Progress in Nuclear Magnetic Resonance Spectroscopy xxx (xxxx) xxx

Contents lists available at ScienceDirect

Progress in Nuclear Magnetic Resonance Spectroscopy

journal homepage: www.elsevier.com/locate/pnmrs

Methyl TROSY spectroscopy: A versatile NMR approach to study challenging biological systems

Stefan Schütz, Remco Sprangers *

Institute of Biophysics and Physical Biochemistry, University of Regensburg, Universitätsstrasse 31, 93053 Regensburg, Germany

Edited by David Neuhaus and David Gadian

ARTICLE INFO

Article history:
Received 5 July 2019
Accepted 25 September 2019
Available online xxxx

Keywords:
Isotope labeling
Large protein complex
TROSY
Dynamics
Interactions
Methyl groups

ABSTRACT

A major goal in structural biology is to unravel how molecular machines function in detail. To that end, solution-state NMR spectroscopy is ideally suited as it is able to study biological assemblies in a near natural environment. Based on methyl TROSY methods, it is now possible to record high-quality data on complexes that are far over 100 kDa in molecular weight. In this review, we discuss the theoretical background of methyl TROSY spectroscopy, the information that can be extracted from methyl TROSY spectra and approaches that can be used to assign methyl resonances in large complexes. In addition, we touch upon insights that have been obtained for a number of challenging biological systems, including the 20S proteasome, the RNA exosome, molecular chaperones and G-protein-coupled receptors. We anticipate that methyl TROSY methods will be increasingly important in modern structural biology approaches, where information regarding static structures is complemented with insights into conformational changes and dynamic intermolecular interactions.

Contents

* Corresponding author.
E-mail address: remco.sprangers@ur.de (R. Sprangers).

https://doi.org/10.1016/j.pnmrs.2019.09.004
0079-6565/

Please cite this article as: S. Schütz and R. Sprangers, Methyl TROSY spectroscopy: A versatile NMR approach to study challenging biological systems, Progress in Nuclear Magnetic Resonance Spectroscopy, https://doi.org/10.1016/j.pnmrs.2019.09.004

1. Introduction

NMR spectroscopy is unique in its ability to study biomolecular structure, interactions and dynamics in a near natural setting. Before the 2000s, NMR spectroscopic studies of assemblies with a molecular weight over 40 kDa were, however, challenging and rare. For these larger systems, rapid spin relaxation rates prevented the routine recording of high-quality NMR spectra [1]. In the last decades, the molecular weight limit of solution-state NMR spectroscopy has been shifted significantly and numerous reports demonstrate that complexes that are far over 100 kDa in size are now amenable to detailed NMR studies. This breakthrough can be ascribed to two important technological advances. On the one hand, sample preparation and isotope labeling methods have been established, where sample deuteration has resulted in significant decreases in transverse relaxation rates [2–9]. On the other hand, the exploitation of transverse relaxation optimized spectroscopy (TROSY) effects [10–12] has resulted in additional and significant sensitivity gains in protein NMR spectroscopy [13,14]. TROSY-based approaches that reduce transverse (T_2) relaxation rates in NMR experiments were initially introduced for ^{1}H, ^{15}N-labeled proteins, and later adapted to aromatic ^{1}H-^{13}C spin systems [15] and $^{13}CH_3$-labeled methyl groups [16].

In our opinion, the combination of specialized methyl labeling schemes and methyl TROSY techniques is one of the most successful approaches that allows for solution-state NMR spectroscopy studies on high molecular weight assemblies [17–19]. In this review, we provide a comprehensive overview of the theoretical background of methyl TROSY spectroscopy. We then discuss the strategies for NMR sample preparation and the approaches that can be exploited to assign methyl group resonances. Finally, we introduce a number of methods that can be used to obtain information regarding protein structure, interactions and dynamics and we will present a small selection of recent and highly impressive applications of methyl TROSY NMR spectroscopy. This review should thereby provide the required background information for people who are interested in applying methyl TROSY techniques to their biological system of interest.

2. The methyl TROSY effect

The sensitivity of an NMR experiment depends on the amount of magnetization that is available at the start of the pulse sequence, the parts of this magnetization that are transferred into detectable magnetization (transfer efficiency) and the rates with which the magnetization terms decays during the experiment (relaxation). In that regard, methyl groups are highly favorable as, first, the initial magnetization results from three equivalent protons that all contribute to the final signal and, second, it is possible to preserve this magnetization for an extended time based on spectroscopic TROSY techniques.

TROSY methods were first exploited in amide groups [11]. For these ^{1}H-^{15}N spin systems the T_2 relaxation is dominated by dipole-dipole (DD) and chemical shift anisotropy (CSA) mechanisms. For a part of the magnetization in an amide group, these relaxation mechanisms interfere destructively, resulting in extended T_2 times. This slowly relaxing magnetization component is selected in a traditional TROSY experiment, whereas the remaining magnetization is actively suppressed during the pulse sequence. For large proteins, this principle results in a significant gain in signal-to-noise, despite the fact that half of the initial magnetization does not contribute to the observable signal. Due to the magnetic field dependence of the CSA, this amide TROSY principle functions optimally around 900 MHz proton frequency and leads to maximum peak heights at 1.5 GHz [11,20]. A similar TROSY principle cannot be exploited for methyl groups, as the methyl group CSAs are too small to interfere significantly with DD relaxation mechanisms.

The spin-system of a ^{13}C-labeled methyl group can be described with 16 energy levels (Fig. 1A) [16,21]. When a methyl group is

Please cite this article as: S. Schütz and R. Sprangers, Methyl TROSY spectroscopy: A versatile NMR approach to study challenging biological systems, Progress in Nuclear Magnetic Resonance Spectroscopy, https://doi.org/10.1016/j.pnmrs.2019.09.004

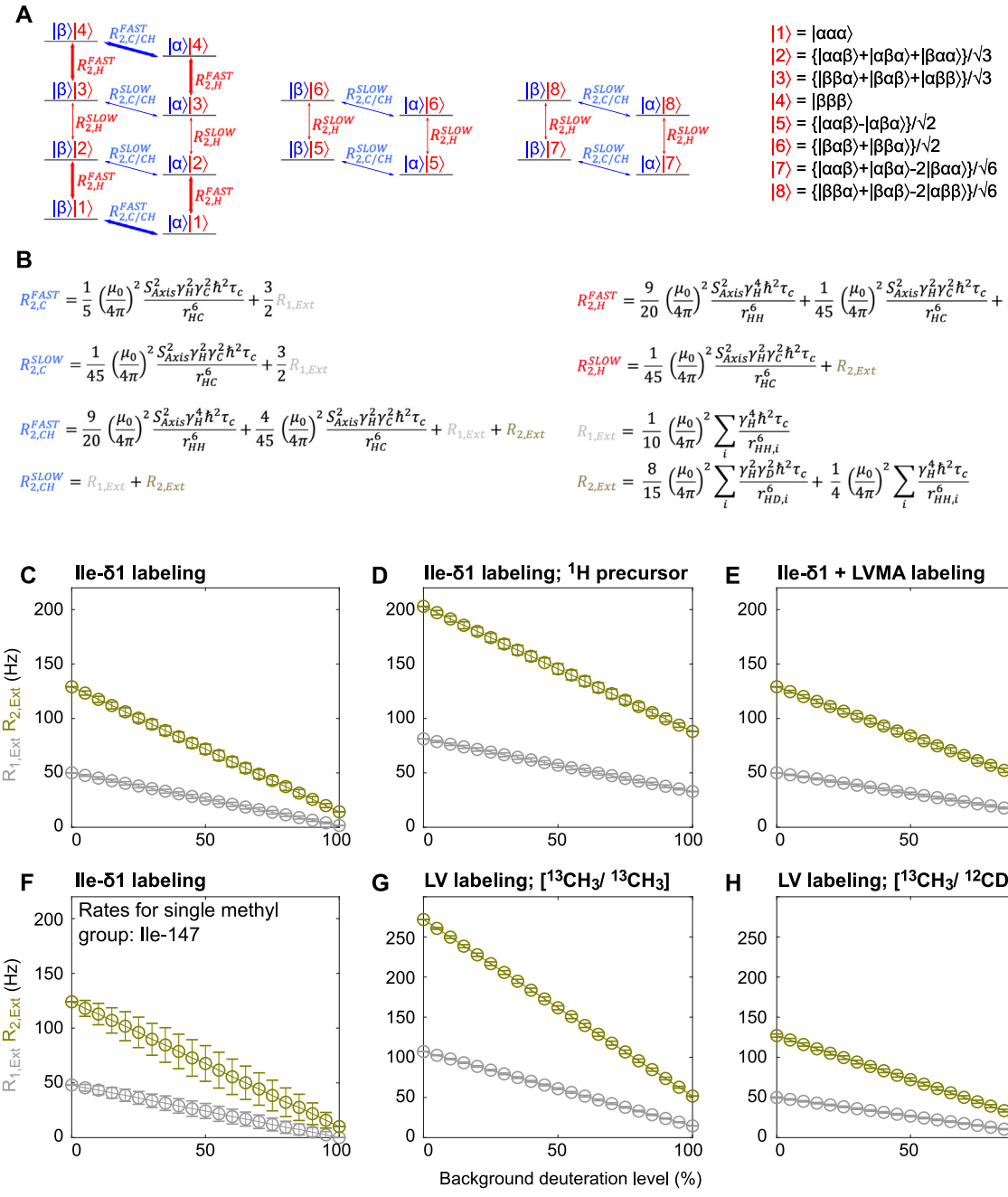

Fig. 1. Relaxation pathways in an isolated methyl group that is part of a large biomolecular complex. A: The methyl group spin system contains three proton spins and the carbon spin which can be described with 16 eigenfunctions that are associated with 16 energy levels. The carbon spin state (α or β) is indicated in blue. The proton spin state (1 to 8) is indicated in red. The thin and bold lines indicate slow and fast relaxation rates that are associated with carbon (blue) or proton (red) transitions. The C/CH subscript in the $R^{SLOW}_{2,C/CH}$ and $R^{FAST}_{2,C/CH}$ rates refer to a carbon relaxation rate in a SQ state ($R^{SLOW}_{2,C}$ or $R^{FAST}_{2,C}$) or in a MQ state ($R^{SLOW}_{2,CH}$ or $R^{FAST}_{2,CH}$). B: The associated (mono-exponential) relaxation rates for the different transitions in A. The subscript 2,C and 2,CH refer to carbon single (C) and multiple quantum rates (CH), respectively, the subscript 2,H refers to the proton relaxation rate. The subscripts 1,EXT and 2,EXT refer to the effects of external protons and deuterons. C-F: The dependence of $R_{1,EXT}$ (gray) and $R_{2,EXT}$ (olive) on the protein deuteration level based on the crystal structure of MSG (PDBID: 1D8C). For each methyl group the $R_{1,EXT}$ and $R_{2,EXT}$ relaxation rates have been determined based on per residue $\Sigma(r^{-6}_{HH})$ and $\Sigma(r^{-6}_{HD})$ values. Subsequently, these rates have been combined to obtain average $R_{1,EXT}$ and $R_{2,EXT}$ rates for the protein. For each deuteration level, 1000 different random proton and deuterium distributions have been used to simulate the random deuteration in the protein and to obtain a distribution for the expected rates. In panel C, the isoleucine Cγ1 atoms are assumed to be fully deuterated, as these atoms are introduced into the protein via the deuterated isoleucine precursor. D: As in C, but where the isoleucine Cγ1 atoms are assumed to be fully protonated, i.e. when a fully protonated isoleucine precursor has been used. E: As in C, but where the methyl groups of valine (γ1 and γ2), leucine (δ1 and δ2), methionine (ε) and alanine (β) are also protonated. F: As in C, but for a single methyl group (I147) in the MSG. Note the large distribution of the rates that a single residue can experience within the ensemble of proteins that make up the NMR sample. These variations in the per residues rates are due to the random and heterogeneous distribution of the proton and deuterium atoms around a specific methyl group. In panels C to E these effects are averaged out as a randomly placed proton is likely to cause strong relaxation in at least one of the isoleucine methyl groups in the protein, while a randomly placed proton it is less likely to cause relaxation in a specific methyl group (e.g. I147; this panel). As a result the averaged rates are larger and more homogeneous in panels C to E than the rates of the individual methyl group as shown in this panel. The large per-residue variation in the relaxation rates caused by external proton and deuterium spins is present in all methyl groups and not restricted to this specific residue. G: As in C, but where the $R_{1,EXT}$ and $R_{2,EXT}$ rates are calculated for leucine and valine methyl resonances in the case that both the pro-(R) and pro-(S) methyl groups are NMR-active (protonated). The close proximity of both methyl groups within one residue results in large relaxation rates. H: As in G, but where each leucine and each valine only contains one NMR active (protonated) methyl group (randomly the pro-(R) or the pro-(S) group). The other methyl group in that residue is fully deuterated. This results in significantly decreased $R_{1,EXT}$ and $R_{2,EXT}$ rates.

Please cite this article as: S. Schütz and R. Sprangers, Methyl TROSY spectroscopy: A versatile NMR approach to study challenging biological systems, Progress in Nuclear Magnetic Resonance Spectroscopy, https://doi.org/10.1016/j.pnmrs.2019.09.004

connected to a large macromolecule, the basis wave-functions can be chosen such that the off-diagonal elements of the density matrix relax in a mono-exponential manner (Fig. 1B) [22–24]. The energy levels are separated into three blocks, between which it is not possible to transfer magnetization by means of chemical shift evolution, $^1J_{C\text{-}H}$ coupling or radio frequency pulses [16,21]. Each of the basis wave functions $|^{13}C\rangle|^1H\rangle$ is written as a combination of the ^{13}C spin state ($|\alpha\rangle$ or $|\beta\rangle$) and the ^1H spin state ($|1\rangle$ to $|8\rangle$) (Fig. 1B). In total, there are 8 possible ^{13}C transitions that are indicated with the horizontal blue lines in Fig. 1A. These transitions separate into 6 slowly relaxing coherences (thin blue lines $R_{2,C}^{SLOW}$ or $R_{2,CH}^{SLOW}$) and two fast relaxing coherences (thick blue lines $R_{2,C}^{FAST}$ or $R_{2,CH}^{FAST}$). The carbon relaxation rates depend on the proton spin state, which is indicated by the subscript "C" for ^{13}C single quantum (SQ) transitions or the subscript "CH" for ^{13}C zero/double quantum (ZQ/DQ). In addition, the 10 possible ^1H transitions are indicated with red vertical lines. These transitions separate into 6 slowly relaxing transitions (thin red lines, $R_{2,H}^{SLOW}$) and 4 fast relaxing coherences (thick red lines, $R_{2,H}^{FAST}$).

The relaxation rates of the magnetization in the methyl group are additionally affected by the presence of proton and deuterium spins that are in close spatial proximity to the methyl group (r^{-6} distance dependence). This is described by an $R_{1,EXT}$ term that takes proton spin flip rates into account and an $R_{2,EXT}$ term that results from the de-phasing of proton magnetization due to long-range ^1H and ^2H dipolar interactions. For a known structure, these latter two relaxation effects can be estimated based on distances between the methyl group and the atoms in the vicinity. It is important to note that the $R_{2,EXT}$ term is significantly lower when the environment of the methyl group is perdeuterated, as an external proton causes around 20-times faster dipolar relaxation than an external deuterium.

Expressions for $R_{2,C}^{SLOW}$, $R_{2,C}^{FAST}$, $R_{2,CH}^{SLOW}$, $R_{2,CH}^{FAST}$, $R_{2,H}^{SLOW}$ and $R_{2,H}^{FAST}$ have been derived, where the proton and carbon CSAs are not taken into account as their contributions to the relaxation rates are very small (Fig. 1B) [21,25]. When the effects of external protons and deuterons are neglected (i.e. when $R_{1,EXT}$ and $R_{2,EXT}$ are assumed to be very small), the equations (Fig. 1B) reveal that (i) the slow ^{13}C single quantum relaxation rate is 1/9 of the fast ^{13}C single quantum relaxation rate ($R_{2,C}^{SLOW} = 1/9 * R_{2,C}^{FAST}$) and (ii) the slow ^{13}C zero/double quantum relaxation ($R_{2,CH}^{SLOW}$) rate is zero. The latter result implies that a part of the zero/double quantum magnetization in a methyl group is insensitive to magnetization losses through dipolar relaxation mechanisms within the methyl group, and only relaxes due to interactions with external protons and deuterons. For a small, perdeuterated, isoleucine-δ1 methyl-labeled protein with a rotational correlation time (τ_c) of 5 ns (corresponding to 8.5 kDa at 20 °C; e.g. ubiquitin) the external protons and deuterons result in relaxation rates that are on the order of $R_{1,EXT} = 0.011\ s^{-1}$ and $R_{2,EXT} = 1.14\ s^{-1}$, when $(\Sigma r_{HH}^{-6})^{-1/6}$ and $(\Sigma r_{HD}^{-6})^{-1/6}$ are assumed to be 5.5 Å and 1.8 Å, respectively. Based on that, the carbon and proton relaxation rates can be estimated to be around: $R_{2,C}^{SLOW} = 0.95\ s^{-1}$, $R_{2,C}^{FAST} = 8.44\ s^{-1}$, $R_{2,CH}^{SLOW} = 1.15\ s^{-1}$, $R_{2,CH}^{FAST} = 26.2\ s^{-1}$, $R_{2,H}^{SLOW} = 2.07\ s^{-1}$, $R_{2,H}^{FAST} = 23.4\ s^{-1}$. For a slowly tumbling protein with a τ_c of 180 ns (corresponding to 650 kDa at 65 °C; 20S proteasome), these rates increase with a factor of 36 (the rates scale linearly with τ_c) and thus increase to around: $R_{1,EXT} = 0.39\ s^{-1}$, $R_{2,EXT} = 40.9\ s^{-1}$, $R_{2,C}^{SLOW} = 34.3\ s^{-1}$, $R_{2,C}^{FAST} = 304\ s^{-1}$, $R_{2,CH}^{SLOW} = 41.3\ s^{-1}$, $R_{2,CH}^{FAST} = 944\ s^{-1}$, $R_{2,H}^{SLOW} = 74.6\ s^{-1}$, $R_{2,H}^{FAST} = 843\ s^{-1}$. First, these numbers indicate that there is a significant difference between the fast and slowly relaxing magnetization terms in highly deuterated proteins (a factor of ~9 for the SQ coherences and a factor of ~29 for the MQ coherences). This observation shows that it is important to design NMR experiments that aim at preserving and selecting the slowly relaxing magnetization terms. Second, these calculated rates show that the MQ relaxation rates are higher than the SQ relaxation rates (by a factor of 1.2 for the slowly relaxing term and by a factor of 3.1 for the fast relaxing term), which is due to significant contributions of dipolar relaxation effects with external protons for MQ coherences. In that regard, it would thus be desirable to avoid the presence of MQ magnetization terms during the pulse sequence. Third, it should be noted that the rates mentioned above will increase significantly when the protein contains a higher proton density, as then $R_{1,EXT}$ and the second term that contributes to $R_{2,EXT}$ will increase rapidly. This is graphically shown in Fig. 1C, where $R_{1,EXT}$ and $R_{2,EXT}$ have been calculated for an isoleucine-δ1 CH_3 labeled protein with a rotational correlation time of 60 ns (80 kDa at 20 °C; MSG; at all deuteration levels the isoleucine-γ1 positions are fully deuterated) at different levels of background deuteration. Upon loss of full background deuteration, the relaxation effects of external protons significantly increase and can, below a specific deuteration level, dominate the overall methyl group relaxation rates. The importance of high deuteration levels close to the methyl groups of interest is highlighted in Fig. 1D, where the $R_{1,EXT}$ and $R_{2,EXT}$ relaxation rates are simulated for MSG when the isoleucine-γ1 positions are fully protonated. Such a sample results from a protein preparation that uses a fully protonated isoleucine precursor (see section below). The graphs in Fig. 1C and D show that the $R_{1,EXT}$ and $R_{2,EXT}$ rates of the protonated isoleucine methyl groups are similar in a protein that is 50% random deuterated and 100% deuterated at the isoleucine-γ1 position and a protein that is per-deuterated, but protonated in the isoleucine-γ1 positions. This highlights the importance of a proper preparation of the precursor molecules that are used to prepare the protein NMR sample. Likewise, the introduction of additional NMR-active (protonated) methyl groups in the protein will increase the $R_{1,EXT}$ and $R_{2,EXT}$ rates, especially in a highly deuterated background (Fig. 1E compared to Fig. 1C). The information gain that the additional (LVMA) methyl groups provide will thus be partially compromised by the increased relaxation that is caused by the higher proton density in the protein. The $R_{1,EXT}$ and $R_{2,EXT}$ relaxation rates for a specific methyl group will strongly depend on the spatial distribution of protons in the protein. As all proteins in the sample are deuterated differently, this will cause a broad distribution of relaxation rates for a specific methyl group (Fig. 1F). It remains to be determined how this spread in relaxation rates for one methyl resonance will influence the quantitative determination of NMR parameters, including residue-specific proton or deuterium T2 relaxation rates. In the above, we focused on the relaxation rates that are experienced by the δ1 methyl groups in isoleucine residues. For methyl groups in other amino acids, it is equally important to ensure that the proton densities around the observed methyl groups are low. The two methyl groups of leucine and valine residues are in close spatial proximity and thus represent a special case, where the protonation of one methyl group can cause significant relaxation in the other methyl group. As a result, relatively high $R_{1,EXT}$ and $R_{2,EXT}$ rates for leucine and valine methyl resonances are expected (Fig. 1G). These high relaxation rates can be reduced by a factor of ~2 when using a labeling scheme that yields leucine and valine residues where randomly only one of the two methyl groups is protonated (and ^{13}C-labeled), whereas the other methyl group is fully deuterated (and not ^{13}C-labeled; see section below) (Fig. 1H). Finally, lower protein deuteration levels will result in smaller differences between the fast and slowly relaxing terms (Fig. 1B), which will reduce the maximal achievable methyl TROSY effect. In summary, TROSY spectra, especially of large assemblies (large τ_c), will benefit significantly from protein deuteration levels that are as high as achievable (Fig. 1C).

Based on density matrix calculations, it can be shown how fast and slowly relaxing magnetization terms decay and are mixed during specific NMR experiments and how this results in the loss of magnetization. In the HSQC experiment [26] (Fig. 2A, red) the first $\pi/2$ pulse splits the initial proton magnetization into two parts, 50% of which relaxes slowly ($R_{2,H}^{SLOW}$) and 50% of which relaxes fast

Please cite this article as: S. Schütz and R. Sprangers, Methyl TROSY spectroscopy: A versatile NMR approach to study challenging biological systems, Progress in Nuclear Magnetic Resonance Spectroscopy, https://doi.org/10.1016/j.pnmrs.2019.09.004

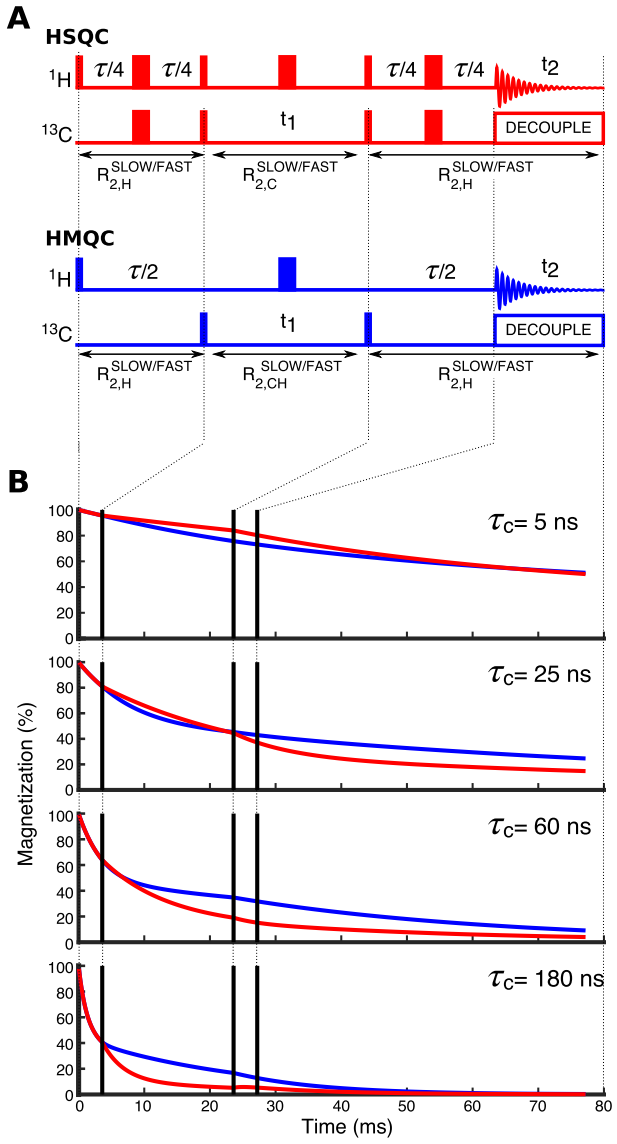

Fig. 2. Relaxation in the HSQC and HMQC experiments. A: Schematic representation of the HSQC (top, red) and HMQC (bottom, blue) experiments. The time τ is set to $1/J_{CH}$, t_1 and t_2 refer to the carbon and proton chemical shift evolution times, respectively. The relaxation mechanisms that are active during the pulse sequence are indicated. B: Simulation of the decay of the magnetization during the HSQC (red) and HMQC (blue) experiments. The data are simulated for methyl groups that are connected to a biomolecule that tumbles with a τ_C of 5, 25, 60 or 180 ns. For the simulations the carbon chemical shift evolution time (t_1) is set to 20 ms. Based on these relaxation rates and the required spectral resolution, it might be advantageous to increase or decrease the maximum carbon acquisition time in real experiments.

($R_{2,H}^{FAST}$) during the first INEPT step of $\tau/2 = 1/(2\ J_{HC}) \sim 4.0$ ms. After the first INEPT step, the amount of slow and fast relaxing magnetization is, due to the relaxation, no longer distributed 50:50. The subsequent π/2 proton pulse results in a mixing of the slowly and fast relaxing coherences, whereas the π/2 carbon pulse ensures the formation of SQ coherence. During carbon chemical shift evolution (t_1), one part of the remaining magnetization relaxes slowly ($R_{2,C}^{SLOW}$), whereas the other part relaxes fast ($R_{2,C}^{FAST}$). The fast and slowly relaxing components are, once again, mixed due to the π/2 proton pulse that follows t_1. During the second INEPT step, the remaining magnetization relaxes in part slowly ($R_{2,H}^{SLOW}$) and in part fast ($R_{2,H}^{FAST}$). During proton chemical shift detection (t_2), the detectable magnetization consists of 8 different parts that each have relaxed differently before, during and after t_1. Importantly, the magnetization that experiences slow relaxation in all three steps only constitutes 18.75% of the total equilibrium magnetization. For large complexes, where R_2 is fast, this results in spectra of significantly reduced quality.

During the first INEPT step in an HMQC experiment [27,28] (Fig. 2A, blue) half of the magnetization relaxes slowly ($R_{2,H}^{SLOW}$) and 50% relaxes fast ($R_{2,H}^{FAST}$), as is the case in the HSQC experiment. The subsequent π/2 carbon pulse creates MQ coherence without mixing the slowly and fast relaxing magnetization terms. During t_1, the slowly decaying magnetization continues to decay slowly with $R_{2,CH}^{SLOW}$, whereas the fast decaying magnetization continues to decay fast with $R_{2,CH}^{FAST}$. The π/2 carbon pulse after t_1, like the one before t_1, does not mix the slowly and fast decaying coherences, and during the second INEPT period the slowly and fast decaying coherences decay with $R_{2,H}^{SLOW}$ and $R_{2,H}^{FAST}$, respectively. During proton chemical shift detection (t_2), the magnetization consists of two parts that either decay slowly or that decay rapidly during the complete HMQC pulse sequence. 50% of the initial magnetization thus experiences slow relaxation during the complete experiment. This complete separation of the slow and fast relaxing pathways increases the quality of NMR spectra significantly. Note that the slowly and fast relaxing magnetization terms give rise to signals at the same frequencies. There is thus no need to actively suppress fast relaxing coherences, as is done in the H-N TROSY experiment, and the remaining slowly relaxing magnetization thus adds to the final signal intensity.

To demonstrate the differences between the HSQC and the HMQC experiments described above, we simulated the decay of the magnetization in a $^{13}CH_3$-labeled methyl group in a number of highly deuterated proteins that are widely used in the NMR field (Fig. 2B, red and blue curves correspond to the HSQC and HMQC experiments, respectively). The simulations focussed on τ_C values of 5 ns (corresponding to 8.5 kDa at 20 °C; ubiquitin), 25 ns (41 kDa at 20 °C; MBP), 60 ns (80 kDa at 20 °C; MSG) and 180 ns (650 kDa at 65 °C; 20S proteasome) (Fig. 2B) used an INEPT time (τ/2) of 3.6 ms, a carbon chemical shift evolution time (t_1) of 20 ms and a proton chemical shift evolution time (t_2) of 50 ms. In practice, these values can be adjusted to further optimize spectral quality. It is important to realize that the decay of the total magnetization during the INEPT transfer, t_1 and t_2 is not mono-exponential, but the sum of a fast and a slowly relaxing part (that each relaxes mono-exponentially). Fig. 2B illustrates that the HMQC experiment (blue) significantly outperforms the HSQC experiment (red) when the molecular weight increases, which is due to the fact that the slowly relaxing magnetization terms are consistently preserved in the HMQC experiment after the first π/2 proton pulse, despite the fact that the SQ magnetization relaxes more slowly than the MQ magnetization during the carbon chemical shift evolution steps.

It should be noted that an additional gain in signal-to-noise for the HSQC experiment through the use of sensitivity enhancement approaches is not possible for methyl groups, as the second coherence transfer pathway is not refocussed for methyl groups when the INEPT delay is set to 1/(2J) [29]. At the same time, the inclusion of a sensitivity enhancement scheme to the HMQC pulse sequence [30] is not advisable, as this results in the loss of the methyl TROSY effect due to the requirement of two additional π/2 proton pulses and thus in spectra that will have significantly impaired quality. In addition, sensitivity enhancement schemes will increase the length of the NMR pulse sequence, which will result in additional relaxation losses, especially for larger protein complexes.

To demonstrate experimentally the high quality of HMQC spectra of methyl-labeled samples, we here recorded spectra of a RecA-like domain (25 kDa) and of the 20S proteasome double α-ring ($\alpha_7\alpha_7$, 350 kDa) at different temperatures (Fig. 3). Both protein samples have been prepared in a highly deuterated background

Please cite this article as: S. Schütz and R. Sprangers, Methyl TROSY spectroscopy: A versatile NMR approach to study challenging biological systems, Progress in Nuclear Magnetic Resonance Spectroscopy, https://doi.org/10.1016/j.pnmrs.2019.09.004

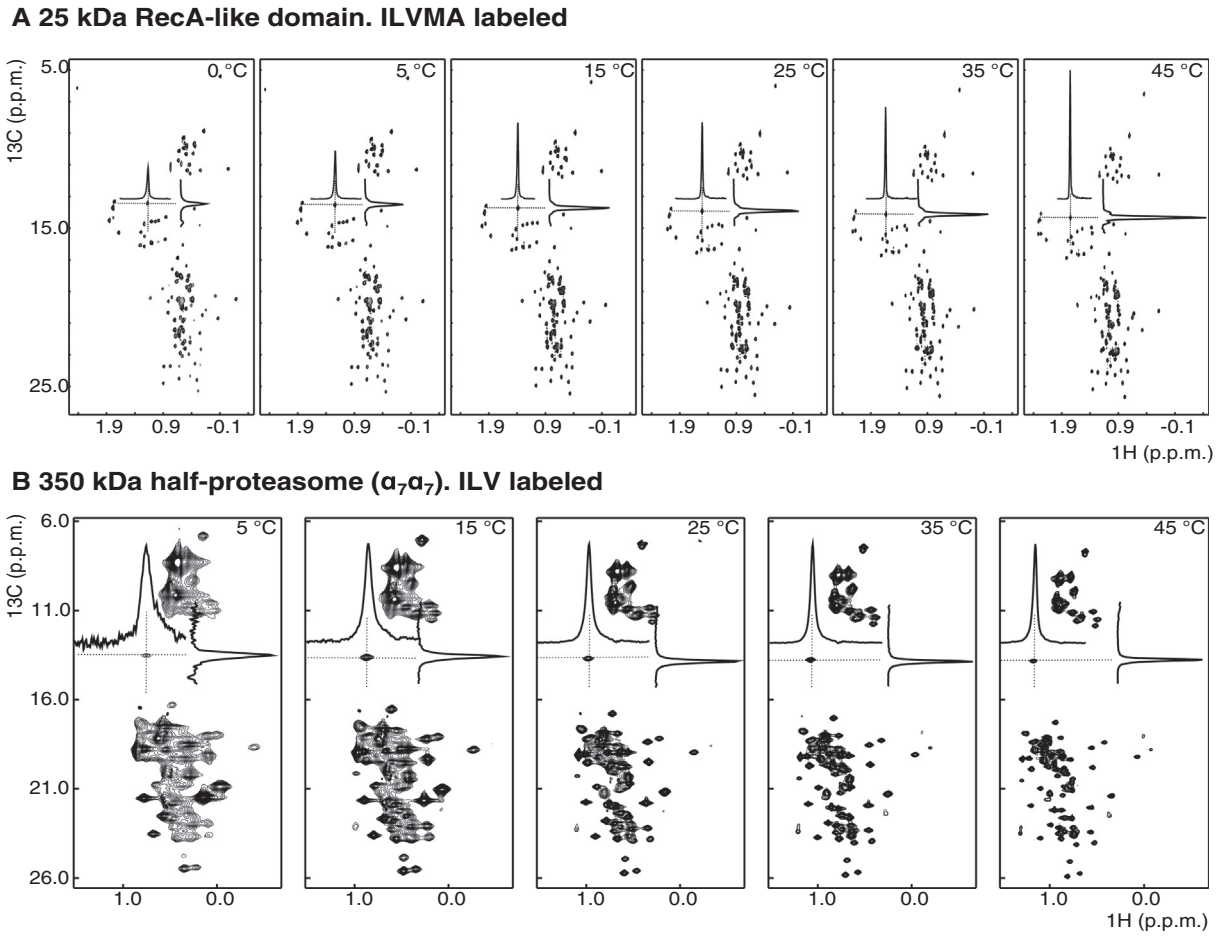

Fig. 3. Temperature-dependence of the quality of methyl TROSY spectra. A: SOFAST methyl TROSY spectra of a 25 kDa ILVMA-labeled RecA-like domain (100 uM protein concentration, D_2O-based buffer), recorded at 800 MHz proton frequency. Each of the spectra was recorded with a carbon acquisition time of 21.2 ms, 4 scans and an inter-scan delay of 0.5 s, which resulted in a total experimental time of 8.5 min. All spectra in A were processed identically using NMRPipe [330] with linear prediction in the carbon dimension and shifted squared sine bell window functions in both dimensions. All spectra are shown with the same contour levels, and the traces have a consistent absolute scaling. With decreasing temperature, the signal-to-noise ratio decreases, whereas the linewidth increases; nevertheless, even at temperatures as low as 0 °C, the spectral quality remains extremely high. B: SOFAST methyl TROSY spectra of the 350 kDa ILV-labeled (only one of the two methyl groups in valine and leucine is randomly labeled) $\alpha_7\alpha_7$ half-proteasome (500 uM protein concentration, D_2O-based buffer), recorded at 800 MHz proton frequency. Each of the spectra was recorded with a carbon acquisition time of 27.6 ms, 32 scans and an inter-scan delay of 0.5 s, which resulted in a total experimental time of 68 min. All spectra in B were processed identically using NMRPipe [330] with linear prediction in the carbon dimension and shifted squared sine bell window functions in both dimensions. The 2D spectra are shown with the same contour levels, and the 1D traces are scaled such that they have the same maximum intensity to visualize the increase in the linewidth with temperature. In addition, a significant reduction in the signal-to-noise ratio can be clearly observed. Despite the relatively low spectral quality at 5 °C, it is still possible to detect a large number of well-resolved resonances for the 350 kDa complex.

(see next section), with NMR-active $^{13}CH_3$ groups in the isoleucine (δ_1), leucine (δ_1 and δ_2), valine (γ_1 and γ_2), alanine and methionine residues (ILVMA labeling; Fig. 3A; RecA-like domain) or at isoleucine (δ_1), leucine (δ_1 or δ_2), valine (γ_1 or γ_2) residues (ILV labeling; Fig. 3B; half-proteasome). All spectra of the RecA-like domain and all spectra of the half-proteasome have been recorded and processed identically. To illustrate the spectral quality, ^1H and ^{13}C traces through a selected resonance are indicated in the spectra. For the RecA-like domain (Fig. 3A), these traces are scaled identically, such that the differences in signal-to-noise at different temperatures are easily visible. From these data, it is clear that the signal-to-noise decreases with decreasing temperature, as is expected. For the half-proteasome, the 1D traces are scaled such that all traces have the same intensity, which highlights the changes in linewidth with temperature. As expected, the linewidths of the methyl resonances increase with decreasing temperature. Importantly, based on the NMR spectra in Fig. 3, it is clear that very high quality spectra of intermediate size proteins can be obtained at very low temperatures (e.g. the 25 kDa RecA-like domain at 0 °C) and that, even for systems that have a molecular weight of 350 kDa, it is possible to record spectra of decent quality at lower temperatures (e.g. the half-proteasome at 15 °C). This demonstrates experimentally that methyl TROSY spectra make very challenging biological systems amenable to NMR spectroscopic studies.

Despite the simplicity of the (methyl TROSY) HMQC experiment [16,28], a number of variations to the four-pulse pulse sequence have been suggested. To increase the sensitivity per time, the use of SOFAST methods has been introduced [31,32,33]. In this approach, the methyl groups are selectively excited with an Ernst-angle pulse. Even for highly deuterated proteins, this results in enhanced longitudinal relaxation of methyl groups and the possibility to reduce the inter-scan recycle delay [32]. As a result, the signal-to-noise per unit of experimental time can be significantly increased. In addition, it was realized that small imperfections in the central π proton pulse in the HMQC experiment result in the presence of additional resonances located at ± ½ J_{CH} from the central carbon resonance [34]. The intensity of these artifacts is on the order of a few percent of the intensity of the central methyl resonances. Nevertheless, for very strong methyl resonances, these

Please cite this article as: S. Schütz and R. Sprangers, Methyl TROSY spectroscopy: A versatile NMR approach to study challenging biological systems, Progress in Nuclear Magnetic Resonance Spectroscopy, https://doi.org/10.1016/j.pnmrs.2019.09.004

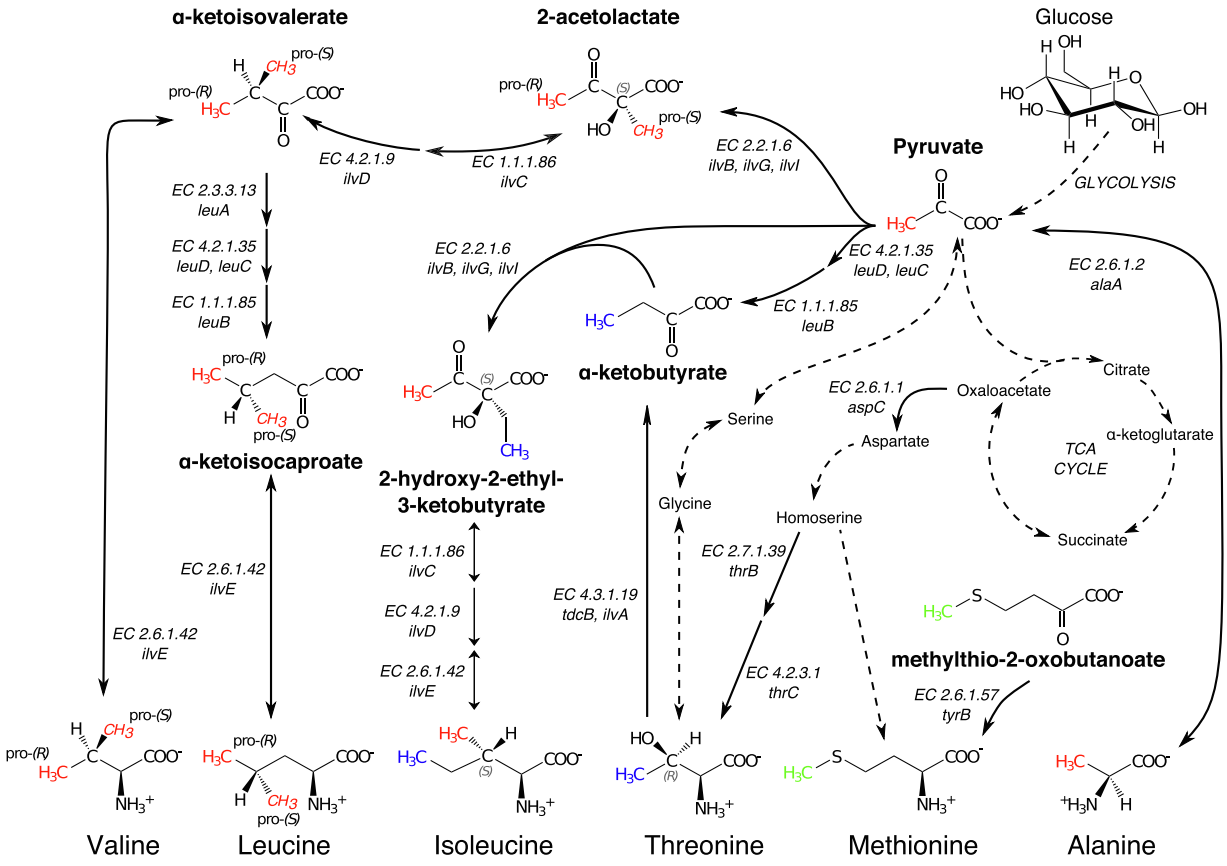

Fig. 4. *E. coli* metabolic pathways that are involved in the biogenesis of methyl-containing amino acids. The methyl-containing amino acids valine, leucine, isoleucine, threonine, methionine and alanine are shown on the bottom. The key metabolites that can be used as precursors for methyl labeling (Table 1), including their structural formulas, are indicated in bold. The color (blue or red) and font-type (italic or upright) of the methyl groups are consistent with the (stereospecific) location in the molecules. Full arrows indicate one-step reactions, while dashed arrows indicate multiple reactions and double-headed arrows indicate reversible reactions. The enzymes that catalyze the reactions are indicted by their EC number, deletion of a number of the corresponding genes from the *E. coli* genome can be exploited to construct strains where specific pathways are blocked (see table 1). The figure has been prepared based on data derived from https://www.genome.jp/kegg/.

undesired resonances can interfere with the spectral analysis. These artifacts, which are not suppressed by gradients or extensive phase cycling, can be efficiently eliminated by the use of a composite (e.g. 90_y-240_x-90_y or 90_y-180_x-90_y) central proton pulse [34].

In summary, the methyl TROSY experiment exploits the interference between ^{1}H-^{1}H and ^{1}H-^{13}C dipolar relaxation mechanisms to preserve slowly relaxing magnetization terms. The strengths of these dipolar interactions are field-independent and as a result, the methyl TROSY experiment functions optimally at all magnetic field strengths. This is in strong contrast to N-H TROSY or aromatic C-H TROSY experiments that exploit CSA relaxation mechanisms that scale with the magnetic field. These latter TROSY techniques thus function optimally at a single magnetic field strength only.

3. Sample preparation: Methyl group labeling

A prerequisite for the recording of high quality methyl TROSY spectra is the preparation of highly deuterated samples (to reduce both $R_{1,EXT}$ and $R_{2,EXT}$; Fig. 1B–F) that contain isolated $^{13}CH_3$-labeled methyl groups. Naturally, these methyl groups are found in around one third of the proteinogenic amino acids (alanine, threonine, valine, leucine, isoleucine and methionine). In this section we describe labeling strategies that are suited for the preparation of NMR samples that contain NMR-active methyl groups in a highly deuterated background.

3.1. *E. coli* -based protein expression

Protein expression in *E. coli* is compatible with growth media that are based on D_2O. In practice, it will not be possible to exclude all protons in the growth medium due to the presence of protons in salts (e.g. crystal water or as part of the KH_2PO_4 and Na_2HPO_4 phosphate stocks) and due to the highly hygroscopic nature of D_2O which results in the absorption of atmospheric water during longer incubation and growth times. In addition, deuterated chemicals, including glucose, have deuteration levels that are below 99% and will thus also introduce protons into the final protein product. In practice it will thus not be possible to prepare protein samples that have a deuteration level that significantly exceeds 99%. Past and current efforts try to optimize the protein over-expression yields such that the high costs that are associated with protein deuteration and isotope labeling are minimized [35–37]. The second advantage of *E. coli* as a protein expression host is that metabolic pathways can be utilized to selectively channel $^{13}CH_3$-labeled methyl groups into specific residues in the target protein (Fig. 4, Table 1). To that end, isotope-labeled amino acids or amino acid precursors are added to the growth medium of the cells. To ensure that these labeled compounds only end up in the target sites and are not "scrambled" into other amino acids, it may be necessary to add additional metabolites or to genetically modify the expression host. Due to the simplicity and reliability of methyl labeling in *E. coli*, this is by far the most commonly used strategy to prepare

Please cite this article as: S. Schütz and R. Sprangers, Methyl TROSY spectroscopy: A versatile NMR approach to study challenging biological systems, Progress in Nuclear Magnetic Resonance Spectroscopy, https://doi.org/10.1016/j.pnmrs.2019.09.004

Table 1
Methyl group isotope labeling strategies.

Labeling	Precursor	Amount (mg/L)	Remarks[a]
Met-ε	L-methionine	50–250 [b]	No scrambling [44]
	4-methylthio-2-ketobutyrate	65	No scrambling [39]
Ile-δ1	α-ketobutyrate [b]	50	No scrambling [1,47]. Cannot be combined with 2-acetolactate.
	2-hydroxy-2-ethyl-3-ketobutyrate	100	Addition of 200 mg/L α-ketoisovalerate to prevent unexpected scrambling into leucine and valine methyl groups. [53,54]
Ile-γ2	2-hydroxy-2-ethyl-3-ketobutyrate	100	Addition of 200 mg/L α-ketoisovalerate to prevent unexpected scrambling into leucine and valine methyl groups. [53,54]
Ile-γ2 + δ1	L-isoleucine	20	Based on an ilvD- and leuB- strain[c]. Addition of 20 mg/L leucine and 20 mg/L valine is required [64].
Leu-δ + Val-γ	α-ketoisovalerate [d]	75–120	No Scrambling [55,57-59]
Leu-δ only	α-ketoisocaproate	150	None [62]
	α-ketoisovalerate	30	Based on an Acl- andVal- strain[c]. 30 mg/L isoleucine and 30 mg/L valine are required [65].
Val-γ only	α-ketoisovalerate [g]	100	Addition of 100 mg/L α-ketoisocaproate to inhibit the use of α-ketoisovalerate in leucine biogenesis [63]
		30	Based on an Acl- and Leu- strain[c]. 30 mg/L isoleucine and 30 mg/L leucine are required [65].
Val-γ2 + Leu-δ2 pro-*(S)*	2-acetolactate 2-[^{13}C]	300	No scrambling [60]
		30	Based on an Acl- strain[c]. 30 mg/L isoleucine is required [65]
Val-γ1 + Leu-δ1 pro-*(R)*	2-acetolactate 4-[^{13}C]	300	No scrambling [60]
		30	Based on an Acl- strain[c.] 30 mg/L isoleucine is required [65]
Val-γ2 pro-*(S)*	2-acetolactate 2-[^{13}C]	300	Addition of 40 mg/L leucine, to inhibit the use of 2-acetolactate in leucine biogenesis [337].
		30	Based on an Acl- and Leu- strain[c]. 30 mg/L isoleucine and 30 mg/L leucine are required [65].
	L-valine γ2-$^{13}CH_3$	100	Addition of 20 mg/L leucine is required[e] [61].
		20	Based on an ilvD- and leuB- strain[c]. Addition of 20 mg/L leucine and 20 mg/L valine is required[c,e] [64].
Val-γ1 pro-*(S)*	2-acetolactate 4-[^{13}C]	300	Addition of 40 mg/L leucine, to inhibit the use of 2-acetolactate in leucine biogenesis [337].
		30	Based on an Acl- and Leu- strain[c]. 30 mg/L isoleucine and 30 mg/L leucine are required [65]
	L-valine γ1-$^{13}CH_3$	100	Addition of 20 mg/L leucine is required[e] [61].
		20	Based on an ilvD- and leuB- strain[c]. Addition of 20 mg/L leucine and 20 mg/L valine is required[c,e][64].
Leu-δ2 pro-*(S)*	2-acetolactate 2-[^{13}C]methyl	30	Based on an Acl- and Val- strain[c]. 30 mg/L isoleucine and 30 mg/L valine are required [65].
	L-leucine δ2-$^{13}CH_3$	20	Addition of 100 mg/L valine is required[e] [61]
		20	Based on an ilvD- and leuB- strain[c]. Addition of 20 mg/L leucine and 20 mg/L valine is required[c,e] [64].
Leu-δ1 pro-*(R)*	2-acetolactate 4-[^{13}C]	30	Based on an Acl- and Val- strain[c]. 30 mg/L isoleucine and 30 mg/L valine are required [65].
	L-leucine δ1-$^{13}CH_3$	20	Addition of 100 mg/L valine is required[e] [61]
		20	Based on an ilvD- and leuB- strain[c]. Addition of 20 mg/L leucine and 20 mg/L valine is required[c,e] [64].
Ala-β	L-alanine	800	Addition of 2.5 g/L glycerol, 2.5 g/L succinate, 60 mg/L isoleucine and 200 mg/L α-ketoisovalerate [69].
		700	Addition of 60 mg/L 2-hydroxy-2-ethyl-3-ketobutyrate, 200 mg/L α-ketoisovalerate [49].
		700 [f]	Addition of 60 mg/L α-ketobutyrate and 200 mg/L α-ketoisovalerate (2–5% scrambling into isoleucine- γ2) [49].
Thr-γ2	L-threonine	50 [g]	Addition of 50 mg/L α-ketobutyrate and 100 mg/L glycine [72].
		25	Based on thrC- strain. Addition of 20 mg/L isoleucine or 25 mg/L α-ketobutyrate [65].
Ile-δ1 + Met-ε	100 mg/L L-methionine + 50 mg/L α-ketobutyrate		

Please cite this article as: S. Schütz and R. Sprangers, Methyl TROSY spectroscopy: A versatile NMR approach to study challenging biological systems, Progress in Nuclear Magnetic Resonance Spectroscopy, https://doi.org/10.1016/j.pnmrs.2019.09.004

Table 1 (*continued*)

Labeling	Precursor	Amount (mg/L)	Remarks[a]
Ile-δ1 + Leu-δ + Val-γ	50 mg/L α-ketobutyrate + 80 mg/L α-ketoisovalerate		
Ile-δ1 + Leu-δ + Val-γ + Ala-β	50 mg/L α-ketobutyrate + 80 mg/L α-ketoisovalerate + 100 mg/L L-alanine		
Ile-δ1 + Leu-δ + Val-γ + Ala-β + Met-ε	50 mg/L α-ketobutyrate + 80 mg/L α-ketoisovalerate + 100 mg/L L-alanine + 100 mg/L L-methionine		
Ile-δ1 + Leu-δ + Val-γ + Ala-β + Met-ε + Thr-γ2	50 mg/L α-ketobutyrate + 80 mg/L α-ketoisovalerate + 100 mg/L L-alanine + 100 mg/L L-methionine + 50 mg/L L-threonine + 100 mg/L glycine		

The incorporation levels of the labeled methyl groups into the target protein should in all cases be very high. Nevertheless, in the author's laboratory, some variation in the absolute incorporation levels are observed, even when producing the same protein multiple times. This is potentially due to differences in the growth of the bacteria and general variations in the final level of protein over expression.

[a] To obtain full protein deuteration is it required to add the additional supplements in their perdeuterated forms.

[b] Amounts can be reduced to 50 mg/L without compromising spectral quality [73,74]. For highly challenging systems αβγ-deuterated methionine can be used [90,92].

[c] The ilvD-, leuB- strain includes deletions for ilvD and leuB; the synthesis of isoleucine from 2-hydroxy-2-ethyl-3-ketobutyrate and the synthesis of α-ketoisocaproate from α-ketoisovalerate are thereby inhibited; Fig. 4. For these deletion strains, a two-phase expression protocol is used. In the growth phase, a supplementation with (deuterated) amino acids that cannot be synthesized by the strain is required. During the expression phase the specifically methyl-labeled amino acids are added, as well as the other required (deuterated) amino acids. The Acl- strain includes deletions for ilvB, ilvG and ilvI; the synthesis of isoleucine, valine and leucine from α-ketobutyrate and pyruvate is inhibited; Fig. 4. The Val- strain includes a deletion for ilvE; the synthesis of valine from α-ketobutyrate and the synthesis of leucine from α-ketoisocaproate are inhibited; Fig. 4. The Leu- strain includes a deletion for leuB; the synthesis of α-ketoisocaproate from α-ketoisovalerate is inhibited; Fig. 4. The thrC- strain contains a deletion of thrC; the synthesis of threonine from homoserine is inhibited; Fig. 4.

[d] Usage of the $^{13}CH_3/^{12}CD_3$-labeled form of 2-ketoisovalerate or 2-ketoisocaproate results in random, non-stereospecific labeling of the two Leu/Val methyl groups as $^{13}CH_3/^{12}CD_3$, which suppresses intra-residue methyl-methyldipolar interactions and enhances spectral resolution.

[e] It is possible to combine the labeling of valine-γ1 with leucine-δ1 or leucine-δ2 and of valine-γ2 with leucine-δ1 or leucine-δ2.

[f] Amounts can be reduced to 50–100 mg/L without compromising labeling efficiency [51,73,74].

[g] Scrambling into Ile-δ1 and Gly. If a Thr-auxotroph strain (thrC-) is used, no scrambling to Gly observed.

samples for methyl TROSY spectroscopy. Most of the labeling schemes that are described below work well in growth media that are based on glucose as a carbon source. If, for example, glycerol is used as a main carbon source, the cellular metabolic pathways change, which can result in a situation where specific precursors are no longer solely used in the corresponding amino acid synthesis pathway.

3.1.1. Methionine-ε

Methionine is one of the most under-represented amino acids in proteins, with an average occurrence of only 1.5 to 2% [38]. Residue-specific methyl-labeling of methionine residues thus results in a limited number of NMR resonances and, consequently, a low degree of signal overlap. In *E. coli*, methionine residues can be labeled with NMR-active methyl groups by two independent strategies (Fig. 4). First, a methionine precursor ([4-^{13}C]-methylthio-2-oxobutanoate; MOB; Table 1) can be added to the minimal growth medium [39]. Second, methionine labeling can be conveniently achieved by the direct addition of methyl-^{13}C-methionine to the growth medium (Table 1), which efficiently represses endogenous methionine synthesis [40]. This latter strategy also functions well in enriched media [41,42]. If required, background amounts of unlabeled methionine in the growth medium can be removed with the enzyme methionine-γ-lyase [43]. As the methyl group of methionine is not J-coupled to the other side chain carbons, it is possible to use fully ^{13}C-labeled methionine or methyl-only labeled methionine. For most applications the use of fully protonated methionine is adequate as the methyl group is distant to other side chain protons due to the connecting sulfur atom. For very large assemblies and in special cases it might be advantageous to use a form of methionine that is deuterated at all but the methyllabeled carbon [44].

3.1.2. Isoleucine-δ1

Isoleucine-δ1 methyl groups are the most frequently used methyl reporters in large protein complexes as the resulting 2D [^{1}H, ^{13}C] spectra are often very well resolved. The labeling of isoleucine-δ1 methyl groups is achieved by the addition of α-ketobutyrate (2-oxobutanoate; Table 1) to the growth medium [1], which is straightforward and cost efficient. The CH_2-CH_3 ethyl moiety of α-ketobutyrate ends up as the $C_{\gamma1}H_2$-$C_{\delta1}H_3$ position in the isoleucine residues (Fig. 4). Depending on the labeling of the α-ketobutyrate, the isoleucine residues can thus be produced in specifically carbon- and deuterium-labeled forms.

Full ^{13}C-labeling of isoleucine residues, which is required to observe intra-residue correlations between the methyl group and the backbone amide resonances, can be achieved with uniformly ^{13}C-labeled α-ketobutyrate in combination with ^{13}C-labeled glucose [45,46]. On the other hand, to record [^{1}H, ^{13}C] spectra that have a very high resolution in the carbon dimension, the Cγ1–Cδ1 J-coupling can be efficiently removed by using α-ketobutyrate that is ^{13}C-labeled only in the methyl group [47]. To suppress dipolar relaxation effects from nearby protons, which is important in high molecular weight complexes, α-ketobutyrate that is deuterated at the CH_2 position should be used. Fully protonated α-ketobutyrate can be conveniently converted into the CD_2 form by incubating the precursor at high pH in D_2O [48]. Indeed, very high-quality NMR spectra of large proteins can be recorded by using ^{2}H, ^{12}C-glucose and 3-d_2-4-^{13}C-α-ketobutyrate in a D_2O-based minimal growth medium [16,48].

The use of α-ketobutyrate as an Ile-δ1 precursor is incompatible with a labeling scheme that simultaneously aims at incorporating stereo-specifically labeled leucine and valine residues based on 2-acetolactate (see below) [49]. This incompatibility of labeling schemes has been overcome by using the isoleucine precursor 2-hydroxy-2-ethyl-3-ketobutyrate (2-aceto-2-hydroxybutanoate) that is closer towards the isoleucine amino acid in the biosynthesis pathway (Fig. 4). Appropriate isotope labeling of this precursor results in efficient isoleucine-δ1 labeling.

Incompatibilities between α-ketobutyrate as an isoleucine precursor and the addition of methyl-labeled alanine have also been reported [49]. In that case, the labeled methyl group from alanine can result in the partial labeling of the isoleucine-γ2 methyl group. The degree of scrambling is, however, low and can often be neglected [50]. In our experience, the level of scrambling of the isotope-labeled methyl group from alanine into isoleucine is less

Please cite this article as: S. Schütz and R. Sprangers, Methyl TROSY spectroscopy: A versatile NMR approach to study challenging biological systems, Progress in Nuclear Magnetic Resonance Spectroscopy, https://doi.org/10.1016/j.pnmrs.2019.09.004

than 2% and does not interfere with most experiments as these small additional resonances rarely result in additional spectral overlap [51].

3.1.3. Isoleucine-γ2

The isoleucine-γ2 methyl groups can be labeled with $^{13}CH_3$ groups using ^{13}C-labeled pyruvate as the sole carbon source in a growth medium that is based on D_2O [52]. In that case, the methyl groups of leucine, valine and isoleucine (γ2) are labeled to ~70%, while the methyl groups in alanine residues are labeled to approximately 40%. One significant drawback of this approach is that partial H-D-exchange at methyl groups results in a mixture of four isotopomeric forms (CH_3, CH_2D, CHD_2 and CD_3) of the methyl group. This complicates the NMR spectra that are obtained, or will result in significant sensitivity losses when specific isotopomers are selected spectroscopically.

Homogeneous labeling of γ2-methyl groups can be achieved by addition of the isoleucine precursor 2-hydroxy-2-ethyl-3-ketobutyrate-4-^{13}C to the growth medium (Fig. 4, Table 1) [53,54]. The precursor can be commercially obtained in its significantly more stable ethyl ester form. Prior to the addition of the precursor to the growth medium it needs to be de-esterified enzymatically or by base treatment [53]. Alternatively, the precursor can be synthesized and stored frozen until usage [54]. Since the precursor is a racemic mixture, only half of the precursor material is utilized by the *E. coli* enzymes. Unexpected scrambling of methyl groups from 2-hydroxy-2-ethyl-3-oxo-butyrate into *proR*-methyls groups of valine and leucine has been observed [53,54].

3.1.4. Leucine-δ1/δ2 and Valine-γ1/γ2

Leucine and valine share a highly overlapping biosynthesis pathway (Fig. 4), where the last common precursor is α-ketoisovalerate (3-methyl-2-oxobutanoate, 2-oxoisovalerate; Table 1) that simultaneously labels leucine and valine residues [55]. The CH_3-CH-CH_3 isopropyl group of the precursor will be incorporated into the isopropyl groups of leucine and valine residues and the labeling of α-ketoisovalerate thus directly determines the labeling in the protein.

Methyl-only ^{13}C-labeled α-ketoisovalerate can be used to ensure that the two leucine and valine methyl groups form isolated spin systems [47,56]. As with isoleucine labeling, this ensures that high resolution two-dimensional proton-carbon correlations can be recorded that do not suffer from carbon-carbon J-couplings. To reduce the proton density and thus the T_2 relaxation rates, the CH proton in α-ketoisovalerate can be replaced by a deuterium. This is conveniently achieved by dissolving the protonated precursor in D_2O at high pH and elevated temperature [48].

The protons of the two methyl groups in the isopropyl moiety are only 2.5 Å apart. Protons in one methyl group thus contribute significantly to the relaxation rates in the other methyl group. These effects can be prevented with the use of α-ketoisovalerate that is randomly fully protonated in one of the two methyl groups and fully deuterated in the other. Use of this form of the precursor results in a non-stereospecific incorporation of $^{13}CH_3$ and $^{12}CD_3$ methyl groups into leucine and valine side chains. Although this results in a protein where only 50% the methyl groups are $^{13}CH_3$-labeled, for larger complexes the spectra will be of superior quality [57–59].

3.1.5. Stereo-specific labeling of Leucine-δ1, Valine-γ1, Leucine-δ2 or Valine-γ2

Spectral overlap in the leucine/valine region of a ^{1}H-^{13}C correlation spectrum increases significantly with increasing molecular complexity. In that case, it is advantageous to stereo-specifically label only one of the two isopropyl methyl groups in leucine and valine residues. Specific labeling of *pro-(S)* (δ2/γ2) methyl groups is possible based on 2-acetolactate (2-Hydroxy-2-methyl-3-oxobutanoate; Table 1) as the methyl group attached to the C2 carbon (italic in Fig. 4) ends up as the *pro-(S)* methyl group, whereas the C4 methyl moiety is incorporated into the *pro-(R)* methyl group [60]. The chemically more stable ethyl ester form of this precursor (Ethyl-2-hydroxy-2-methyl-3-oxobutanoate) is commercially available and can be de-esterified at high pH prior to usage. Alternatively, it has been shown that stereo-specific $^{13}CH_3$-labeling of one of the leucine and/or valine methyl groups can be achieved by the direct addition of these synthesized and stereo-specifically labeled amino acids to the minimal growth medium [61]. This latter method offers the possibility for the simultaneous labeling of valine-γ1 and leucine-δ2 or valine-γ2 and leucine-δ1 methyl groups.

3.1.6. Leucine- or Valine-specific methyl labeling

The resonances of the methyl groups of leucine and valine residues in part share a common spectral region (Fig. 5A). For large molecular assemblies that contain many unique leucine and valine residues it might thus be desirable to label either only leucine or only valine residues.

To label solely leucine residues, α-ketoisocaproate (4-methyl-2-oxopentanoate, 2-oxoisocaproate) can be used (Fig. 4, Table 1), which is suited for large complexes when the methyl groups in the precursor are randomly $^{13}CH_3/^{12}CD_3$-labeled [62]. To specifically label valine residues only, NMR-active α-ketoisovalerate or 2-(*S*)-acetolactate can be used in combination with (deuterated) α-ketoisocaproate (Table 1). In that manner, the leucine biosynthesis pathway is saturated with an NMR-inactive compound while the NMR-active precursor can be fully incorporated into valine residues [63]. Alternatively, the leucine pathway can be inhibited by the direct addition of (deuterated) leucine to the growth medium.

An alternative strategy for valine-specific methyl labeling is the use of an *E. coli* strain that lacks the dihydro-acid dehydratase and 3-isopropylmalate dehydrogenase enzymes (ΔilvD and ΔleuB, respectively) [64]. In this background, the biosynthesis of isoleucine from α-ketobutyrate and the biosynthesis of leucine from α-ketoisovalerate are blocked (Fig. 4). Growth medium that is supplemented with α-ketoisovalerate, (perdeuterated) leucine and isoleucine then results in labeling of valine methyl groups only (Table 1). Likewise, deletion of the ilvB, ilvG, ilvI genes inhibits the acetolactate synthase pathway and interferes with leucine/valine and isoleucine biosynthesis. In this background, (labeled) isoleucine or 2-hydroxy-2-ethyl-3-ketobutyrate must be added for isoleucine production and α-ketoisovalerate or acetolactate are required to produce leucine and valine [65] (Table 1). Finally, deletion of the leuB gene has been used to specifically label valine residues [65]. An advantage of these auxotrophic expression strains is that reduced amounts of the labeled amino acids/ precursors are required to achieve full label incorporation [64].

3.1.7. Alanine-β

Alanine is one of the most abundant amino acids [38] and is found both in protein cores and on surfaces [66]. The short alanine side chain provides the advantage that motions in the methyl group are correlated with motions of the backbone. Optimal spectral resolution can be achieved when the incorporated alanine is deuterated at the Cα-position and carbon-labeled only at the Cβ-position.

Within the cell, alanine is readily metabolized into pyruvate, a central metabolite in many biosynthesis pathways (Fig. 4). Supplementing the *E. coli* growth medium with NMR-active alanine therefore results in significant isotope scrambling. To prevent this, the minimal growth medium can be supplemented with the other 19 amino acids in their NMR-inactive forms [67]. Due to the high costs

Please cite this article as: S. Schütz and R. Sprangers, Methyl TROSY spectroscopy: A versatile NMR approach to study challenging biological systems, Progress in Nuclear Magnetic Resonance Spectroscopy, https://doi.org/10.1016/j.pnmrs.2019.09.004

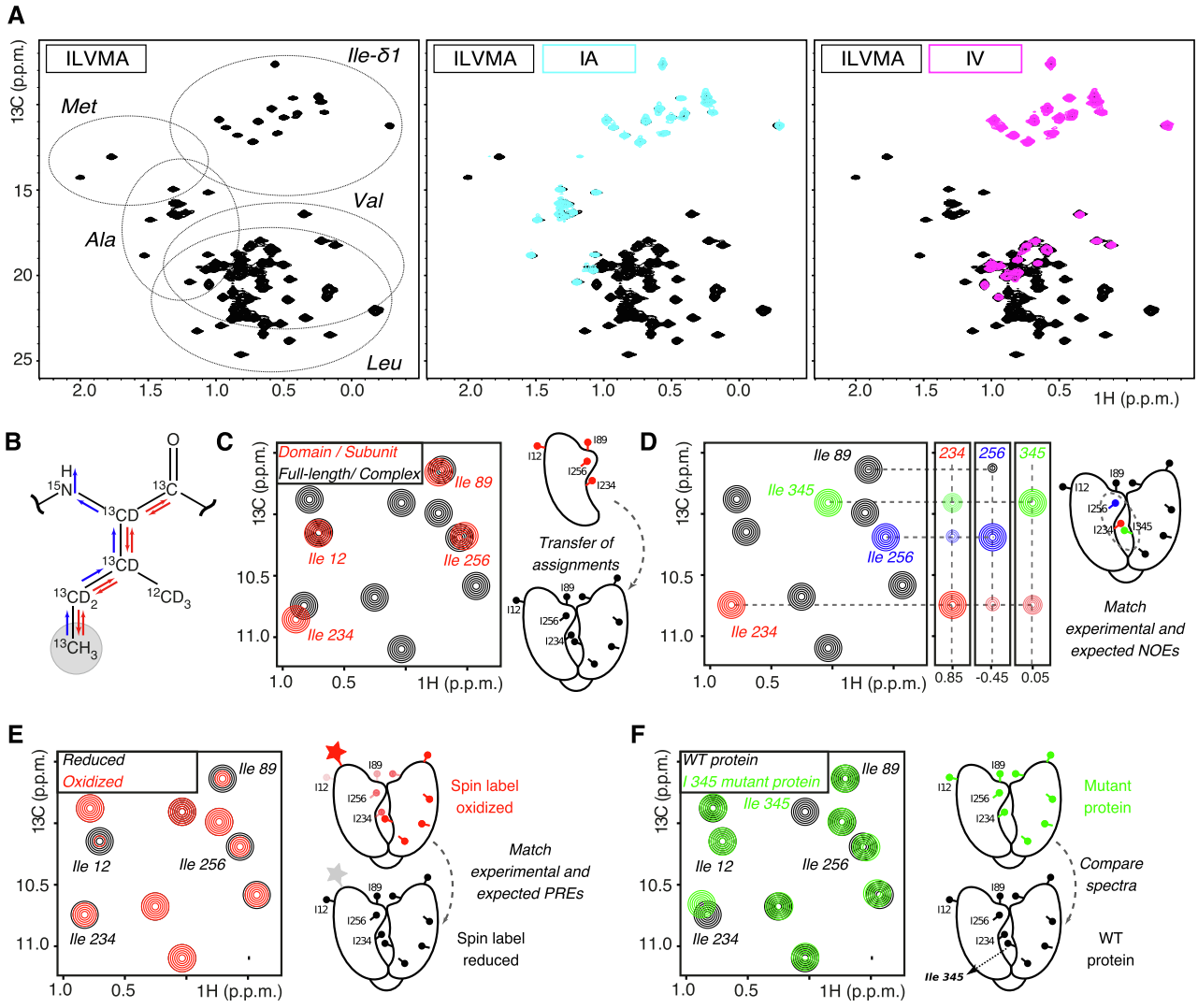

Fig. 5. Methyl group assignment strategies. A: In an ILVMA-labeled methyl TROSY spectrum (black), the individual amino acid types can be identified based on samples that are NMR-active only in IA (cyan, middle) or IV (magenta, right) methyl groups. Note the significant overlap in the chemical shift ranges of methyl resonances from alanine and valine residues and from valine and leucine residues. In the IA-labeled sample, the scrambling of methyl groups from alanine to leucine and valine was suppressed by the addition of NMR-inactive α-ketoisovalerate (Table 1). In IV-labeled samples, the scrambling of the labeled α-ketoisovalerate precursor into leucine was suppressed by the addition of NMR-inactive α-ketoisocaproate (Table 1). B: Assignment of methyl resonances is possible through the transfer of methyl group magnetization to the protein backbone (blue arrows). Alternatively, "out-and-back" experiments (red arrows) can be used to correlate methyl group resonances with a subset of side chain resonances. C: Schematic representation of the divide-and-conquer approach. The resonances from a representative smaller part of the complex (red) can be assigned; these assignments can subsequently be transferred to the full assembly (black resonances). Note that some resonances can shift between the smaller part and the full assembly, as indicated for e.g. residue 234. Provided such shift changes are small relative to the dispersion of the other signals, the approach can still give unambiguous results. D: Schematic representation of the structure-based assignment of methyl resonances. The measured NOE intensities (experimental distances) are matched with known distances from a three- dimensional structure. The displayed "strips" represent data from a C-C-H NOESY experiment. E: Schematic representation of PRE-assisted assignment of methyl groups. A spin label is attached to the protein based on the known structure. The experimental PREs are subsequently matched with distances that are known from the structure; the weaker the signal in the oxidized spectrum (relative to the corresponding signal in the control, i.e. reduced, spectrum), the shorter the distance between the methyl group and the spin label. F: Schematic representation of the assignment of a methyl resonance (isoleucine 345) based on mutagenesis. The HMQC spectra of the WT (black) and mutant (green) proteins are compared. The resonance of isoleucine 345 is absent in the mutant spectrum. Note the additional chemical shift perturbations (e.g. in isoleucine 234) in the mutant protein that are due to slight changes of the local structure. In some cases, these changes can be of such an extent that an unambiguous assignment is not possible.

of deuterated amino acids this approach is not suitable for the large-scale production of perdeuterated proteins. As an alternative, perdeuterated rich medium that is supplemented with methyl-labeled alanine has been used. However, this approach suffers from low incorporation levels due to the presence of NMR-inactive alanine in the growth medium [68]. Currently, the most cost-efficient way to prevent metabolic scrambling from [*methyl*-^{13}C]-2-^{2}H-alanine into other methyl groups is by the simultaneous addition of α-ketoisovalerate, succinate, and isoleucine (e.g. in a deuterated form) to the D_2O-based M9 minimal growth medium (Table 1) [69].

3.1.8. Threonine-γ2

Compared with other methyl-containing amino acids, threonine has a high propensity to be found on protein surfaces and at nucleotide binding sites, which is due to its capability to form side chain hydrogen bonds [66,70]. Unfortunately, labeling of threonine is challenging due to many crosslinks between the biosynthesis pathways of threonine and other amino acids (Fig. 4). First attempts to methyl-label threonine residues were based on the use of [2-^{13}C]-glycerol as a carbon source [71] This strategy suffers from low labeling efficiency, severe isotope scrambling even in the presence of supplemented alanine, isoleucine, methionine, lysine

Please cite this article as: S. Schütz and R. Sprangers, Methyl TROSY spectroscopy: A versatile NMR approach to study challenging biological systems, Progress in Nuclear Magnetic Resonance Spectroscopy, https://doi.org/10.1016/j.pnmrs.2019.09.004

and α-ketoisovalerate and the formation of the $^{13}CHD_2$ isotopomer when the growth medium is based on D_2O.

Since the production of U-[^{2}H]-[*methyl*-$^{13}CH_3$] threonine has been established, the amino acid can be added directly to the growth medium [72]. To prevent scrambling of NMR-active nuclei into isoleucine residues, the growth medium needs to be further supplemented with α-ketobutyrate, whereas the degradation of the added threonine into acetyl-CoA and glycine can be inhibited by the addition of perdeuterated glycine (Table 1). Alternatively, undesired conversion of supplemented threonine can be circumvented by use of a Thr-auxotrophic expression strain (ΔthrC) [73], which also enhances the incorporation efficiency into the over-expressed protein (Table 1) [65].

3.1.9. Combinatorial labeling of methyl groups

To increase the information content in NMR spectra, it is often desirable to label several methyl-containing amino acids at the same time. Most of the methyl labeling schemes described above can be combined and the simultaneous labeling of all methyl-bearing amino acids (ILVMAT) is feasible [73,74]. In the authors' laboratory, we routinely exploit IM-labeling, especially of very large protein complexes where the proton density should be reduced to a minimum [75]. For intermediate sized complexes, we have good experience with ILVM- and ILVMA-labeling [51]. This latter scheme is convenient as the scrambling of alanine methyl groups into other sites in the protein is efficiently inhibited by the NMR-active LV precursor α-ketoisovalerate. For the combinatorial IA-labeling we routinely use the "standard" isoleucine precursor α-ketobutyrate instead of 2-hydroxy-2-ethyl-3-ketobutyrate [49], as isotope scrambling from alanine into isoleucine-γ2 groups is in practice low and the additional signals usually do not interfere with the spectral analysis (Table 1).

3.2. Cell-based protein expression in eukaryotes

The labeling strategies discussed so far rely on *E. coli* as the expression host. The main advantages for the use of bacteria as expression systems are their short generation cycles, their ability to grow in perdeuterated minimal media, the relatively low costs, even for labeled cultures, and their well-understood biochemical pathways. As a result, the vast majority of (methyl-labeled) NMR samples have been prepared by over-expression of the protein in *E. coli*. Nevertheless, simple bacterial expression hosts have their shortcomings, as they lack sophisticated chaperones and a machinery that can perform (essential) post-translational modifications, and more advanced expression host might be required.

3.2.1. Yeast

A widely used eukaryotic expression host for the large-scale production of ^{13}C- and ^{15}N-labeled proteins is the yeast species *Pichia pastoris* [76,77], where protein expression is controlled by the *AOX1* (alcohol oxidase 1) promotor that can be induced with methanol. Importantly, protein deuteration to levels of around 80%, which are required for efficient methyl TROSY NMR spectroscopy, is possible [77]. The labeling of Ile-δ1 methyl groups [78,79] has been successfully achieved by supplementing the growth medium with α-ketobutyrate (see above), although with incorporation levels that are only around 50%. On the other hand, methyl group labeling in leucine and valine residues through addition of α-ketoisovalerate appears to be more challenging as the incorporation levels are below 5%, indicating that further optimization is required. The production of deuterated and methyl-labeled proteins has also been established in *Kluyveromyces lactis* [80,81], where protein expression is controlled by the *LAC4* promotor that can be induced with galactose, comparable to protein over-expression in *E. coli*. The isotope incorporation rates reach 95% in medium that contains ^{13}C-glucose and ^{15}N-ammonium chloride [45] and perdeuteration of proteins has been reported [81]. The labeling of methyl groups using D_2O-based growth medium supplemented with α-ketobutyrate and α-ketoisovalerate results in methyl-specific labeling of the isoleucine residues with 60–70% efficiency. The labeling efficiency of leucine and valine residues is on the order of a few percent but can be enhanced by the addition of labeled valine to the growth medium. Current efforts actively pursue the optimization of these methyl labeling strategies [82] and will ensure that in the future the production of highly deuterated, methyl-labeled samples can be routinely performed in yeast.

3.2.2. Insect cells

Baculovirus-infected Sf9 insect cells are not capable of growing on minimal media that contain only one carbon and one nitrogen source, as 10 out of the 20 proteinogenic amino acids are essential. To label proteins with NMR-active nuclei, amino acids in rich expression media can be replaced by NMR-active ones [83]. The labeling efficiencies are, however, low as the supplemented labeled amino acids are diluted with unlabeled metabolites from essential growth supplements [84]. To overcome these challenges, defined minimal growth media that do not require yeast extract have been developed [85]. These have resulted in the incorporation of the essential amino acids phenylalanine, tyrosine and valine with 90% efficiency and in uniform ^{15}N- and ^{13}C/^{15}N-labeling [86–88]. To improve low expression yield in the absence of yeast extract without reducing the incorporation of specific amino acids, more sophisticated growth protocols and media compositions have been developed [89]. Recent advances have shown that methionine labeling in insect cells is also possible in combination with partial deuteration [90–92]. The latter is achieved by supplementing the expression medium with a subset of (partially) deuterated amino acids, deuterated algal extract and deuterated, methyl-labeled methionine. This tour-de-force approach resulted in considerable signal-to-noise gains compared to the protonated form of the complex. Interestingly, the labeling of alanine residues with 45% efficiency has also been achieved in insect cells when the interconversion of alanine to pyruvate has been inhibited with the transaminase inhibitor β-chloro-l-alanine [93]. Finally, it has been shown that the production of uniformly labeled, deuterated proteins in insect cells is more economical when the medium is supplemented with ^{2}H, ^{13}C, ^{15}N-labeled protein hydrolysate from *Pichia pastoris* [94] or algal amino acid extracts [95].

3.2.3. Mammalian cells

A major drawback of protein labeling and expression in higher eukaryotic cells is their inability to grow or even survive in perdeuterated media [96–98]. Therefore, mammalian cells have, so far, not been successfully used to produce deuterated, ^{13}C-methyl-labeled proteins for the application of methyl TROSY NMR. Nevertheless, recent advances in labeling schemes in mammalian cells provide first insights into the future applicability for the production of specifically NMR-active protein complexes. As an example, amino acid-type specific labeling [99] as well as uniform ^{13}C/^{15}N-labeling in Chinese hamster ovary (CHO) cells have been reported [100]. In addition, partial deuteration has been achieved based on the use of partially deuterated amino acids [101]. As with expression systems based on insect cells, methionine labeling can be accomplished by addition of the methyl-labeled amino acid to the mammalian expression medium [102].

3.3. Cell-free protein expression

Cell-free protein expression systems have been developed to facilitate the production of difficult (e.g. toxic or unstable) target proteins for NMR spectroscopy [103]. Recent improvements of

the cell-free expression systems now allow the production of milligrams of labeled target protein from as little as a milliliter of reaction mixture [104–106]. An advantage of open cell-free expression systems is that cofactors, chaperones or (deuterated) membrane mimetics can be added to the reaction chamber [107]. This is especially useful for membrane proteins that can then directly fold in the presence of a suitable detergent, without the need for post-translational re-solubilization of the protein [108,109]. In the cell-free expression setup, both uniform and amino acid-type selective labeling are feasible, by adding either all or a subset of the amino acids in a labeled form [103–105,110]. The metabolic turnover rates are reduced to a minimum in a cell-free expression system and the labeling of single amino acids, which can be challenging *in vivo* due to label scrambling, becomes readily feasible. As a prerequisite for methyl TROSY NMR spectroscopy, perdeuteration of the target protein is possible in cell-free expression systems by supplementing amino acids in their deuterated form [105,111], eventually accompanied by deuteration of the cell extract [112]. Based on this, cell-free expression can produce samples that result in high-quality NMR spectra of membrane proteins [113] and high molecular weight complexes [112]. The stereo-array isotope labeling (SAIL) approach makes use of the cell-free expression system in an unprecedented manner [114]. Here, every single amino acid is added in a deliberately labeled form. Thereby, protein labeling is optimized with regard to NMR-based structure calculations and relaxation [115]. This approach can thus be expected to facilitate the preparation of high-quality protein samples for methyl TROSY-based techniques [116]. An interesting approach in cell-free expression is to use crude amino acid mixtures that already contain the desired labeling pattern. In this manner, the labeling scheme from *E. coli* proteins can be directly transferred to the cell-free-expressed target protein [117].

3.4. Partial isotope labeling

In all the approaches discussed above, isotope labeling is introduced throughout the sequence of the full-length protein. For large, single-chain proteins or for large asymmetric multi-subunit complexes, the large number of unique methyl groups will result in significant spectral overlap. To overcome these limitations, NMR isotope labeling can be restricted to a part of the protein (complex). Two of these approaches are segmental isotope labeling and LEGO NMR.

All segmental isotope labeling approaches rely on the ligation of two or more protein fragments that are differentially labeled. The proteins that are thereby produced can, for instance, be NMR-active in only a part of the polypeptide chain, whereas the remaining part remains NMR-invisible. One successfully exploited method for the ligation of two protein fragments relies on an intein [118–121] or a so-called split intein reaction [122]. This ligation reaction can take place either *in vitro* after separate purification of the two fragments or *in vivo* after sequential expression of the two constructs within one cell [123,124]. Alternatively, segmental isotope labeling can be realized based on the sortase A enzyme that catalyzes an *in vitro* transpeptidation reaction [125–130]. It should be noted that the intein- and sortase-based ligation approaches depend on the presence of (short) specific amino acid sequences at the ligation site. In addition, it is required that both fragments are stable in isolation. These two considerations determine where the potential ligation sites are within a protein chain. Based on protein ligation methods, it is thus now possible to ligate a (smaller) methyl labeled fragment to a (larger and fully deuterated) protein. The resulting methyl TROSY NMR spectra will then contain signals from only the portion of the protein that is NMR-active.

The LEGO NMR approach is designed to prepare large and asymmetric protein complexes that are NMR-active in only a subset of the subunits [131]. This method is designed for protein complexes that cannot be reconstituted *in vitro* from individually expressed and purified proteins. In brief, the LEGO NMR approach exploits the sequential expression of differentially labeled and unlabeled subunits of a complex. These two parts of the final complex then spontaneously assemble within the (*E. coli*) expression system and can subsequently be purified in a straightforward manner.

3.5. Post-translational isotope labeling

The labeling strategies discussed above rely on the introduction of the NMR-active isotopes during protein expression. Alternatively, it is possible to add methyl groups to specific sites in (purified) proteins in a post-translational manner, which circumvents limitations with the expression of NMR-active proteins. To that end, methionine, lysine and cysteine residues have been successfully used. The, in part, harsh chemical conditions that are required might render these approaches inadequate for the labeling of marginally stable proteins.

3.5.1. Methionine

First attempts to use methionine methyl groups as probes for NMR spectroscopy date back to the late 1980s. In these studies, an additional methyl group was attached to the sulfur atom of methionine residues by alkylation with ^{13}C-methyliodide. The S-[^{13}C]-methylmethionine that was obtained was subsequently reduced to arbitrarily remove one of the two methyl groups. This results in the formation of the protein with enriched labeling in methionine $^{13}CH_3$-methyl groups [132–135].

3.5.2. Lysine

Lysine residues are prominent sites for post-translational modifications, and many cellular proteins contain methylated lysine residues. *In vitro*, a near complete methylation of the ε-amino group can be achieved by reductive alkylation in the presence of a mild reducing agent using formaldehyde as a methyl donor [136,137]. The reaction conditions can be adjusted to favor either mono- or dimethylation [138,139]. The degeneracy within dimethylated lysine residues can thereby improve the signal-to-noise ratio. This approach can be complemented based on lysine-methyltransferases that use S-adenosyl-methionine (SAM) as a methyl donor to selectively catalyze mono-, di- or trimethylation reactions [140]. The applicability of lysine methylation has been demonstrated in a variety of NMR studies [141–148].

3.5.3. Cysteine

To attach NMR-active methyl groups to the reactive thiol group in cysteine residues, the protein can be incubated with ^{13}C-labeled MMTS (methyl-methanethiosulfonate), which results in the formation of S-methylthiocysteine (MTC) [149]. Interestingly, this approach appears to work well for large proteins in a protonated background [150], as the introduced label is surface exposed and thus remote from protons in the protein.

One important advantage of the methyl groups that are introduced on lysine or cysteine residues is that these groups have highly specific chemical shifts. This makes the resulting resonances easily identifiable, even in a background that contains other NMR-active methyl groups.

4. Assignment of methyl group chemical shifts

The assignment of methyl resonances to specific methyl groups in the protein is a prerequisite for the analysis of NMR data with high spatial resolution. For methyl groups in large complexes, this process can be time-consuming and challenging, especially when

Please cite this article as: S. Schütz and R. Sprangers, Methyl TROSY spectroscopy: A versatile NMR approach to study challenging biological systems, Progress in Nuclear Magnetic Resonance Spectroscopy, https://doi.org/10.1016/j.pnmrs.2019.09.004

traditional methyl resonance assignment strategies, which rely on assigned backbone resonances, fail. Here, we discuss some of the assignment strategies that have proven to be successful.

4.1. Assignment of the residue type

The methyl chemical shifts of most residue types localize to specific spectral regions (Fig. 5A). Partial overlap of those regions, however, can prevent the unambiguous assignment of a resonance to a specific residue type. These assignment uncertainties can be resolved by preparing methyl-labeled samples that only contain a subset of the NMR-active residues. As an example, based on an IA-labeled sample and an IV-labeled sample it is possible to unambiguously link all resonances from an ILVMA-labeled protein to specific residue types (Fig. 5A). Secondly, methyl resonances in a 2D methyl TROSY HMQC spectrum can be assigned to specific residues spectroscopically, based on unique non-methyl carbon resonances in the side chain. As an example, the differences in the typical chemical shifts of leucine C_β and valine C_α resonances can be used to identify if a methyl group resonance results from a leucine or a valine residue [151].

The assignment of the two methyl resonances in valine and leucine residues to the *pro-(R)* ($\gamma1/\delta1$) and *pro-(S)* ($\gamma2/\delta2$) positions is possible by differential carbon-labeling of these sites. First, this can be achieved through the use of a mixture of 10% $^{13}C_6$- and 90% $^{12}C_6$-glucose [45,152–155]. Due to the metabolic pathways in *E. coli*, this results in samples that are only labeled to 10%. However, the NMR-active *pro-(R)* groups will always have an NMR-active neighboring carbon atom, whereas the NMR-active *pro-(S)* groups will have a neighboring carbon that is most likely NMR-inactive. Based on the presence or absence of one-bond C_{methyl}-C J-couplings, it is thus possible to assign methyl groups to *pro-(R)* or *pro-(S)* groups. Experimentally, this is possible for instance with the use of constant-time HSQC spectra, where methyl groups that have an NMR-active carbon neighbor will have a phase that is opposite to the methyl groups that lack an NMR-active carbon neighbor. Secondly, it is possible to use 100% $^{13}C_6$-glucose and sub-saturating (66%) amounts of 2-[^{13}C]-methyl-acetolactate [156]. In that case, the *pro-(R)* groups are ^{13}C-labeled to 33% and always have an NMR-active neighboring carbon, whereas the *pro-(S)* groups have an NMR-active carbon neighbor in 33% of the cases and an NMR-inactive carbon neighbor in 66% of the cases. As a result, the *pro-(R)* and *pro-(S)* groups both arise with 33% of the maximum intensity in CT HSQC spectra, but with opposite signs and can thus be differentiated in a straightforward manner. Alternatively, *pro-(S)* groups can be selectively labeled directly based on the appropriate precursors [60] (see Table 1 and above).

4.2. Methyl assignment via through-bond correlations

For smaller proteins that are up to approximately 50 kDa, it is possible to assign protein backbone resonances through traditional methods. Based on this assignment, methyl groups can be correlated to the specific residues based on TOCSY approaches [157]. Due to fast signal relaxation processes, this TOCSY approach will fail for larger proteins, and in those cases full deuteration and special methyl labeling schemes are required to link methyl groups to the protein backbone [45,158]. In one such approach, the losses that occur during the TOSCY transfer times are prevented by using COSY-type magnetization transfer steps as this ensures that magnetization from the methyl groups is solely transferred to a limited number of side chain and/ or backbone nuclei [159] (Fig. 5B). These experiments benefit from labeling schemes that result in "linearized" spin systems in leucine and valine residues, for example through the use of $^{13}CH_3/^{12}CD_3$-labeled precursors [57]. Alternatively, more sensitive methyl-detected "out-and-back" experiments have been introduced, where the methyl resonances are correlated with a number of side chain carbon atoms (Fig. 5B). To simultaneously record spectra for methyl-bearing side chains of different length, a SIM-HMCM(CGCBCA)CO experiment has been developed [160]. Alternatively, one can record a set of experiments where the magnetization is transferred to a single carbon atom that is either one, two or three bonds remote from the methyl group [161]. It has been shown that complete backbone and ILV methyl group assignments can be obtained with a single NMR sample, which significantly reduces the experimental costs [162].

These methyl-detected "out-and-back" strategies have been extended to facilitate the assignment of alanine methyl group resonances through a 4D HMCMCACO-type experiment [163]. In addition, it has been shown that alanine and isoleucine-$\gamma2$ methyl groups can be simultaneously assigned [164], where the isoleucine spin system is "linearized" with the use of selective pulses. Finally, threonine-$\gamma2$ and alanine methyl groups can be assigned through a strategy that exploits the spectroscopic selection of $^{13}CHD_2$ isotopomers that are present in proteins that have been grown in a D_2O-based medium containing protonated glucose [52,165].

The assignment of methionine methyl resonances by spectroscopic through-bond methods is very challenging as the methyl group is an isolated spin system. Only for low molecular weight proteins (up to 20 kDa) is it possible to exploit small long-range ^{13}C-^{13}C and ^{1}H-^{13}C J-couplings to link the methyl group to the rest of the side chain [166].

4.3. Divide-and-conquer

For most proteins that have a molecular weight over 50 kDa, the assignment of the backbone becomes challenging [167]. In the divide-and-conquer approach, a large molecular complex or multi-domain protein is dissected into smaller building blocks that are amenable to standard assignment experiments (Fig. 5C). When the fold of the building blocks is the same in isolation and in the intact complex, it is possible to transfer the assignments from the small part onto the larger assembly. This strategy has turned out to be useful for e.g. symmetric multi-subunit assemblies, in case the individual subunits can be prepared in a monomeric form [17]. Changes in the chemical shifts between the monomer and the fully assembled complex are often limited, especially in the core of the protein building block. In addition, the divide-and-conquer approach has been successfully applied to complexes that contain more than one unique subunit [168] and to large multi-domain proteins where domains can be purified in isolation [44,75,169,170]. The transferred assignments can be independently confirmed based on the comparison of the chemical shifts of additional carbon atoms in the side chains or based on NOESY or mutagenesis experiments (see below).

4.4. Assignment based on NOEs

Even for very large complexes, it is possible to record methyl-methyl NOE contacts with high sensitivity [17]. These spectra provide information about resonances of methyl groups that are close (<5–10 Å) in space (Fig. 5D). These data can validate or suggest assignments when high-resolution structural information of the complex is available, as experimental NOE cross-peak patterns can be compared with known distances. Experimentally, NOEs between methyl groups are readily obtained with the use of 3D HMQC-NOESY [171] or 4D HMQC-NOESY-HMQC [172,173] experiments, which can be combined with SOFAST approaches [174]. Due to the lower dispersion of the proton chemical shifts in methyl groups, H-C-H correlations are usually less informative than C-C-H correlations. The recent development of non-uniform sampling

Please cite this article as: S. Schütz and R. Sprangers, Methyl TROSY spectroscopy: A versatile NMR approach to study challenging biological systems, Progress in Nuclear Magnetic Resonance Spectroscopy, https://doi.org/10.1016/j.pnmrs.2019.09.004

(NUS)-based experiments [175,176] allows for the relatively fast recording of 4D H-C-C-H correlations that provide unambiguous information on methyl groups that are close in space [177].

4.5. Assignment with paramagnetic probes

When high-resolution structural data of the protein under investigation are available, it is possible to derive assignments based on paramagnetic centers that are introduced to specific sites on the protein (Fig. 5E). These sites can be introduced to the protein either through linkage of a tag to one [178,179] or two cysteine residues [180], or through binding of a specific metal ion to a lanthanide binding peptide tag [181–184], a double His-motif [185] or a naturally occurring metal binding site [186–188]. Experimentally determined pseudo-contact shifts (PCS) and paramagnetic relaxation enhancement (PRE) rates can then be compared to back-calculated parameters. By placing the tags at different sites on the protein, it is possible to obtain near complete resonance assignments [179,189]. The success of this assignment method strongly depends on the number of tagged sites and on the ability to take potential motions of the spin label into account during the back-calculation of the data.

4.6. Methyl assignment via site-directed mutagenesis

For very large and challenging protein complexes and for situations where structural information of sufficient quality is lacking, the assignment strategies mentioned above might not be suitable. In those cases, a limited or full methyl group assignment can be obtained through a mutagenesis approach (Fig. 5F). In this approach, a methyl-bearing residue of interest is mutated into a closely related amino acid (e.g. isoleucine to valine), without distorting the fold of the protein. Methyl TROSY spectra are subsequently recorded for the wild-type and for the mutant protein [190]. In the ideal case, both spectra are identical apart from one (alanine, methionine, threonine, isoleucine) or two (valine, leucine) resonances that are absent in the spectrum of the mutated protein. These resonance(s) then correspond to the methyl group(s) of the mutated residue. To prevent the appearance of additional methyl group resonances due to the introduced assignment mutation (e.g. in the isoleucine to valine mutant example above) it is beneficial to refrain from labeling the amino acid type that is introduced. In practice, the assignment procedure can be complicated if the introduced mutation results in severe chemical shift perturbations of other resonances so that the peak reporting on the mutation can no longer be unambiguously identified [17]. In such a case, it might be necessary to record spectra for a large number of individual mutations to be able to distinguish between primary and secondary chemical shift changes [191]. In practice, the mutagenesis approach has proven to be a successful means for obtaining methyl group assignments of large complexes [75,191–193]. This is especially true in cases where a full resonance assignment is not required and where, based on prior data, it is possible to identify a specific region of the protein that is of (biological) interest.

4.7. Chemical shift prediction

Based on knowledge of the protein structure, it is theoretically possible to predict the chemical shift of (methyl group) resonances. However, despite numerous efforts, chemical shift predictions of methyl groups are often unreliable, which is due to inaccuracies in the protein structure, dynamics within the protein and inaccuracies in the prediction algorithms. Future research on the prediction of side chain chemical shifts using CH3shift [194], PROSHIFT [195] and SHIFTX2 [196] will continue to improve the reliability of the method. Currently, the prediction algorithms are successfully used as a driving force within automatic assignment protocols (see below).

4.8. Automated methyl assignments

Automated strategies try to facilitate the tedious processes that accompany the methyl group assignment process. These programs use experimental NMR data and a protein structure as input and ideally result in a complete and reliable assignment of all methyl group resonances. The programs MAP-XS [197,198] and FLAMEnGO [199,200] use a swapping procedure to reach convergence between measured and predicted NOEs. Both programs can include additional data such as PREs, RDCs, and PCS as well as assignments from mutagenesis or chemical shift predictions. The programs MAGMA [201] and MAGIC [202] exploit graph theory to correlate experimental and back-calculated NOE patterns. In the experience of the authors' group, the latter program is able to suggest reasonable methyl group assignments for intermediate sized proteins that have labeled methyl groups in isoleucine, leucine, valine, alanine and methionine residues. It is, however, necessary to confirm experimentally at least a number of the computationally obtained assignments, which can be done with a limited number of assignment mutants.

5. HMQC-based experiments

Based on (assigned) methyl TROSY spectra, it is possible to obtain information regarding biomolecular interactions [19], dynamics and structure. These aspects will be discussed in more detail below.

5.1. Interactions

Biomolecular interactions can be conveniently and quantitatively studied using chemical shift perturbations (CSPs) in methyl TROSY spectra. An advantage for the study of interactions based on methyl groups is that protein binding sites are often enriched in hydrophobic, methyl-bearing amino acids [203]. At the same time, complex formation often results in methyl group CSPs that are smaller compared to those observed in proton-nitrogen spectra, which is most likely due to the intrinsic mobility of long methyl-containing side chains and the relatively small carbon chemical shift range of specific methyl groups, and the fact that amide group CSPs, unlike methyl group CSPs, are highly sensitive to changes in hydrogen-bonding.

5.1.1. Methionine scanning

A major drawback of methyl TROSY methods is that only parts of the protein are NMR-visible. As a result, the experiment is "blind" to protein regions that are devoid of methyl-bearing side chains. One way to overcome this bottleneck is through the introduction of methyl-containing residues at specific sites of interest [204]. This idea was extended in the methionine scanning approach where a large number of reporter methionine residues are, one at a time, introduced by mutation at solvent-exposed sites. The introduced methionine residues can be instantaneously assigned by the appearance of a new resonance in the NMR spectrum. Based on CSPs of the reporter resonance and on CSPs of naturally occurring methyl resonances, the site of interest can be classified as being part of the binding pocket, as being essential for binding or as being outside the binding pocket. The methionine scanning method has been successfully applied to study protein:protein [204,205] and large protein:RNA complexes [75]. In addition, the methionine scanning approach can also be exploited to determine dynamics at parts of the protein that contains no natu-

Please cite this article as: S. Schütz and R. Sprangers, Methyl TROSY spectroscopy: A versatile NMR approach to study challenging biological systems, Progress in Nuclear Magnetic Resonance Spectroscopy, https://doi.org/10.1016/j.pnmrs.2019.09.004

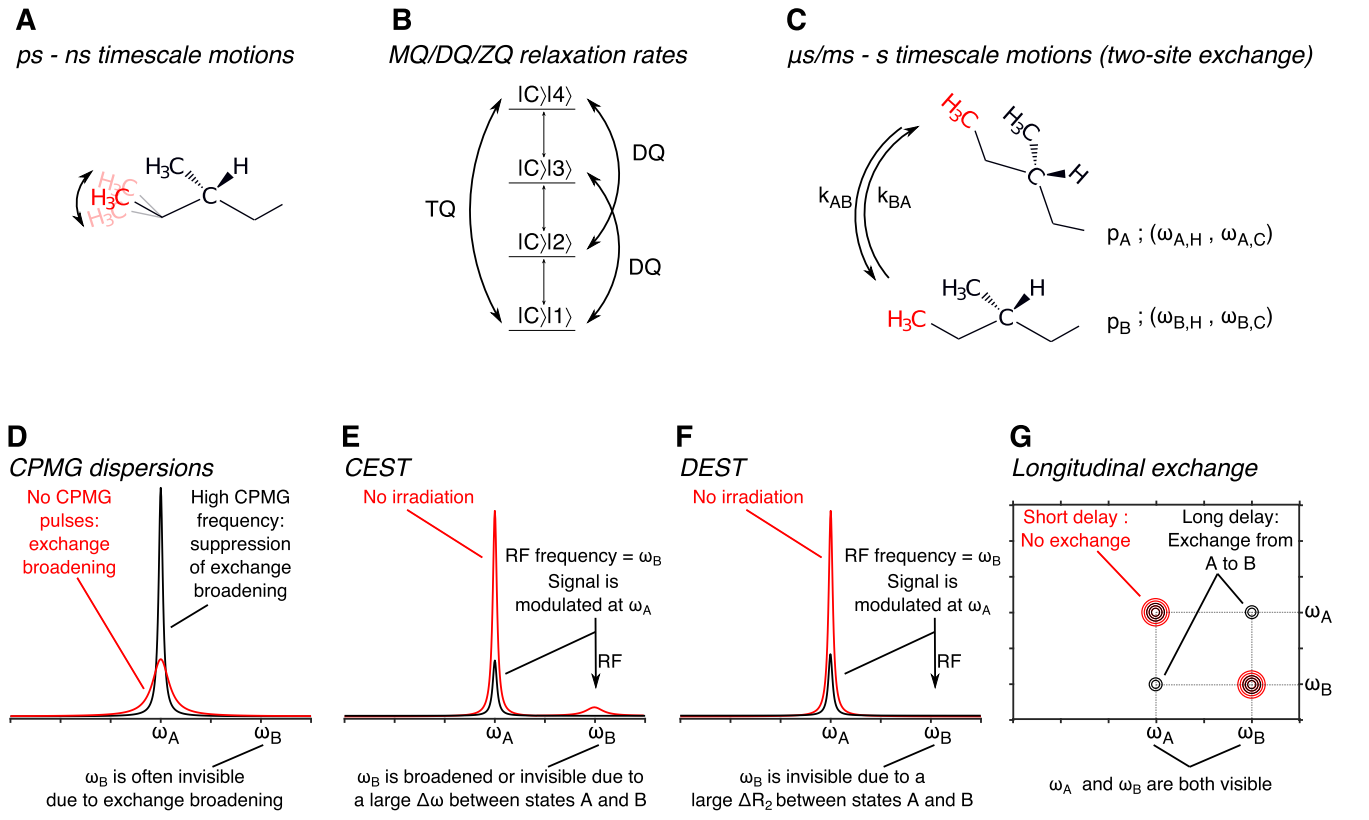

Fig. 6. Protein dynamics. A: Fast (ps-ns timescale) side chain motions can be described with a local order parameter. B: The measurement of DQ and TQ relaxation rates in methyl groups can be exploited to extract methyl group order parameters. C: Slower timescale motions (μs/ms to s timescales) can be described through an exchange process. In that process state A (with population p_A and chemical shifts $\omega_{A,H}$ and $\omega_{A,C}$) changes conformation into state B (p_B and chemical shifts $\omega_{B,H}$ and $\omega_{B,C}$) through the associated rates k_{AB} and k_{BA}. In reality, the exchange process and motional models can be more complicated (three-, four- or *n*- site exchange [331]). D: Schematic representation of the CPMG relaxation dispersion experiment. The exchange broadening of the resonance line of the visible major population p_A (red) is suppressed through the application of a π pulse train (black). Based on the experimentally determined dependence of the linewidth on the CPMG frequency, it is possible to extract information regarding p_A, p_B, $|\Delta\omega|$, k_{AB} and k_{BA}. Note that SQ, MQ and TQ CPMG experiments have different dependencies on $|\Delta\omega|$. E: Schematic representation of the CEST experiment. In case an RF field is applied at the frequency of a minor conformation that resonates at ω_B, this results in a decrease of the intensity of the signal at ω_A (black line). Based on the experimentally determined dependence of the intensity of the major resonances at ω_A on the intensity and frequency of the applied RF pulse, it is possible to extract information regarding p_A, p_B, $\Delta\omega$, k_{AB} and k_{BA}. F: Schematic representation of the DEST experiment. As in the CEST experiment, the resonance line of the major conformation (red) is modulated through the application of an RF field at the minor (black), invisible conformation. The resonance lines of the second conformation (p_B) are too broad to be observed directly (R_2 is too fast), but can be observed indirectly. G: Schematic representation of a longitudinal exchange experiment. During a variable mixing time the protein changes conformation. Depending on the length of the delay, the exchange rates and populations can be determined.

ral methyl groups. Especially for very large systems, it can be highly efficient to place a single methyl-containing group in a specific region of interest. In that light, methionine residues, as well as post-translationally modified cysteine residues (see above) provide the advantage of resulting in NMR spectra that do not suffer from extensive spectral overlap.

5.2. Dynamics

A unique aspect that NMR spectroscopy contributes to structural biology is its ability to study protein motions on timescales that range from pico-/ nanoseconds to hours or days [206]. These dynamics play a central role in processes that include protein folding, biomolecular interactions, enzyme catalysis and allostery. Based on methyl TROSY spectroscopy it is now possible to extract information regarding protein dynamics for complexes that are far over 100 kDa in molecular weight.

5.2.1. Pico- to nanosecond timescale motions

Biomolecules undergo numerous motions on the picosecond to nanosecond timescale that are associated with e.g. loop motions, rotameric jumps of side chains and the wobbling of side chains within one rotameric state (Fig. 6A). These motions are often described by an order parameter (S^2). For methyl group containing side chains, there exists a wide range of experiments that are able to quantify these fast timescale motions [207]. Many of those methods require the labeling of the methyl group as either $^{13}CHD_2$ [208–210] or $^{13}CH_2D$ [209,211–213] Here we will focus on those experiments that can be performed on $^{13}CH_3$ groups, as these samples are most routinely prepared during the studies of high molecular weight complexes. The experiments to extract $^{13}CH_3$ order parameters are complicated by dipolar cross-correlation mechanisms. To overcome this challenge, it is possible to select individual proton transitions in the NMR experiment such that semi-quantitative estimates of side chain mobility can be obtained [213].

5.2.1.1. MQ/DQ/ZQ relaxation rates. The MQ coherence in the HMQC experiment contains ZQ (zero quantum) and DQ (double quantum) terms that are interconverted by the central π proton pulse. The ZQ and DQ terms relax differently, which can be exploited to enhance spectral resolution beyond that in the HMQC experiment [214,215]. Within the $^{13}CH_3$ group a number of ^1H–^1H dipolar cross-correlation rates can be exploited to extract information regarding side chain motions. In particular, the determination of 'forbidden' DQ/TQ (triple quantum) transitions [216–218] provides a direct measure of the methyl group order parameter (Fig. 6B).

Please cite this article as: S. Schütz and R. Sprangers, Methyl TROSY spectroscopy: A versatile NMR approach to study challenging biological systems, Progress in Nuclear Magnetic Resonance Spectroscopy, https://doi.org/10.1016/j.pnmrs.2019.09.004

These approaches have been applied to a wide variety of systems to reveal detailed information on protein entropy and allostery [168,219,220] In addition, information regarding fast protein side chain motions can be extracted from ΔR_{MQ} (=R_{DQ}-R_{ZQ}) and R_{MQ} rates [215,221–223], as well as from the B_0 field-dependence of MQ relaxation rates [224,225]. A semi-quantitative measure of fast timescale dynamics of methyl groups can also be obtained straightforwardly from the analysis of peak intensities in HMQC and HSQC spectra [226].

5.2.2. Micro- to millisecond timescale motions

Biological processes often take place on the μs, ms or second timescale. When the exchange rates that are associated with these processes are slower than the chemical shift difference between two states (slow or intermediate exchange), these processes can be efficiently probed using NMR spectroscopic methods (Fig. 6C). The analysis of these motions is often based on the assumption that the exchange process involves two states. More complex exchange processes can be quantified; however, care needs to be taken that sufficient data are available to justify the analysis with models that have many more degrees of freedom [227,228].

5.2.2.1. CPMG relaxation dispersion experiments. Relaxation dispersion measurements (Fig. 6D) are ideally suited to study motions that take place on the ms timescale, a rate with which many enzymatic reactions take place. Relaxation dispersion experiments rely on the ability to suppress dephasing of magnetization that is caused by a chemical or conformational exchange process. For a two-state process (A ⇄ B), the data provide information regarding the rate of the exchange process (kinetics, $k_{ex} = k_{AB} + k_{BA}$) and the populations of both states (thermodynamics, p_A and p_B, where $p_B/p_A = k_{AB}/k_{BA}$). In addition, the magnitude of the chemical shift difference ($|\Delta\omega| = |\omega_B-\omega_A|$) between state A and state B can be derived [228,229]. Based on the state of the magnetization during the determination of the exchange process, the experiment is sensitive to the carbon or proton chemical shift difference or to a combination of these. Importantly, exchange parameters can also be derived when the second state is only very weakly populated and not directly observable in the NMR spectra. Recent technological advances allow for the application of very high CPMG frequencies (over 5 kHz), such that fast exchange processes can also be quantified accurately [230], thereby providing insights into rotameric jumps that were otherwise not detectable [231]. These approaches can likely be directly extended to methyl groups.

In a SQ (single quantum) experiment the relaxation dispersion profiles depend on the chemical shift difference of either carbon [232,233] or protons [234,235]. The ^{13}C SQ experiment can be applied to high molecular weight systems [236]; however, the sensitivity of the experiment is reduced due to the fact that the methyl TROSY principle is not active throughout the complete sequence. In the ^{1}H SQ CPMG relaxation experiment the slowly and fast relaxing magnetization terms are not mixed after the first π/2 proton pulse and this sequence thus benefits from a full methyl TROSY effect [234]. Consequently, this experiment is applicable to challenging systems and of equal sensitivity to the MQ experiment that is described below. It should be noted that proton and carbon SQ relaxation experiments can also be conveniently recorded on large proteins that are labeled with $^{13}CHD_2$ groups [237–240].

In MQ (multiple quantum) relaxation dispersion experiments the obtained profiles depend on a combination of the proton and carbon chemical shift difference [241]. This aspect makes MQ dispersion sensitive to exchange processes that might not be detectable in one of the SQ experiments, as the latter only provide information when the proton (^{1}H SQ) or the carbon (^{13}C SQ) chemical shift difference is non-zero. At the same time, the analysis of MQ relaxation data is challenging, as the degrees of freedom that determine the relaxation profiles are higher. The MQ dispersion experiment fully exploits the methyl TROSY principle as it is devoid of π/2 proton pulses that mix fast and slowly relaxing coherences. Multiple studies have exploited MQ relaxation dispersion experiments to study methyl dynamics in large systems that are not amenable to standard ^{1}H-^{15}N or ^{13}C SQ based experiments [17,168,190,242–244].

The strength of proton TQ (triple quantum) relaxation dispersion experiments on methyl groups results from the fact that these depend on three times the proton chemical shift difference, which is equivalent to increasing the static magnetic field by a factor of three [245]. This gives rise to significantly larger dispersion profiles (larger $\Delta R_{2,eff}$) and thus allows for the measurement of accurate relaxation dispersion data, even for resonances that have a relatively small $|\Delta\omega_H|$ between the two exchanging states. In addition, the increase in the effective chemical shift difference between SQ and TQ experiments results in a shift towards an exchange regime that is slower on the NMR chemical shift timescale, such that exchange parameters can be more accurately extracted for faster exchange processes. Despite the lack of a full methyl TROSY effect during the pulse sequence, TQ relaxation dispersion experiments have been successfully applied to the half-proteasome ($\alpha_7\alpha_7$; Fig. 3) that has a molecular weight of 360 kDa [245]. The dependence of the dispersion profiles on $3^*\Delta\omega_H$ has recently also been exploited in the design of a sensitive experiment that allows for the determination of the diffusion constant of sparsely populated protein states [246].

Methyl ^{1}H DQ (double quantum) experiments have also been developed [247], albeit without exploiting the methyl TROSY principle. The resulting relaxation dispersion curves depend on $2^*\Delta\omega_H$ and thus complement SQ and TQ data.

In summary, a large number of relaxation dispersion experiments for methyl groups are now available. In practice, the accuracy of the extracted exchange parameters will significantly increase when data from different experiments are combined and when these data are recorded on spectrometers that have different magnetic field strengths. As an example, it has been shown that simultaneous fitting of SQ, DQ and TQ data significantly enhances the accuracy of the extracted parameters [247]. In addition, approaches have been developed that allow for the determination of the sign of Δω, which is important for the reconstruction of spectra of "invisible states" i.e. minor states whose population and/or exchange properties render their own signals undetectable, but whose existence and properties may be inferred by analyzing their effects on signals of the major species [248,249].

Several software packages that are able to analyze CPMG dispersion profiles have been developed. These include GUARDD [250], CPMG Fit (Palmer laboratory, Columbia University), CATIA [251], cpmg_fit (Korzhnev laboratory, UConn), NESSY [252], relax [253], ShereKhan [254], Glove [255], ChemEx (Bouvignies laboratory, Paris) and PINT [256]. The applicability of these software packages strongly depends on the specific experiments that are to be analyzed, the number of magnetic fields that have been used, the number of independent experiments that need to be analyzed simultaneously, the exchange model that is considered and the assumptions that have been made in the formulas that describe the exchange process.

5.2.2.2. $R_{1\rho}$ relaxation dispersion experiments. A number of $R_{1\rho}$ relaxation dispersion experiments have been designed for methyl groups. Compared to CPMG relaxation dispersion experiments, $R_{1\rho}$ experiments can in general monitor faster exchange processes. The published experiments focus on the use of $^{13}CHD_2$ labeled methyl groups, as this removes cross-correlated dipolar spin relaxation pathways. Based on such a labeling scheme, it is possible to measure ^{1}H and ^{13}C $R_{1\rho}$ relaxation dispersion profiles [257–259].

Please cite this article as: S. Schütz and R. Sprangers, Methyl TROSY spectroscopy: A versatile NMR approach to study challenging biological systems, Progress in Nuclear Magnetic Resonance Spectroscopy, https://doi.org/10.1016/j.pnmrs.2019.09.004

Due to dipolar cross-correlation within $^{13}CH_3$-labeled methyl groups, the design of $R_{1\rho}$ experiments for this widely-used labeling scheme is unfortunately highly challenging.

5.2.2.3. CEST, DEST. In CEST (Chemical Exchange Saturation Transfer) experiments the resonance of a minor, NMR-invisible state is saturated. If the corresponding exchange process is on a ms timescale, this saturation can be detected through the loss of intensity of the major, NMR-visible state [260]. When the proton frequency is systematically irradiated, the experiment can fully benefit from the methyl TROSY effect [261–263]. As an alternative, the carbon frequency can be saturated [264]. The ^{13}C CEST experiment suffers from the absence of a methyl TROSY effect; nevertheless, it is possible to extract quantitative information regarding chemical shifts of invisible excited states [236]. For large proteins, the sensitivity of ^{13}C-CEST experiments can be significantly enhanced by making use of CHD_2-labeled methyl groups [265]. Recent advances show that the recording of CEST experiments can be speeded up by the application of dedicated saturation schemes, where a number of frequencies are simultaneously saturated [266–268].

DEST (Dark-state Exchange Saturation Transfer) experiments can be applied to a smaller (slowly relaxing) protein that transiently associates with a binding partner to form a large (fast relaxing) complex. The large difference in R_2 between the free and bound states of the complex forms the basis for the DEST experiment. A weak RF field is applied at a frequency that is remote from the resonance of the free protein, but that is able to saturate the broad lines from the large complex. Due to the exchange of the small protein with the large complex, the resonances of the NMR-visible small protein are reduced in intensity. The dependence of this signal attenuation on the RF offset provides direct information on the kinetics of the exchange process. The DEST approach was initially developed for ^{15}N-labeled samples [269] and has recently been extended to $^{13}CH_3$-labeled side chains [270,271].

5.2.2.4. Longitudinal exchange. In the situation where the kinetics of the exchange process are slow ($k_{ex} \ll |\Delta\omega|$; often higher ms timescales) and the populations of both states are of comparable magnitude, it is possible to observe the resonances of both states directly. In such cases, exchange processes can be conveniently determined based on longitudinal exchange measurements [272]. These experiments can be extended to methyl groups [190,192,193,273], where it should be noted that the methyl TROSY effect is in part sacrificed as an additional $\pi/2$ proton pulse is required to bring both the proton and the carbon part of the magnetization into the longitudinal state. In the longitudinal ZZ-exchange experiment, the chemical shift of one nucleus is recorded before an exchange delay, whereas the chemical shift of the second nucleus is recorded after the delay time. When the protein changes conformation during the delay time, a cross peak appears that has the frequency of one state in the first dimension and the frequency of the other state in the second dimension. The exchange rates and the populations that are associated with the exchange process can be extracted from the intensity of the cross- and auto-peaks in a series of spectra that are recorded with different delay times [190,274].

5.2.2.5. Real-time NMR. When the kinetics of a (biological) process are very slow (seconds or slower), they cannot be detected using the methods mentioned above. These slow processes can be caused by significant structural rearrangements that have energy barriers that are larger than a couple of kcal/mol. Alternatively, non-equilibrium slow processes can be induced by a sudden change in the sample conditions that is brought about with a rapid mixing device (to modulate pH, salt, concentration of a denaturant or substrate) [275,276], with a laser pulse (e.g. to remove a photo-labile chemical group) or with a pressure jump [277]. The time dependence of these slow processes can be obtained through the rapid recording of a series of NMR spectra e.g. based on fast pulsing methods. In combination with methyl TROSY methods, a time resolution of 10 min or better can be achieved for complexes that have a molecular weight in the MDa range [278,279].

The number of reports that exploit methyl TROSY techniques to gain insights into functionally important dynamics of challenging biomolecular systems is steadily growing and covers widely different aspects of biology, including DNA polymerases [280], membrane chaperones [281], membrane channels [282], nucleosomes [244], AAA+ proteins [283,284] and glucokinase enzymes [285]. These data highlight the importance of methyl TROSY methods in complementing our knowledge of static structures with information on protein dynamics.

5.3. Structure

Methyl-methyl distance restraints are an important source of structural information and can improve the quality of structural models of intermediate-sized proteins significantly [286]. It is possible to extract inter-methyl distances for differentially methyl-labeled samples, even in very large protein complexes [17,49]. Based on the "exact NOE" approach, the accuracy of the extracted structural information can be further improved [287]. For large protein complexes it is, however, not possible to determine a full three-dimensional structure *a priori* based on methyl-methyl distances alone.

Alternatively, structural information can also be derived from PRE rates that directly report on the distance between a methyl group and a spin label that is introduced into the protein at a specific location. Indeed, PRE measurements have provided direct information on dynamic protein complexes and have revealed insights into structural states that are sampled [51,193]. In addition, PRE measurements can provide information on the quaternary structure of very large protein:RNA complexes [288].

Additional structural information can be obtained from accurate $^1H_{methyl}$-$^{13}C_{methyl}$ and $^{13}C_{methyl}$-^{13}C residual dipolar couplings (RDCs) in large methyl-labeled complexes [50,289–292]. The interpretation of these RDCs can, however, be challenging, as long methyl-bearing side chains can undergo extensive motions, including fast timescale motions and rotameric jumps, that modulate the dipolar coupling measurement. Despite these challenges, RDC measurements can provide direct information on changes in protein structure that can take place, for example, on ligand binding [293,294]. Finally, in an impressive study, RDC measurements on methyl groups have been extended such that information on sparely populated excited states were obtained [295].

Local structural information regarding the rotameric state of valine side chains can be directly deducted from chemical shifts [296]. This information can complement intermediate resolution crystal structures, where the exact localization of side chains is often uncertain.

Despite these advances, it is not feasible to determine high-quality NMR structures of large complexes based on methyl data only. This is due to the sparseness of the data that results in a very limited number of measurements compared to the number of unknown atom coordinates. When methyl TROSY data are complemented with other data, it is, however, possible to unravel structural information for proteins that are far larger than those routinely studied [297].

6. Applications involving methyl TROSY

The ultimate goal of the methodology described in this review is to obtain atomic resolution insights into the structure, interactions

Please cite this article as: S. Schütz and R. Sprangers, Methyl TROSY spectroscopy: A versatile NMR approach to study challenging biological systems, Progress in Nuclear Magnetic Resonance Spectroscopy, https://doi.org/10.1016/j.pnmrs.2019.09.004

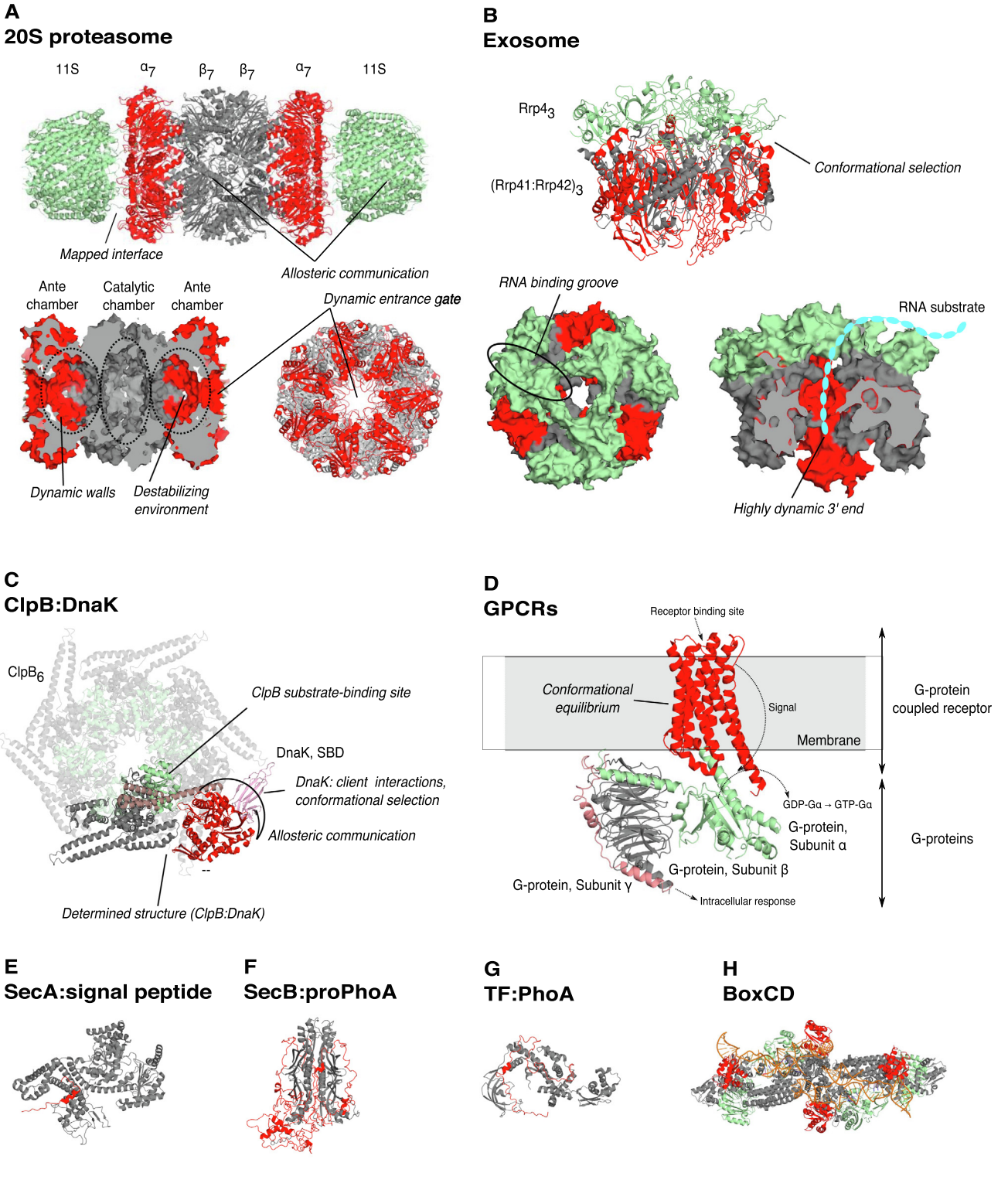

Fig. 7. Mechanistic and structural insights into large molecular machines. A: The 20S proteasome [332] complex. The α and β subunits and the 11S activator are colored red, gray and green respectively. The panel at the left bottom displays the interior of the complex. Important biological findings are indicated. The top and bottom left panels are side views of the complex, the bottom right panel is a top view of the complex towards the entrance pore. B: The RNA exosome [333]. The Rrp41, Rrp42 and Rrp4 subunits are colored red, gray and green respectively. The panel on the right bottom displays the interior of the complex, where the active sites are located. The RNA substrate is displayed schematically in cyan. Important biological insights that are derived from methyl TROSY NMR spectra are indicated. The top panel and the bottom right panel are side views of the complex, the bottom left panel is a top view towards the entrance pore. C: Structure of the ClpB/DnaK complex, as revealed by methyl TROSY NMR data. The model that is shown is based on a superposition of the structures of the dimeric ClpB/DnaK complex [305], the hexameric ClpB complex [334] and the structure of Hsp70 [335]. ClpB is colored in gray and green, whereas DnaK is colored in red, pink and salmon. D: Structure representing a GPCR:G-protein complex [336]. The GPCR is colored red, the lipid membrane is indicated with a gray box. The trimeric G-protein complex is colored green (α-subunit), gray (β-subunit) and salmon (γ-subunit). E: Structure of the SecA:signal peptide complex [44]. SecA is colored in gray, the signal peptide in red. F: Structure of the SecB:proPhoA complex [74]. SecB is colored in gray, one of the possible conformations of the unfolded PhoA peptide is shown in red. G: Structure of the trigger factor (TF) chaperone in complex with PhoA [73]. TF is colored in gray, PhoA in red. H: Structure of the BoxCD complex [288]. The NOP5 subunits are colored gray, L7A red, Fibrillarin green and the RNA in orange.

Please cite this article as: S. Schütz and R. Sprangers, Methyl TROSY spectroscopy: A versatile NMR approach to study challenging biological systems, Progress in Nuclear Magnetic Resonance Spectroscopy, https://doi.org/10.1016/j.pnmrs.2019.09.004

and dynamics of large biological machines. In the following, we will describe a few systems that have been extensively studied, without trying to provide a full overview of all published examples. We focus on three kinds of large cellular systems: enzymes that degrade proteins/RNA (barrel-shaped proteases and RNases), chaperones that ensure that cellular proteins are well folded and G-protein-coupled receptors (GPCRs).

6.1. Barrel-shaped protease: The 20S proteasome complex

The 20S proteasome is a molecular machine that hydrolyses proteins that have been targeted for degradation (Fig. 7A) [298]. The proteasome from *Thermoplasma acidophilum* contains 14 α and 14 β subunits that are arranged into four homo-heptameric rings with an $\alpha_7\beta_7\beta_7\alpha_7$ architecture. The four rings form three chambers, with the catalytic chamber located between the two β_7 rings. Methyl TROSY spectra of the 670 kDa complex are of very high quality and benefit from the 14-fold symmetry and from the fact that samples can be prepared that are NMR-active only in one of the two different subunits [17]. An almost complete assignment of labeled methyl groups in the complex has been achieved through divide-and-conquer and mutagenesis approaches. Based on this, it was found that the complex is unexpectedly mobile, both inside the chambers, as well as around the substrate entrance pore [17,193,273]. Importantly, these reports show that it is possible to extract quantitative data on complexes that are far over 100 kDa in molecular weight. The importance of protein motions in the 20S proteasome has been further demonstrated by the identification of an allosteric network that connects the entrance pore and active sites that are 75 Å apart [292]. Information of this kind is normally not accessible based on static structures only, which highlights the important role methyl TROSY methods can play in elucidating biomolecular function. When the substrate is inside the 20S proteasome, it is kept in an unfolded state, which is important to facilitate rapid hydrolysis of the peptide backbone [299]. The hydrolysis of the substrate peptide bonds is subsequently catalyzed through the N-terminal threonine, of which the amino group pKa value was determined to be 6.3 based on methyl TROSY data [300]. Methyl TROSY NMR studies on the 20S proteasome have also been exploited in the search for proteasome inhibitors that can serve as pharmaceutical compounds [301–303], thereby further expanding the applicability of the method.

6.2. Barrel-shaped RNase: the exosome complex

The exosome is a 180–270 kDa complex that degrades RNA in the 3′ to 5′ direction [304]. In recent years, the authors' laboratory has extensively studied the molecular mechanisms behind this molecular machine from *Sulfolobus solfataricus* that contains three catalytic Rrp41-Rrp42 heterodimers in the core and three Rrp4 proteins in the cap (Fig. 7B). Interestingly, methyl TROSY NMR spectra revealed that the 180 kDa core of the complex samples structurally different conformations [168] that correlate with the interaction between the Rrp41-Rrp42 core barrel and the Rrp4 RNA binding proteins. Based on MQ dispersion experiments and on longitudinal exchange experiments, the populations and exchange rates that are associated with these conformational changes could be accurately quantified. The motions in the exosome core were not anticipated, as multiple static crystal structures of the complex display only a single conformation. This important finding highlights the fact that molecular motions might often escape detection and indicates the importance of studies that aim at localizing and quantifying dynamic processes in biomolecular complexes. A large-scale methionine scanning approach was subsequently used to determine how substrate RNA is channeled towards the active sites that are located in the interior of the complex [75]. It was found that the RNA covers an extended surface patch of Rrp4. The local interaction strength between the substrate RNA and the exosome increases in a stepwise manner, which facilitates the translocation of the substrate RNA towards the active sites. Inside the exosome barrel, the substrate is highly mobile and the RNA rapidly engages with and dissociates from the three active sites [236]. As for the proteasome, methyl TROSY NMR data clearly provide unique insights into large molecular machines.

6.3. Chaperones: ClpB:DnaK

The bacterial ClpB chaperone (Hsp104 in eukaryotes) belongs to the AAA+ family and uses ATP to re-solubilize protein aggregates. ClpB acts in concert with the DnaK (Hsp70) chaperone (Fig. 7C). Based on impressive methyl TROSY NMR studies, an atomic resolution model of the complex between the two chaperones could be constructed [305]. This model provides insights into how the ClpB NTD destabilizes client proteins, such that they can be further processed by the ClpB central pore [306]. The flexible DnaK chaperone interacts promiscuously with client proteins through a conformational selection mechanism and thereby increases the conformational space that substrate proteins sample, which aids substrate folding [263,307–309]. Interestingly, methyl TROSY-based experiments on bacterial and eukaryotic chaperones revealed that allosteric communication between the different domains in the DnaK chaperone changed during evolution, demonstrating the importance of structural studies that take the dynamic nature of proteins into account [310,311].

6.4. Chaperones: Hsp90

The Hsp90 chaperone is a highly abundant protein that assists in protein folding and degradation which makes it an important target for anti-cancer drugs [287]. The 180 kDa dimer of Hsp90 undergoes large ATP-dependent structural changes during the catalytic cycle that can be observed in methyl TROSY spectra [294]. Molecular details of the interaction between Hsp90 and the co-chaperone p23 as well as between Hsp90 and the client protein Tau could be revealed based on methyl TROSY NMR experiments [169,312]. In those studies, a very long substrate binding groove has been identified that explains how multiple weak interactions between client proteins and the chaperone contribute to the chaperone function. Additionally, these studies provided a rationale for how the Hsp90 chaperone, in contrast to DnaK (Hsp70), specifically recruits late folding intermediates.

These examples on two chaperone systems display the power of methyl TROSY methods for studies of large and sometimes highly dynamic or fuzzy complexes. Similarly, high-resolution structural information has been obtained for the dynamic complexes of the SecA protein with a translocation signal sequence [44], as well as of the SecB and trigger factor chaperones with client proteins [74,73,313]. The quality of these structures significantly benefits from the high sensitivity and information density of methyl-methyl NOE data [56].

6.5. Membrane proteins: GPCRs

GPCRs are eukaryotic receptors with seven transmembrane helices that interact with external ligands, including neurotransmitters, metabolites and hormones. This interaction leads to conformational changes within the protein that, through the action of G-proteins, results in the activation of cellular signaling pathways (Fig. 7D). GPCRs are highly important pharmaceutical targets and therefore of prime interest for structural biology studies. This is reflected in the fact that over 300 structures of 60 different receptors in complex with a large variety of ligands have been

Please cite this article as: S. Schütz and R. Sprangers, Methyl TROSY spectroscopy: A versatile NMR approach to study challenging biological systems, Progress in Nuclear Magnetic Resonance Spectroscopy, https://doi.org/10.1016/j.pnmrs.2019.09.004

determined. Due to the role of the inherent structural flexibility of GPCRs, NMR spectroscopy is an ideal tool to relate conformational dynamics with functions. Indeed, methyl TROSY spectroscopy has been able to correlate conformational changes in GPCRs with activity in the presence and absence of agonists, antagonists and G-protein-mimetic nanobodies for the β1-adrenergic receptor [314], the β2-adrenergic receptor [90,91,145], the leukotriene B4 receptor BLT2 [315], the neurotensin receptor 1 [316], the adenosine A2A receptor [79], the μ-opioid receptor [148,317] and the M2 muscarinic acetylcholine receptor [318]. Interestingly, the dynamic behavior of GPCRs depends on the membrane-mimicking environment the protein is embedded in, indicating the importance of the lipid bilayer for function [92]. This finding is also important for structural and functional methyl TROSY studies that have been performed in a large number of different membrane-mimicking environments, including nanodiscs [92,315,319] that can closely resemble the natural environment of the receptor. Due to the high biological interest in GPCR function, a large number of strategies have been exploited to prepare suitable NMR samples where NMR-active methyl groups have been introduced in methionine [90–92,314,316–319], isoleucine [79,315,319] and methylated lysine residues [145,148] and proteins have been expressed in *E. coli* [315,316], *P. pastoris* [79] or insect cells [90–92,148,314,318,319]. Recently, phosphorylation has been shown to modulate the conformations that GPCRs sample [319], providing an extra layer of regulation. Current research focusses on unraveling the complex allosteric mechanism that links the agonist-binding pocket to the end of a signaling event to understand the mechanism that underlies receptor activation and how this is linked to protein dynamics [79,148,314]. It should be noted that in addition to methyl TROSY approaches, elegant ^{19}F NMR methods have been used to study the conformational changes in GPCRs [320,321]. In addition to the GPCRs themselves, the heterotrimeric G-protein complex is also being actively studied, and for the α-subunits it has been shown that this protein is significantly more rigid in complex with GTP as compared to GDP [322,323]. In summary, a combination of several state-of-the-art NMR spectroscopic studies have been able to link protein dynamics with transmembrane signaling pathways.

6.6. Integrated structural biology

None of the applications mentioned above relied solely on the use of NMR spectroscopic techniques and it is well recognized that the combination of multiple structural methods provides clear advantages. To that end, significant efforts aim at integrating complementary methods [324]. Recently, the strength of this integrative approach was impressively shown and allowed the determination of a structure of the 390 kDa Box C/D enzyme [288]. To that end, methyl TROSY NMR data were combined with small angle scattering data (SANS, SAXS) and the knowledge of static crystal structures.

7. Conclusion and outlook

Importantly, recent progress in NMR spectroscopy, and especially in methyl TROSY-based methods, now permits detailed studies of high molecular weight complexes. At the same time, cryo-electron microscopy (EM) has undergone a revolution that has improved the achievable resolution significantly [325,326]. As a result, an overlapping regime has emerged in which both methods can be applied to the same biomolecular complexes. This opens up new and exciting possibilities to study molecular machines in great detail. In such an approach, three-dimensional models of large complexes can be reconstructed based on EM data. Different structural classes that are found in EM ensembles can suggest the presence of larger conformational changes, sometimes even in a time-resolved manner [327]. These dynamic processes can subsequently be studied quantitatively and in extraordinary detail based on methyl TROSY NMR data. In addition, interactions of molecular machines with (small or large) interaction partners can be analyzed based on methyl TROSY spectra, which are also ideally suited to identify regulatory allosteric networks. Studies that successfully combine the recent advances in both cryo-EM and methyl TROSY NMR spectroscopy are now appearing [328,329], and display insights into the potential which arises from the combination of both methods.

In this light, methyl TROSY-based NMR will become increasingly important as it provides a broad range of atomic resolution insights into biomolecular structure, interactions and motions. We are excited about the developments in NMR spectroscopy and the current and future possibilities these will bring.

Acknowledgments

We would like to thank all members of the Sprangers group for continuous stimulating discussions. We especially would like to thank Philip Wurm and Jan Overbeck for their remarks on the manuscript and for the valuable discussion. R.S. would like to thank Lewis Kay for past and present support. We apologize to authors of studies that have not been cited. This work has been supported by the European Union's Seventh Framework Programme (FP7/2007–2013), ERC Grant 616052 (RS).

References

[1] K.H. Gardner, L.E. Kay, Production and Incorporation of ^{15}N, ^{13}C, ^{2}H (1 H-δ1 Methyl) Isoleucine into Proteins for Multidimensional NMR Studies, J. Am. Chem. Soc. 119 (1997) 7599–7600, https://doi.org/10.1021/ja9706514.

[2] D.M. LeMaster, Chiral beta and random fractional deuteration for the determination of protein sidechain conformation by NMR, FEBS Lett. 223 (1987) 191–196.

[3] M.A. Markus, K.T. Dayie, P. Matsudaira, G. Wagner, Effect of deuteration on the amide proton relaxation rates in proteins. Heteronuclear NMR experiments on villin 14T, J. Magn. Reson. B. 105 (1994) 192–195.

[4] R.A. Venters, B.T. Farmer, C.A. Fierke, L.D. Spicer, Characterizing the use of perdeuteration in NMR studies of large proteins: 13C, 15N and 1H assignments of human carbonic anhydrase II, J. Mol. Biol. 264 (1996) 1101–1116.

[5] M. Sattler, S.W. Fesik, Use of deuterium labeling in NMR: overcoming a sizeable problem, Struct. Lond. Engl. 1993 (4) (1996) 1245–1249.

[6] R.A. Venters, C.C. Huang, B.T. Farmer, R. Trolard, L.D. Spicer, C.A. Fierke, High-level 2H/13C/15N labeling of proteins for NMR studies, J. Biomol. NMR 5 (1995) 339–344.

[7] S. Grzesiek, J. Anglister, H. Ren, A. Bax, Carbon-13 line narrowing by deuterium decoupling in deuterium/carbon-13/nitrogen-15 enriched proteins. Application to triple resonance 4D J connectivity of sequential amides, J. Am. Chem. Soc. 115 (1993) 4369–4370, https://doi.org/10.1021/ja00063a068.

[8] T. Yamazaki, W. Lee, C.H. Arrowsmith, D.R. Muhandiram, L.E. Kay, A suite of triple resonance NMR experiments for the backbone assignment of 15N, 13C, 2H labeled proteins with high sensitivity, J. Am. Chem. Soc. 116 (1994) 11655–11666, https://doi.org/10.1021/ja00105a005.

[9] T. Yamazaki, W. Lee, M. Revington, D.L. Mattiello, F.W. Dahlquist, C.H. Arrowsmith, L.E. Kay, An HNCA pulse scheme for the backbone assignment of 15N,13C,2H-labeled proteins: application to a 37-kDa Trp repressor-DNA complex, J. Am. Chem. Soc. 116 (1994) 6464–6465, https://doi.org/10.1021/ja00093a069.

[10] M. Gueron, J.L. Leroy, R.H. Griffey, Proton nuclear magnetic relaxation of nitrogen-15-labeled nucleic acids via dipolar coupling and chemical shift anisotropy, J. Am. Chem. Soc. 105 (1983) 7262–7266, https://doi.org/10.1021/ja00363a009.

[11] K. Pervushin, R. Riek, G. Wider, K. Wüthrich, Attenuated T2 relaxation by mutual cancellation of dipole-dipole coupling and chemical shift anisotropy indicates an avenue to NMR structures of very large biological macromolecules in solution, Proc. Natl. Acad. Sci. U. S. A. 94 (1997) 12366–12371.

[12] R. Riek, G. Wider, K. Pervushin, K. Wüthrich, Polarization transfer by cross-correlated relaxation in solution NMR with very large molecules, Proc. Natl. Acad. Sci. U. S. A. 96 (1999) 4918–4923.

Please cite this article as: S. Schütz and R. Sprangers, Methyl TROSY spectroscopy: A versatile NMR approach to study challenging biological systems, Progress in Nuclear Magnetic Resonance Spectroscopy, https://doi.org/10.1016/j.pnmrs.2019.09.004

[13] G. Wider, K. Wüthrich, NMR spectroscopy of large molecules and multimolecular assemblies in solution, Curr. Opin. Struct. Biol. 9 (1999) 594–601.
[14] R. Riek, K. Pervushin, K. Wüthrich, TROSY and CRINEPT: NMR with large molecular and supramolecular structures in solution, Trends Biochem. Sci. 25 (2000) 462–468.
[15] K. Pervushin, R. Riek, G. Wider, K. Wüthrich, Transverse Relaxation-Optimized Spectroscopy (TROSY) for NMR studies of aromatic spin systems in ^{13}C-labeled proteins, J. Am. Chem. Soc. 120 (1998) 6394–6400, https://doi.org/10.1021/ja980742g.
[16] V. Tugarinov, P.M. Hwang, J.E. Ollerenshaw, L.E. Kay, Cross-correlated relaxation enhanced 1H–13C NMR spectroscopy of methyl groups in very high molecular weight proteins and protein complexes, J. Am. Chem. Soc. 125 (2003) 10420–10428, https://doi.org/10.1021/ja030153x.
[17] R. Sprangers, L.E. Kay, Quantitative dynamics and binding studies of the 20S proteasome by NMR, Nature 445 (2007) 618–622, https://doi.org/10.1038/nature05512.
[18] R. Sprangers, A. Velyvis, L.E. Kay, Solution NMR of supramolecular complexes: providing new insights into function, Nat. Methods 4 (2007) 697–703, https://doi.org/10.1038/nmeth1080.
[19] S. Wiesner, R. Sprangers, Methyl groups as NMR probes for biomolecular interactions, Curr. Opin. Struct. Biol. 35 (2015) 60–67, https://doi.org/10.1016/j.sbi.2015.08.010.
[20] K. Takeuchi, H. Arthanari, G. Wagner, Perspective: revisiting the field dependence of TROSY sensitivity, J. Biomol. NMR 66 (2016) 221–225, https://doi.org/10.1007/s10858-016-0075-4.
[21] J.E. Ollerenshaw, V. Tugarinov, L.E. Kay, Methyl TROSY: explanation and experimental verification, Magn. Reson. Chem. 41 (2003) 843–852, https://doi.org/10.1002/mrc.1256.
[22] L.G. Werbelow, A.G. Marshall, Internal rotation and nonexponential methyl nuclear relaxation for macromolecules, J. Magn. Reson. 1969 (11) (1973) 299–313, https://doi.org/10.1016/0022-2364(73)90055-3.
[23] L.E. Kay, J.H. Prestegard, Methyl group dynamics from relaxation of double quantum filtered NMR signals. Application to deoxycholate, J. Am. Chem. Soc. 109 (1987) 3829–3835, https://doi.org/10.1021/ja00247a002.
[24] L.E. Kay, D.A. Torchia, The effects of dipolar cross correlation on 13C methyl-carbon T1, T2, and NOE measurements in macromolecules, J. Magn. Reson. 1969 (95) (1991) 536–547, https://doi.org/10.1016/0022-2364(91)90167-R.
[25] V. Tugarinov, P.M. Hwang, J.E. Ollerenshaw, L.E. Kay, Cross-correlated relaxation enhanced ^{1} H– ^{13} C NMR spectroscopy of methyl groups in very high molecular weight proteins and protein complexes, J. Am. Chem. Soc. 125 (2003) 10420–10428, https://doi.org/10.1021/ja030153x.
[26] G. Bodenhausen, D.J. Ruben, Natural abundance nitrogen-15 NMR by enhanced heteronuclear spectroscopy, Chem. Phys. Lett. 69 (1980) 185–189, https://doi.org/10.1016/0009-2614(80)80041-8.
[27] L. Mueller, Sensitivity enhanced detection of weak nuclei using heteronuclear multiple quantum coherence, J. Am. Chem. Soc. 101 (1979) 4481–4484, https://doi.org/10.1021/ja00510a007.
[28] A. Bax, R.H. Griffey, B.L. Hawkins, Correlation of proton and nitrogen-15 chemical shifts by multiple quantum NMR, J. Magn. Reson. 1969 (55) (1983) 301–315, https://doi.org/10.1016/0022-2364(83)90241-X.
[29] J. Schleucher, M. Schwendinger, M. Sattler, P. Schmidt, O. Schedletzky, S.J. Glaser, O.W. Sørensen, C. Griesinger, A general enhancement scheme in heteronuclear multidimensional NMR employing pulsed field gradients, J. Biomol. NMR 4 (1994) 301–306.
[30] J. Cavanagh, M. Rance, Sensitivity-enhanced NMR techniques for the study of biomolecules, in: Annu. Rep. NMR Spectrosc., Elsevier, 1993, pp. 1–58, https://doi.org/10.1016/S0066-4103(08)60264-1.
[31] C. Amero, P. Schanda, M.A. Durá, I. Ayala, D. Marion, B. Franzetti, B. Brutscher, J. Boisbouvier, Fast two-dimensional NMR spectroscopy of high molecular weight protein assemblies, J. Am. Chem. Soc. 131 (2009) 3448–3449, https://doi.org/10.1021/ja809880p.
[32] P. Schanda, B. Brutscher, Very fast two-dimensional NMR spectroscopy for real-time investigation of dynamic events in proteins on the time scale of seconds, J. Am. Chem. Soc. 127 (2005) 8014–8015, https://doi.org/10.1021/ja051306e.
[33] P. Schanda, E. Kupce, B. Brutscher, SOFAST-HMQC experiments for recording two-dimensional heteronuclear correlation spectra of proteins within a few seconds, J. Biomol. NMR 33 (2005) 199–211, https://doi.org/10.1007/s10858-005-4425-x.
[34] L.E. Kay, Artifacts can emerge in spectra recorded with even the simplest of pulse schemes: an HMQC case study, J. Biomol. NMR (2019), https://doi.org/10.1007/s10858-019-00227-7.
[35] M. Cai, Y. Huang, R. Yang, R. Craigie, G.M. Clore, A simple and robust protocol for high-yield expression of perdeuterated proteins in Escherichia coli grown in shaker flasks, J. Biomol. NMR 66 (2016) 85–91, https://doi.org/10.1007/s10858-016-0052-y.
[36] E.S. O'Brien, D.W. Lin, B. Fuglestad, M.A. Stetz, T. Gosse, C. Tommos, A.J. Wand, Improving yields of deuterated, methyl labeled protein by growing in H2O, J. Biomol. NMR 71 (2018) 263–273, https://doi.org/10.1007/s10858-018-0200-7.
[37] S.B. Azatian, N. Kaur, M.P. Latham, Increasing the buffering capacity of minimal media leads to higher protein yield, J. Biomol. NMR 73 (2019) 11–17, https://doi.org/10.1007/s10858-018-00222-4.
[38] P. McCaldon, P. Argos, Oligopeptide biases in protein sequences and their use in predicting protein coding regions in nucleotide sequences, Proteins 4 (1988) 99–122, https://doi.org/10.1002/prot.340040204.
[39] M. Fischer, K. Kloiber, J. Häusler, K. Ledolter, R. Konrat, W. Schmid, Synthesis of a 13C-methyl-group-labeled methionine precursor as a useful tool for simplifying protein structural analysis by NMR spectroscopy, Chem. Biochem. Eur. J. Chem. Biol. 8 (2007) 610–612, https://doi.org/10.1002/cbic.200600551.
[40] D.C. Muchmore, L.P. McIntosh, C.B. Russell, D.E. Anderson, F.W. Dahlquist, Expression and nitrogen-15 labeling of proteins for proton and nitrogen-15 nuclear magnetic resonance, Methods Enzymol. 177 (1989) 44–73.
[41] M.J. DellaVecchia, W.K. Merritt, Y. Peng, T.W. Kirby, E.F. DeRose, G.A. Mueller, B. Van Houten, R.E. London, NMR analysis of [methyl-13C]methionine UvrB from Bacillus caldotenax reveals UvrB-domain 4 heterodimer formation in solution, J. Mol. Biol. 373 (2007) 282–295, https://doi.org/10.1016/j.jmb.2007.07.045.
[42] X. Zheng, G.A. Mueller, E.F. DeRose, R.E. London, Solution characterization of [methyl-(13)C]methionine HIV-1 reverse transcriptase by NMR spectroscopy, Antiviral Res. 84 (2009) 205–214, https://doi.org/10.1016/j.antiviral.2009.07.021.
[43] J. Klopp, A. Winterhalter, R. Gébleux, D. Scherer-Becker, C. Ostermeier, A.D. Gossert, Cost-effective large-scale expression of proteins for NMR studies, J. Biomol. NMR 71 (2018) 247–262, https://doi.org/10.1007/s10858-018-0179-0.
[44] I. Gelis, A.M.J.J. Bonvin, D. Keramisanou, M. Koukaki, G. Gouridis, S. Karamanou, A. Economou, C.G. Kalodimos, Structural basis for signal-sequence recognition by the translocase motor SecA as determined by NMR, Cell. 131 (2007) 756–769, https://doi.org/10.1016/j.cell.2007.09.039.
[45] K.H. Gardner, X. Zhang, K. Gehring, L.E. Kay, Solution NMR studies of a 42 KDa *Escherichia Coli* maltose binding protein/β-cyclodextrin complex: chemical shift assignments and analysis, J. Am. Chem. Soc. 120 (1998) 11738–11748, https://doi.org/10.1021/ja982019w.
[46] J.B. Jordan, H. Kovacs, Y. Wang, M. Mobli, R. Luo, C. Anklin, J.C. Hoch, R.W. Kriwacki, Three-dimensional 13C-detected CH3-TOCSY using selectively protonated proteins: facile methyl resonance assignment and protein structure determination, J. Am. Chem. Soc. 128 (2006) 9119–9128, https://doi.org/10.1021/ja058587a.
[47] P.J. Hajduk, D.J. Augeri, J. Mack, R. Mendoza, J. Yang, S.F. Betz, S.W. Fesik, NMR-based screening of proteins containing ^{13} C-labeled methyl groups, J. Am. Chem. Soc. 122 (2000) 7898–7904, https://doi.org/10.1021/ja000350l.
[48] V. Tugarinov, V. Kanelis, L.E. Kay, Isotope labeling strategies for the study of high-molecular-weight proteins by solution NMR spectroscopy, Nat. Protoc. 1 (2006) 749–754, https://doi.org/10.1038/nprot.2006.101.
[49] R. Kerfah, M.J. Plevin, O. Pessey, O. Hamelin, P. Gans, J. Boisbouvier, Scrambling free combinatorial labeling of alanine-β, isoleucine-δ1, leucine-proS and valine-proS methyl groups for the detection of long range NOEs, J. Biomol. NMR 61 (2015) 73–82, https://doi.org/10.1007/s10858-014-9887-2.
[50] R. Godoy-Ruiz, C. Guo, V. Tugarinov, Alanine methyl groups as NMR probes of molecular structure and dynamics in high-molecular-weight proteins, J. Am. Chem. Soc. 132 (2010) 18340–18350, https://doi.org/10.1021/ja1083656.
[51] J.P. Wurm, I. Holdermann, J.H. Overbeck, P.H.O. Mayer, R. Sprangers, Changes in conformational equilibria regulate the activity of the Dcp2 decapping enzyme, Proc. Natl. Acad. Sci. U. S. A. 114 (2017) 6034–6039, https://doi.org/10.1073/pnas.1704496114.
[52] M.K. Rosen, K.H. Gardner, R.C. Willis, W.E. Parris, T. Pawson, L.E. Kay, Selective methyl group protonation of perdeuterated proteins, J. Mol. Biol. 263 (1996) 627–636, https://doi.org/10.1006/jmbi.1996.0603.
[53] A.M. Ruschak, A. Velyvis, L.E. Kay, A simple strategy for ^{13}C, ^{1}H labeling at the Ile-γ2 methyl position in highly deuterated proteins, J. Biomol. NMR 48 (2010) 129–135, https://doi.org/10.1007/s10858-010-9449-1.
[54] I. Ayala, O. Hamelin, C. Amero, O. Pessey, M.J. Plevin, P. Gans, J. Boisbouvier, An optimized isotopic labelling strategy of isoleucine-γ2 methyl groups for solution NMR studies of high molecular weight proteins, Chem. Commun. Camb. Engl. 48 (2012) 1434–1436, https://doi.org/10.1039/c1cc12932e.
[55] N.K. Goto, K.H. Gardner, G.A. Mueller, R.C. Willis, L.E. Kay, A robust and cost-effective method for the production of Val, Leu, Ile (delta 1) methyl-protonated 15N-, 13C-, 2H-labeled proteins, J. Biomol. NMR 13 (1999) 369–374.
[56] J.D. Gross, V.M. Gelev, G. Wagner, A sensitive and robust method for obtaining intermolecular NOEs between side chains in large protein complexes, J. Biomol. NMR 25 (2003) 235–242.
[57] V. Tugarinov, L.E. Kay, Ile, Leu, and Val methyl assignments of the 723-residue malate synthase G using a new labeling strategy and novel NMR methods, J. Am. Chem. Soc. 125 (2003) 13868–13878, https://doi.org/10.1021/ja030345s.
[58] V. Tugarinov, L.E. Kay, An isotope labeling strategy for methyl TROSY spectroscopy, J. Biomol. NMR 28 (2004) 165–172, https://doi.org/10.1023/B:JNMR.0000013824.93994.1f.
[59] R. Lichtenecker, M.L. Ludwiczek, W. Schmid, R. Konrat, Simplification of protein NOESY spectra using bioorganic precursor synthesis and NMR spectral editing, J. Am. Chem. Soc. 126 (2004) 5348–5349, https://doi.org/10.1021/ja049679n.
[60] P. Gans, O. Hamelin, R. Sounier, I. Ayala, M.A. Durá, C.D. Amero, M. Noirclerc-Savoye, B. Franzetti, M.J. Plevin, J. Boisbouvier, Stereospecific isotopic labeling of methyl groups for NMR spectroscopic studies of high-molecular-weight proteins, Angew. Chem. Int. Ed Engl. 49 (2010) 1958–1962, https://doi.org/10.1002/anie.200905660.

Please cite this article as: S. Schütz and R. Sprangers, Methyl TROSY spectroscopy: A versatile NMR approach to study challenging biological systems, Progress in Nuclear Magnetic Resonance Spectroscopy, https://doi.org/10.1016/j.pnmrs.2019.09.004

[61] Y. Miyanoiri, M. Takeda, K. Okuma, A.M. Ono, T. Terauchi, M. Kainosho, Differential isotope-labeling for Leu and Val residues in a protein by E. coli cellular expression using stereo-specifically methyl labeled amino acids, J. Biomol. NMR 57 (2013) 237–249, https://doi.org/10.1007/s10858-013-9784-0.

[62] R.J. Lichtenecker, N. Coudevylle, R. Konrat, W. Schmid, Selective isotope labelling of leucine residues by using α-ketoacid precursor compounds, Chembiochem Eur. J. Chem. Biol. 14 (2013) 818–821, https://doi.org/10.1002/cbic.201200737.

[63] R.J. Lichtenecker, K. Weinhäupl, L. Reuther, J. Schörghuber, W. Schmid, R. Konrat, Independent valine and leucine isotope labeling in Escherichia coli protein overexpression systems, J. Biomol. NMR 57 (2013) 205–209, https://doi.org/10.1007/s10858-013-9786-y.

[64] Y. Miyanoiri, Y. Ishida, M. Takeda, T. Terauchi, M. Inouye, M. Kainosho, Highly efficient residue-selective labeling with isotope-labeled Ile, Leu, and Val using a new auxotrophic E. coli strain, J. Biomol. NMR 65 (2016) 109–119, https://doi.org/10.1007/s10858-016-0042-0.

[65] Y.R. Monneau, Y. Ishida, P. Rossi, T. Saio, S.-R. Tzeng, M. Inouye, C.G. Kalodimos, Exploiting E. coli auxotrophs for leucine, valine, and threonine specific methyl labeling of large proteins for NMR applications, J. Biomol. NMR 65 (2016) 99–108, https://doi.org/10.1007/s10858-016-0041-1.

[66] S. Miller, J. Janin, A.M. Lesk, C. Chothia, Interior and surface of monomeric proteins, J. Mol. Biol. 196 (1987) 641–656.

[67] Z. Serber, W. Straub, L. Corsini, A.M. Nomura, N. Shimba, C.S. Craik, P. Ortiz de Montellano, V. Dötsch, Methyl groups as probes for proteins and complexes in in-cell NMR experiments, J. Am. Chem. Soc. 126 (2004) 7119–7125, https://doi.org/10.1021/ja049977k.

[68] R.L. Isaacson, P.J. Simpson, M. Liu, E. Cota, X. Zhang, P. Freemont, S. Matthews, A new labeling method for methyl transverse relaxation-optimized spectroscopy NMR spectra of alanine residues, J. Am. Chem. Soc. 129 (2007) 15428–15429, https://doi.org/10.1021/ja0761784.

[69] I. Ayala, R. Sounier, N. Usé, P. Gans, J. Boisbouvier, An efficient protocol for the complete incorporation of methyl-protonated alanine in perdeuterated protein, J. Biomol. NMR 43 (2009) 111–119, https://doi.org/10.1007/s10858-008-9294-7.

[70] S. Biswas, M. Guharoy, P. Chakrabarti, Dissection, residue conservation, and structural classification of protein-DNA interfaces, Proteins Struct. Funct. Bioinforma 74 (2009) 643–654, https://doi.org/10.1002/prot.22180.

[71] K. Sinha, L. Jen-Jacobson, G.S. Rule, Specific labeling of threonine methyl groups for NMR studies of protein-nucleic acid complexes, Biochemistry 50 (2011) 10189–10191, https://doi.org/10.1021/bi201496d.

[72] A. Velyvis, A.M. Ruschak, L.E. Kay, An economical method for production of (2)H, (13)CH3-threonine for solution NMR studies of large protein complexes: application to the 670 kDa proteasome, PloS One 7 (2012), https://doi.org/10.1371/journal.pone.0043725 e43725.

[73] T. Saio, X. Guan, P. Rossi, A. Economou, C.G. Kalodimos, Structural basis for protein antiaggregation activity of the trigger factor chaperone, Science 344 (2014) 1250494, https://doi.org/10.1126/science.1250494.

[74] C. Huang, P. Rossi, T. Saio, C.G. Kalodimos, Structural basis for the antifolding activity of a molecular chaperone, Nature 537 (2016) 202–206, https://doi.org/10.1038/nature18965.

[75] M.A. Cvetkovic, J.P. Wurm, M.J. Audin, S. Schütz, R. Sprangers, The Rrp4-exosome complex recruits and channels substrate RNA by a unique mechanism, Nat. Chem. Biol. 13 (2017) 522–528, https://doi.org/10.1038/nchembio.2328.

[76] Y. Laroche, V. Storme, J. De Meutter, J. Messens, M. Lauwereys, High-level secretion and very efficient isotopic labeling of tick anticoagulant peptide (TAP) expressed in the methylotrophic yeast, Pichia pastoris, Biotechnol. Nat. Publ. Co. 12 (1994) 1119–1124.

[77] W.D. Morgan, A. Kragt, J. Feeney, Expression of deuterium-isotope-labelled protein in the yeast pichia pastoris for NMR studies, J. Biomol. NMR 17 (2000) 337–347.

[78] L. Clark, J.A. Zahm, R. Ali, M. Kukula, L. Bian, S.M. Patrie, K.H. Gardner, M.K. Rosen, D.M. Rosenbaum, Methyl labeling and TROSY NMR spectroscopy of proteins expressed in the eukaryote Pichia pastoris, J. Biomol. NMR 62 (2015) 239–245, https://doi.org/10.1007/s10858-015-9939-2.

[79] L.D. Clark, I. Dikiy, K. Chapman, K.E. Rödström, J. Aramini, M.V. LeVine, G. Khelashvili, S.G. Rasmussen, K.H. Gardner, D.M. Rosenbaum, Ligand modulation of sidechain dynamics in a wild-type human GPCR, ELife 6 (2017), https://doi.org/10.7554/eLife. 28505.

[80] T. Sugiki, I. Shimada, H. Takahashi, Stable isotope labeling of protein by Kluyveromyces lactis for NMR study, J. Biomol. NMR 42 (2008) 159–162, https://doi.org/10.1007/s10858-008-9276-9.

[81] M. Miyazawa-Onami, K. Takeuchi, T. Takano, T. Sugiki, I. Shimada, H. Takahashi, Perdeuteration and methyl-selective (1)H, (13)C-labeling by using a Kluyveromyces lactis expression system, J. Biomol. NMR 57 (2013) 297–304, https://doi.org/10.1007/s10858-013-9789-8.

[82] R. Suzuki, M. Sakakura, M. Mori, M. Fujii, S. Akashi, H. Takahashi, Methyl-selective isotope labeling using α-ketoisovalerate for the yeast Pichia pastoris recombinant protein expression system, J. Biomol. NMR 71 (2018) 213–223, https://doi.org/10.1007/s10858-018-0192-3.

[83] W.J. Walton, A.J. Kasprzak, J.T. Hare, T.M. Logan, An economic approach to isotopic enrichment of glycoproteins expressed from Sf9 insect cells, J. Biomol. NMR 36 (2006) 225–233, https://doi.org/10.1007/s10858-006-9086-x.

[84] A.D. Gossert, W. Jahnke, Isotope labeling in insect cells, in: H.S. Atreya (Ed.), Isot. Labeling Biomol. NMR, Springer, Netherlands, Dordrecht, 2012, pp. 179–196, https://doi.org/10.1007/978-94-007-4954-2_10.

[85] A. Strauss, F. Bitsch, B. Cutting, G. Fendrich, P. Graff, J. Liebetanz, M. Zurini, W. Jahnke, Amino-acid-type selective isotope labeling of proteins expressed in Baculovirus-infected insect cells useful for NMR studies, J. Biomol. NMR 26 (2003) 367–372.

[86] A. Strauss, F. Bitsch, G. Fendrich, P. Graff, R. Knecht, B. Meyhack, W. Jahnke, Efficient uniform isotope labeling of Abl kinase expressed in Baculovirus-infected insect cells, J. Biomol. NMR 31 (2005) 343–349, https://doi.org/10.1007/s10858-005-2451-3.

[87] N. Vajpai, A. Strauss, G. Fendrich, S.W. Cowan-Jacob, P.W. Manley, S. Grzesiek, W. Jahnke, Solution conformations and dynamics of ABL kinase-inhibitor complexes determined by NMR substantiate the different binding modes of imatinib/nilotinib and dasatinib, J. Biol. Chem. 283 (2008) 18292–18302, https://doi.org/10.1074/jbc.M801337200.

[88] W. Jahnke, R.M. Grotzfeld, X. Pellé, A. Strauss, G. Fendrich, S.W. Cowan-Jacob, S. Cotesta, D. Fabbro, P. Furet, J. Mestan, A.L. Marzinzik, Binding or bending: distinction of allosteric Abl kinase agonists from antagonists by an NMR-based conformational assay, J. Am. Chem. Soc. 132 (2010) 7043–7048, https://doi.org/10.1021/ja101837n.

[89] A.D. Gossert, A. Hinniger, S. Gutmann, W. Jahnke, A. Strauss, C. Fernández, A simple protocol for amino acid type selective isotope labeling in insect cells with improved yields and high reproducibility, J. Biomol. NMR 51 (2011) 449–456, https://doi.org/10.1007/s10858-011-9570-9.

[90] Y. Kofuku, T. Ueda, J. Okude, Y. Shiraishi, K. Kondo, M. Maeda, H. Tsujishita, I. Shimada, Efficacy of the β_2-adrenergic receptor is determined by conformational equilibrium in the transmembrane region, Nat. Commun. 3 (2012) 1045, https://doi.org/10.1038/ncomms2046.

[91] R. Nygaard, Y. Zou, R.O. Dror, T.J. Mildorf, D.H. Arlow, A. Manglik, A.C. Pan, C. W. Liu, J.J. Fung, M.P. Bokoch, F.S. Thian, T.S. Kobilka, D.E. Shaw, L. Mueller, R. S. Prosser, B.K. Kobilka, The dynamic process of β(2)-adrenergic receptor activation, Cell 152 (2013) 532–542, https://doi.org/10.1016/j.cell.2013.01.008.

[92] Y. Kofuku, T. Ueda, J. Okude, Y. Shiraishi, K. Kondo, T. Mizumura, S. Suzuki, I. Shimada, Functional dynamics of deuterated β2 -adrenergic receptor in lipid bilayers revealed by NMR spectroscopy, Angew. Chem. Int. Ed Engl. 53 (2014) 13376–13379, https://doi.org/10.1002/anie.201406603.

[93] Y. Kofuku, T. Yokomizo, S. Imai, Y. Shiraishi, M. Natsume, H. Itoh, M. Inoue, K. Nakata, S. Igarashi, H. Yamaguchi, T. Mizukoshi, E. Suzuki, T. Ueda, I. Shimada, Deuteration and selective labeling of alanine methyl groups of β2-adrenergic receptor expressed in a baculovirus-insect cell expression system, J. Biomol. NMR 71 (2018) 185–192, https://doi.org/10.1007/s10858-018-0174-5.

[94] C. Opitz, S. Isogai, S. Grzesiek, An economic approach to efficient isotope labeling in insect cells using homemade 15N-, 13C- and 2H-labeled yeast extracts, J. Biomol. NMR 62 (2015) 373–385, https://doi.org/10.1007/s10858-015-9954-3.

[95] A. Sitarska, L. Skora, J. Klopp, S. Roest, C. Fernández, B. Shrestha, A.D. Gossert, Affordable uniform isotope labeling with (2)H, (13)C and (15)N in insect cells, J. Biomol. NMR 62 (2015) 191–197, https://doi.org/10.1007/s10858-015-9935-6.

[96] J.J. Katz, H.L. Crespi, Deuterated organisms: cultivation and uses, Science 151 (1966) 1187–1194.

[97] R.A. Uphaus, M.I. Blake, J.J. Katz, Deuterium isotope effects in *Nicotiana tabacum*, Can. J. Bot. 53 (1975) 2128–2133, https://doi.org/10.1139/b75-239.

[98] S. Kubo, N. Nishida, Y. Udagawa, O. Takarada, S. Ogino, I. Shimada, A gel-encapsulated bioreactor system for NMR studies of protein-protein interactions in living mammalian cells, Angew. Chem. Int. Ed. 52 (2013) 1208–1211, https://doi.org/10.1002/anie.201207243.

[99] D.F. Wyss, J.M. Withka, M.H. Knoppers, K.A. Sterne, M.A. Recny, G. Wagner, 1H resonance assignments and secondary structure of the 13.6 kDa glycosylated adhesion domain of human CD2, Biochemistry 32 (1993) 10995–11006.

[100] J.W. Lustbader, S. Birken, S. Pollak, A. Pound, B.T. Chait, U.A. Mirza, S. Ramnarain, R.E. Canfield, J.M. Brown, Expression of human chorionic gonadotropin uniformly labeled with NMR isotopes in Chinese hamster ovary cells: an advance toward rapid determination of glycoprotein structures, J. Biomol. NMR 7 (1996) 295–304.

[101] P.E. Coughlin, F.E. Anderson, E.J. Oliver, J.M. Brown, S.W. Homans, S. Pollak, J. W. Lustbader, Improved resolution and sensitivity of triple-resonance NMR methods for the structural analysis of proteins by use of a backbone-labeling strategy, J. Am. Chem. Soc. 121 (1999) 11871–11874, https://doi.org/10.1021/ja993083w.

[102] E.J. Beatty, M.C. Cox, T.A. Frenkiel, B.M. Tam, A.B. Mason, R.T. MacGillivray, P.J. Sadler, R.C. Woodworth, Interlobe communication in 13C-methionine-labeled human transferrin, Biochemistry 35 (1996) 7635–7642, https://doi.org/10.1021/bi960684g.

[103] T. Kigawa, Y. Muto, S. Yokoyama, Cell-free synthesis and amino acid-selective stable isotope labeling of proteins for NMR analysis, J. Biomol. NMR 6 (1995) 129–134.

[104] T. Kigawa, T. Yabuki, Y. Yoshida, M. Tsutsui, Y. Ito, T. Shibata, S. Yokoyama, Cell-free production and stable-isotope labeling of milligram quantities of proteins, FEBS Lett. 442 (1999) 15–19.

[105] T. Torizawa, M. Shimizu, M. Taoka, H. Miyano, M. Kainosho, Efficient production of isotopically labeled proteins by cell-free synthesis: a practical protocol, J. Biomol. NMR 30 (2004) 311–325, https://doi.org/10.1007/s10858-004-3534-2.

Please cite this article as: S. Schütz and R. Sprangers, Methyl TROSY spectroscopy: A versatile NMR approach to study challenging biological systems, Progress in Nuclear Magnetic Resonance Spectroscopy, https://doi.org/10.1016/j.pnmrs.2019.09.004

[106] F. Katzen, G. Chang, W. Kudlicki, The past, present and future of cell-free protein synthesis, Trends Biotechnol. 23 (2005) 150–156, https://doi.org/10.1016/j.tibtech.2005.01.003.
[107] D. Schwarz, F. Junge, F. Durst, N. Frölich, B. Schneider, S. Reckel, S. Sobhanifar, V. Dötsch, F. Bernhard, Preparative scale expression of membrane proteins in Escherichia coli-based continuous exchange cell-free systems, Nat. Protoc. 2 (2007) 2945–2957, https://doi.org/10.1038/nprot.2007.426.
[108] C. Klammt, D. Schwarz, K. Fendler, W. Haase, V. Dötsch, F. Bernhard, Evaluation of detergents for the soluble expression of alpha-helical and beta-barrel-type integral membrane proteins by a preparative scale individual cell-free expression system, FEBS J. 272 (2005) 6024–6038, https://doi.org/10.1111/j.1742-4658.2005.05002.x.
[109] R. Kalmbach, I. Chizhov, M.C. Schumacher, T. Friedrich, E. Bamberg, M. Engelhard, Functional cell-free synthesis of a seven helix membrane protein: in situ insertion of bacteriorhodopsin into liposomes, J. Mol. Biol. 371 (2007) 639–648, https://doi.org/10.1016/j.jmb.2007.05.087.
[110] D.A. Vinarov, B.L. Lytle, F.C. Peterson, E.M. Tyler, B.F. Volkman, J.L. Markley, Cell-free protein production and labeling protocol for NMR-based structural proteomics, Nat. Methods 1 (2004) 149–153, https://doi.org/10.1038/nmeth716.
[111] A. Koglin, C. Klammt, N. Trbovic, D. Schwarz, B. Schneider, B. Schäfer, F. Löhr, F. Bernhard, V. Dötsch, Combination of cell-free expression and NMR spectroscopy as a new approach for structural investigation of membrane proteins, Magn. Reson. Chem. MRC 44 (2006) S17–S23, https://doi.org/10.1002/mrc.1833, Spec No.
[112] T. Etezady-Esfarjani, S. Hiller, C. Villalba, K. Wüthrich, Cell-free protein synthesis of perdeuterated proteins for NMR studies, J. Biomol. NMR 39 (2007) 229–238, https://doi.org/10.1007/s10858-007-9188-0.
[113] M. Etzkorn, T. Raschle, F. Hagn, V. Gelev, A.J. Rice, T. Walz, G. Wagner, Cell-free expressed bacteriorhodopsin in different soluble membrane mimetics: biophysical properties and NMR accessibility, Struct. Lond. Engl. 1993 (21) (2013) 394–401, https://doi.org/10.1016/j.str.2013.01.005.
[114] M. Kainosho, T. Torizawa, Y. Iwashita, T. Terauchi, A. Mei Ono, P. Güntert, Optimal isotope labelling for NMR protein structure determinations, Nature 440 (2006) 52–57, https://doi.org/10.1038/nature04525.
[115] M. Takeda, T. Ikeya, P. Güntert, M. Kainosho, Automated structure determination of proteins with the SAIL-FLYA NMR method, Nat. Protoc. 2 (2007) 2896–2902, https://doi.org/10.1038/nprot.2007.423.
[116] M. Kainosho, Y. Miyanoiri, T. Terauchi, M. Takeda, Perspective: next generation isotope-aided methods for protein NMR spectroscopy, J. Biomol. NMR 71 (2018) 119–127, https://doi.org/10.1007/s10858-018-0198-x.
[117] R. Linser, V. Gelev, F. Hagn, H. Arthanari, S.G. Hyberts, G. Wagner, Selective methyl labeling of eukaryotic membrane proteins using cell-free expression, J. Am. Chem. Soc. 136 (2014) 11308–11310, https://doi.org/10.1021/ja504791j.
[118] H. Paulus, Protein splicing and related forms of protein autoprocessing, Annu. Rev. Biochem. 69 (2000) 447–496, https://doi.org/10.1146/annurev.biochem.69.1.447.
[119] Y. Minato, T. Ueda, A. Machiyama, I. Shimada, H. Iwaï, Segmental isotopic labeling of a 140 kDa dimeric multi-domain protein CheA from Escherichia coli by expressed protein ligation and protein trans-splicing, J. Biomol. NMR 53 (2012) 191–207, https://doi.org/10.1007/s10858-012-9628-3.
[120] R. Xu, B. Ayers, D. Cowburn, T.W. Muir, Chemical ligation of folded recombinant proteins: segmental isotopic labeling of domains for NMR studies, Proc. Natl. Acad. Sci. U. S. A. 96 (1999) 388–393.
[121] K. Severinov, T.W. Muir, Expressed protein ligation, a novel method for studying protein-protein interactions in transcription, J. Biol. Chem. 273 (1998) 16205–16209.
[122] X.Q. Liu, Protein-splicing intein: genetic mobility, origin, and evolution, Annu. Rev. Genet. 34 (2000) 61–76, https://doi.org/10.1146/annurev.genet.34.1.61.
[123] S. Züger, H. Iwai, Intein-based biosynthetic incorporation of unlabeled protein tags into isotopically labeled proteins for NMR studies, Nat. Biotechnol. 23 (2005) 736–740, https://doi.org/10.1038/nbt1097.
[124] M. Muona, A.S. Aranko, V. Raulinaitis, H. Iwai, Segmental isotopic labeling of multi-domain and fusion proteins by protein trans-splicing in vivo and in vitro, Nat. Protoc. 5 (2010) 574–587, https://doi.org/10.1038/nprot.2009.240.
[125] H. Mao, S.A. Hart, A. Schink, B.A. Pollok, Sortase-mediated protein ligation: a new method for protein engineering, J. Am. Chem. Soc. 126 (2004) 2670–2671, https://doi.org/10.1021/ja039915e.
[126] Y. Kobashigawa, H. Kumeta, K. Ogura, F. Inagaki, Attachment of an NMR-invisible solubility enhancement tag using a sortase-mediated protein ligation method, J. Biomol. NMR 43 (2009) 145–150, https://doi.org/10.1007/s10858-008-9296-5.
[127] L. Freiburger, M. Sonntag, J. Hennig, J. Li, P. Zou, M. Sattler, Efficient segmental isotope labeling of multi-domain proteins using Sortase A, J. Biomol. NMR 63 (2015) 1–8, https://doi.org/10.1007/s10858-015-9981-0.
[128] R. Zhang, R. Wu, G. Joachimiak, S.K. Mazmanian, D.M. Missiakas, P. Gornicki, O. Schneewind, A. Joachimiak, Structures of sortase B from Staphylococcus aureus and Bacillus anthracis reveal catalytic amino acid triad in the active site, Struct. Lond. Engl. 1993 (12) (2004) 1147–1156, https://doi.org/10.1016/j.str.2004.06.001.
[129] P.R. Race, M.L. Bentley, J.A. Melvin, A. Crow, R.K. Hughes, W.D. Smith, R.B. Sessions, M.A. Kehoe, D.G. McCafferty, M.J. Banfield, Crystal structure of Streptococcus pyogenes sortase A: implications for sortase mechanism, J. Biol. Chem. 284 (2009) 6924–6933, https://doi.org/10.1074/jbc.M805406200.
[130] F.P. Williams, A.G. Milbradt, K.J. Embrey, R. Bobby, Segmental isotope labelling of an individual bromodomain of a tandem domain BRD4 using Sortase A, PloS One 11 (2016), https://doi.org/10.1371/journal.pone.0154607 e0154607.
[131] M. Mund, J.H. Overbeck, J. Ullmann, R. Sprangers, LEGO-NMR spectroscopy: a method to visualize individual subunits in large heteromeric complexes, Angew. Chem. Int. Ed Engl. 52 (2013) 11401–11405, https://doi.org/10.1002/anie.201304914.
[132] W.C. Jones, T.M. Rothgeb, F.R. Gurb, Letter: Specific enrichment with 13-C of the methionine methyl groups of sperm whale myoglobin, J. Am. Chem. Soc. 97 (1975) 3875–3877.
[133] W.C. Jones, T.M. Rothgeb, F.R. Gurd, Nuclear magnetic resonance studies of sperm whale myoglobin specifically enriched with 13C in the methionine methyl groups, J. Biol. Chem. 251 (1976) 7452–7460.
[134] C.M. Deber, M.A. Moscarello, D.D. Wood, Conformational studies on 13C-enriched human and bovine myelin basic protein, in solution and incorporated into liposomes, Biochemistry 17 (1978) 898–903.
[135] R.E. Hardy, K. Dill, Magnetic resonance study of glycophorin A-containing 13C-enriched methionines, FEBS Lett. 143 (1982) 327–331.
[136] G.E. Means, R.E. Feeney, Reductive alkylation of amino groups in proteins, Biochemistry 7 (1968) 2192–2201, https://doi.org/10.1021/bi00846a023.
[137] G.E. Means, Reductive alkylation of proteins, J. Protein Chem. 3 (1984) 121–130, https://doi.org/10.1007/BF01024842.
[138] S.T. Larda, M.P. Bokoch, F. Evanics, R.S. Prosser, Lysine methylation strategies for characterizing protein conformations by NMR, J. Biomol. NMR 54 (2012) 199–209, https://doi.org/10.1007/s10858-012-9664-z.
[139] S.J. Abraham, S. Hoheisel, V. Gaponenko, Detection of protein-ligand interactions by NMR using reductive methylation of lysine residues, J. Biomol. NMR 42 (2008) 143–148, https://doi.org/10.1007/s10858-008-9274-y.
[140] F.-X. Theillet, S. Liokatis, J.O. Jost, B. Bekei, H.M. Rose, A. Binolfi, D. Schwarzer, P. Selenko, Site-specific mapping and time-resolved monitoring of lysine methylation by high-resolution NMR spectroscopy, J. Am. Chem. Soc. 134 (2012) 7616–7619, https://doi.org/10.1021/ja301895f.
[141] G.R. Moore, M.C. Cox, D. Crowe, M.J. Osborne, F.I. Rosell, J. Bujons, P.D. Barker, M.R. Mauk, A.G. Mauk, N epsilon, N epsilon-dimethyl-lysine cytochrome c as an NMR probe for lysine involvement in protein-protein complex formation, Biochem. J. 332 (Pt 2) (1998) 439–449.
[142] J.T. Ashfield, T. Meyers, D. Lowne, P.G. Varley, J.R. Arnold, P. Tan, J.C. Yang, L.G. Czaplewski, T. Dudgeon, J. Fisher, Chemical modification of a variant of human MIP-1alpha; implications for dimer structure, Protein Sci. Publ. Protein Soc. 9 (2000) 2047–2053, https://doi.org/10.1110/ps.9.10.2047.
[143] S.J. Abraham, T. Kobayashi, R.J. Solaro, V. Gaponenko, Differences in lysine pKa values may be used to improve NMR signal dispersion in reductively methylated proteins, J. Biomol. NMR 43 (2009) 239–246, https://doi.org/10.1007/s10858-009-9306-2.
[144] S.J. Abraham, R.C. Cheng, T.A. Chew, C.M. Khantwal, C.W. Liu, S. Gong, R.K. Nakamoto, M. Maduke, 13C NMR detects conformational change in the 100-kD membrane transporter ClC-ec1, J. Biomol. NMR 61 (2015) 209–226, https://doi.org/10.1007/s10858-015-9898-7.
[145] M.P. Bokoch, Y. Zou, S.G.F. Rasmussen, C.W. Liu, R. Nygaard, D.M. Rosenbaum, J.J. Fung, H.-J. Choi, F.S. Thian, T.S. Kobilka, J.D. Puglisi, W.I. Weis, L. Pardo, R.S. Prosser, L. Mueller, B.K. Kobilka, Ligand-specific regulation of the extracellular surface of a G-protein-coupled receptor, Nature 463 (2010) 108–112, https://doi.org/10.1038/nature08650.
[146] Y. Hattori, K. Furuita, I. Ohki, T. Ikegami, H. Fukada, M. Shirakawa, T. Fujiwara, C. Kojima, Utilization of lysine ^{13}C-methylation NMR for protein-protein interaction studies, J. Biomol. NMR 55 (2013) 19–31, https://doi.org/10.1007/s10858-012-9675-9.
[147] K. Möbius, K. Nordsieck, A. Pichert, S.A. Samsonov, L. Thomas, J. Schiller, S. Kalkhof, M. Teresa Pisabarro, A.G. Beck-Sickinger, D. Huster, Investigation of lysine side chain interactions of interleukin-8 with heparin and other glycosaminoglycans studied by a methylation-NMR approach, Glycobiology 23 (2013) 1260–1269, https://doi.org/10.1093/glycob/cwt062.
[148] R. Sounier, C. Mas, J. Steyaert, T. Laeremans, A. Manglik, W. Huang, B.K. Kobilka, H. Déméné, S. Granier, Propagation of conformational changes during μ-opioid receptor activation, Nature 524 (2015) 375–378, https://doi.org/10.1038/nature14680.
[149] T.L. Religa, A.M. Ruschak, R. Rosenzweig, L.E. Kay, Site-directed methyl group labeling as an NMR probe of structure and dynamics in supramolecular protein systems: applications to the proteasome and to the ClpP protease, J. Am. Chem. Soc. 133 (2011) 9063–9068, https://doi.org/10.1021/ja202259a.
[150] A.R. Galiakhmetov, E.A. Kovrigina, C. Xia, J.-J.P. Kim, E.L. Kovrigin, Application of methyl-TROSY to a large paramagnetic membrane protein without perdeuteration: 13C-MMTS-labeled NADPH-cytochrome P450 oxidoreductase, J. Biomol. NMR 70 (2018) 21–31, https://doi.org/10.1007/s10858-017-0152-3.
[151] W. Hu, A.T. Namanja, S. Wong, Y. Chen, Selective editing of Val and Leu methyl groups in high molecular weight protein NMR, J. Biomol. NMR 53 (2012) 113–124, https://doi.org/10.1007/s10858-012-9629-2.
[152] D. Neri, T. Szyperski, G. Otting, H. Senn, K. Wüthrich, Stereospecific nuclear magnetic resonance assignments of the methyl groups of valine and leucine in the DNA-binding domain of the 434 repressor by biosynthetically directed fractional 13C labeling, Biochemistry 28 (1989) 7510–7516.

Please cite this article as: S. Schütz and R. Sprangers, Methyl TROSY spectroscopy: A versatile NMR approach to study challenging biological systems, Progress in Nuclear Magnetic Resonance Spectroscopy, https://doi.org/10.1016/j.pnmrs.2019.09.004

[153] H.S. Atreya, K.V. Chary, Selective "unlabeling" of amino acids in fractionally 13C labeled proteins: an approach for stereospecific NMR assignments of CH3 groups in Val and Leu residues, J. Biomol. NMR 19 (2001) 267–272.
[154] C. Hilty, G. Wider, C. Fernández, K. Wüthrich, Stereospecific assignments of the isopropyl methyl groups of the membrane protein OmpX in DHPC micelles, J. Biomol. NMR 27 (2003) 377–382.
[155] V. Tugarinov, L.E. Kay, Stereospecific NMR assignments of prochiral methyls, rotameric states and dynamics of valine residues in malate synthase G, J. Am. Chem. Soc. 126 (2004) 9827–9836, https://doi.org/10.1021/ja048738u.
[156] M.J. Plevin, O. Hamelin, J. Boisbouvier, P. Gans, A simple biosynthetic method for stereospecific resonance assignment of prochiral methyl groups in proteins, J. Biomol. NMR 49 (2011) 61–67, https://doi.org/10.1007/s10858-010-9463-3.
[157] M. Sattler, J. Schleucher, C. Griesinger, Heteronuclear multidimensional NMR experiments for the structure determination of proteins in solution employing pulsed field gradients, Prog. Nucl. Magn. Reson. Spectrosc. 34 (1999) 93–158, https://doi.org/10.1016/S0079-6565(98)00025-9.
[158] C. Hilty, C. Fernández, G. Wider, K. Wüthrich, Side chain NMR assignments in the membrane protein OmpX reconstituted in DHPC micelles, J. Biomol. NMR 23 (2002) 289–301.
[159] V. Tugarinov, L.E. Kay, Side chain assignments of Ile delta 1 methyl groups in high molecular weight proteins: an application to a 46 ns tumbling molecule, J. Am. Chem. Soc. 125 (2003) 5701–5706, https://doi.org/10.1021/ja021452+.
[160] V. Tugarinov, V. Venditti, G. Marius Clore, A NMR experiment for simultaneous correlations of valine and leucine/isoleucine methyls with carbonyl chemical shifts in proteins, J. Biomol. NMR 58 (2014) 1–8, https://doi.org/10.1007/s10858-013-9803-1.
[161] K. Sinha, L. Jen-Jacobson, G.S. Rule, Divide and conquer is always best: sensitivity of methyl correlation experiments, J. Biomol. NMR 56 (2013) 331–335, https://doi.org/10.1007/s10858-013-9751-9.
[162] A. Krejcirikova, V. Tugarinov, 3D-TROSY-based backbone and ILV-methyl resonance assignments of a 319-residue homodimer from a single protein sample, J. Biomol. NMR 54 (2012) 135–143, https://doi.org/10.1007/s10858-012-9667-9.
[163] D. Sheppard, C. Guo, V. Tugarinov, 4D 1H–13C NMR spectroscopy for assignments of alanine methyls in large and complex protein structures, J. Am. Chem. Soc. 131 (2009) 1364–1365, https://doi.org/10.1021/ja808202q.
[164] D. Sheppard, C. Guo, V. Tugarinov, Methyl-detected "out-and-back" NMR experiments for simultaneous assignments of Alabeta and Ilegamma2 methyl groups in large proteins, J. Biomol. NMR 43 (2009) 229–238, https://doi.org/10.1007/s10858-009-9305-3.
[165] C. Guo, V. Tugarinov, Selective 1H–13C NMR spectroscopy of methyl groups in residually protonated samples of large proteins, J. Biomol. NMR 46 (2010) 127–133, https://doi.org/10.1007/s10858-009-9393-0.
[166] A. Bax, F. Delaglio, S. Grzesiek, G.W. Vuister, Resonance assignment of methionine methyl groups and chi 3 angular information from long-range proton-carbon and carbon-carbon J correlation in a calmodulin-peptide complex, J. Biomol. NMR 4 (1994) 787–797.
[167] V. Tugarinov, R. Muhandiram, A. Ayed, L.E. Kay, Four-dimensional NMR spectroscopy of a 723-residue protein: chemical shift assignments and secondary structure of malate synthase g, J. Am. Chem. Soc. 124 (2002) 10025–10035.
[168] M.J.C. Audin, G. Dorn, S.A. Fromm, K. Reiss, S. Schütz, M.K. Vorländer, R. Sprangers, The archaeal exosome: identification and quantification of site-specific motions that correlate with cap and RNA binding, Angew. Chem. Int. Ed Engl. 52 (2013) 8312–8316, https://doi.org/10.1002/anie.201302811.
[169] G.E. Karagöz, A.M.S. Duarte, H. Ippel, C. Uetrecht, T. Sinnige, M. van Rosmalen, J. Hausmann, A.J.R. Heck, R. Boelens, S.G.D. Rüdiger, N-terminal domain of human Hsp90 triggers binding to the cochaperone p23, Proc. Natl. Acad. Sci. U. S. A. 108 (2011) 580–585, https://doi.org/10.1073/pnas.1011867108.
[170] A.A. Ogunjimi, S. Wiesner, D.J. Briant, X. Varelas, F. Sicheri, J. Forman-Kay, J.L. Wrana, The ubiquitin binding region of the Smurf HECT domain facilitates polyubiquitylation and binding of ubiquitylated substrates, J. Biol. Chem. 285 (2010) 6308–6315, https://doi.org/10.1074/jbc.M109.044537.
[171] S.W. Fesik, E.R.P. Zuiderweg, Heteronuclear three-dimensional nmr spectroscopy. A strategy for the simplification of homonuclear two-dimensional NMR spectra, J. Magn. Reson. 1969 (78) (1988) 588–593, https://doi.org/10.1016/0022-2364(88)90144-8.
[172] G.M. Clore, L.E. Kay, A. Bax, A.M. Gronenborn, Four-dimensional 13C/13C-edited nuclear Overhauser enhancement spectroscopy of a protein in solution: application to interleukin 1 beta, Biochemistry 30 (1991) 12–18.
[173] E.R.P. Zuiderweg, A.M. Petros, S.W. Fesik, E.T. Olejniczak, Four-dimensional [13C,1H,13C,1H] HMQC-NOE-HMQC NMR spectroscopy: resolving tertiary nuclear Overhauser effect distance constraints in the spectra of larger proteins, J. Am. Chem. Soc. 113 (1991) 370–372, https://doi.org/10.1021/ja00001a060.
[174] P. Rossi, Y. Xia, N. Khanra, G. Veglia, C.G. Kalodimos, 15N and 13C- SOFAST-HMQC editing enhances 3D-NOESY sensitivity in highly deuterated, selectively [1H,13C]-labeled proteins, J. Biomol. NMR 66 (2016) 259–271, https://doi.org/10.1007/s10858-016-0074-5.
[175] S. Hiller, I. Ibraghimov, G. Wagner, V.Y. Orekhov, Coupled decomposition of four-dimensional NOESY spectra, J. Am. Chem. Soc. 131 (2009) 12970–12978, https://doi.org/10.1021/ja902012x.
[176] M. Mobli, J.C. Hoch, Nonuniform sampling and non-Fourier signal processing methods in multidimensional NMR, Prog. Nucl. Magn. Reson. Spectrosc. 83 (2014) 21–41, https://doi.org/10.1016/j.pnmrs.2014.09.002.
[177] J. Ying, F. Delaglio, D.A. Torchia, A. Bax, Sparse multidimensional iterative lineshape-enhanced (SMILE) reconstruction of both non-uniformly sampled and conventional NMR data, J. Biomol. NMR 68 (2017) 101–118, https://doi.org/10.1007/s10858-016-0072-7.
[178] Y.-Z. Pan, B. Quade, K.D. Brewer, M. Szabo, J.D. Swarbrick, B. Graham, J. Rizo, Sequence-specific assignment of methyl groups from the neuronal SNARE complex using lanthanide-induced pseudocontact shifts, J. Biomol. NMR 66 (2016) 281–293, https://doi.org/10.1007/s10858-016-0078-1.
[179] V. Venditti, N.L. Fawzi, G.M. Clore, Automated sequence- and stereo-specific assignment of methyl-labeled proteins by paramagnetic relaxation and methyl-methyl nuclear Overhauser enhancement spectroscopy, J. Biomol. NMR 51 (2011) 319–328, https://doi.org/10.1007/s10858-011-9559-4.
[180] P.H.J. Keizers, A. Saragliadis, Y. Hiruma, M. Overhand, M. Ubbink, Design, synthesis, and evaluation of a lanthanide chelating protein probe: CLaNP-5 yields predictable paramagnetic effects independent of environment, J. Am. Chem. Soc. 130 (2008) 14802–14812, https://doi.org/10.1021/ja8054832.
[181] X.-C. Su, K. McAndrew, T. Huber, G. Otting, Lanthanide-binding peptides for NMR measurements of residual dipolar couplings and paramagnetic effects from multiple angles, J. Am. Chem. Soc. 130 (2008) 1681–1687, https://doi.org/10.1021/ja076564l.
[182] T. Saio, K. Ogura, M. Yokochi, Y. Kobashigawa, F. Inagaki, Two-point anchoring of a lanthanide-binding peptide to a target protein enhances the paramagnetic anisotropic effect, J. Biomol. NMR 44 (2009) 157–166, https://doi.org/10.1007/s10858-009-9325-z.
[183] K. Barthelmes, A.M. Reynolds, E. Peisach, H.R.A. Jonker, N.J. DeNunzio, K.N. Allen, B. Imperiali, H. Schwalbe, Engineering encodable lanthanide-binding tags into loop regions of proteins, J. Am. Chem. Soc. 133 (2011) 808–819, https://doi.org/10.1021/ja104983t.
[184] A.W. Barb, G.P. Subedi, An encodable lanthanide binding tag with reduced size and flexibility for measuring residual dipolar couplings and pseudocontact shifts in large proteins, J. Biomol. NMR 64 (2016) 75–85, https://doi.org/10.1007/s10858-015-0009-6.
[185] A. Bahramzadeh, H. Jiang, T. Huber, G. Otting, Two Histidines in an α-Helix: A Rigid Co2+-Binding Motif for PCS Measurements by NMR Spectroscopy, Angew. Chem. Int. Ed Engl. 57 (2018) 6226–6229, https://doi.org/10.1002/anie.201802501.
[186] M. John, C. Schmitz, A.Y. Park, N.E. Dixon, T. Huber, G. Otting, Sequence-specific and stereospecific assignment of methyl groups using paramagnetic lanthanides, J. Am. Chem. Soc. 129 (2007) 13749–13757, https://doi.org/10.1021/ja0744753.
[187] F. Flügge, T. Peters, Complete assignment of Ala, Ile, Leu, Met and Val methyl groups of human blood group A and B glycosyltransferases using lanthanide-induced pseudocontact shifts and methyl-methyl NOESY, J. Biomol. NMR 70 (2018) 245–259, https://doi.org/10.1007/s10858-018-0183-4.
[188] A. Velyvis, H.K. Schachman, L.E. Kay, Assignment of Ile, Leu, and Val methyl correlations in supra-molecular systems: an application to aspartate transcarbamoylase, J. Am. Chem. Soc. 131 (2009) 16534–16543, https://doi.org/10.1021/ja906978r.
[189] M. Lescanne, S.P. Skinner, A. Blok, M. Timmer, L. Cerofolini, M. Fragai, C. Luchinat, M. Ubbink, Methyl group assignment using pseudocontact shifts with PARAssign, J. Biomol. NMR 69 (2017) 183–195, https://doi.org/10.1007/s10858-017-0136-3.
[190] R. Sprangers, A. Gribun, P.M. Hwang, W.A. Houry, L.E. Kay, Quantitative NMR spectroscopy of supramolecular complexes: dynamic side pores in ClpP are important for product release, Proc. Natl. Acad. Sci. U. S. A. 102 (2005) 16678–16683, https://doi.org/10.1073/pnas.0507370102.
[191] C. Amero, M. Asunción Durá, M. Noirclerc-Savoye, A. Perollier, B. Gallet, M.J. Plevin, T. Vernet, B. Franzetti, J. Boisbouvier, A systematic mutagenesis-driven strategy for site-resolved NMR studies of supramolecular assemblies, J. Biomol. NMR 50 (2011) 229–236, https://doi.org/10.1007/s10858-011-9513-5.
[192] A. Neu, U. Neu, A.-L. Fuchs, B. Schlager, R. Sprangers, An excess of catalytically required motions inhibits the scavenger decapping enzyme, Nat. Chem. Biol. 11 (2015) 697–704, https://doi.org/10.1038/nchembio.1866.
[193] T.L. Religa, R. Sprangers, L.E. Kay, Dynamic regulation of archaeal proteasome gate opening as studied by TROSY NMR, Science 328 (2010) 98–102, https://doi.org/10.1126/science.1184991.
[194] A.B. Sahakyan, W.F. Vranken, A. Cavalli, M. Vendruscolo, Structure-based prediction of methyl chemical shifts in proteins, J. Biomol. NMR 50 (2011) 331–346, https://doi.org/10.1007/s10858-011-9524-2.
[195] J. Meiler, PROSHIFT: protein chemical shift prediction using artificial neural networks, J. Biomol. NMR 26 (2003) 25–37.
[196] B. Han, Y. Liu, S.W. Ginzinger, D.S. Wishart, SHIFTX2: significantly improved protein chemical shift prediction, J. Biomol. NMR 50 (2011) 43–57, https://doi.org/10.1007/s10858-011-9478-4.
[197] Y. Xu, M. Liu, P.J. Simpson, R. Isaacson, E. Cota, J. Marchant, D. Yang, X. Zhang, P. Freemont, S. Matthews, Automated assignment in selectively methyl-labeled proteins, J. Am. Chem. Soc. 131 (2009) 9480–9481, https://doi.org/10.1021/ja9020233.
[198] Y. Xu, S. Matthews, MAP-XSII: an improved program for the automatic assignment of methyl resonances in large proteins, J. Biomol. NMR 55 (2013) 179–187, https://doi.org/10.1007/s10858-012-9700-z.
[199] F.-A. Chao, L. Shi, L.R. Masterson, G. Veglia, FLAMEnGO: a fuzzy logic approach for methyl group assignment using NOESY and paramagnetic relaxation enhancement data, J. Magn. Reson. San Diego Calif 1997 (214) (2012) 103–110, https://doi.org/10.1016/j.jmr.2011.10.008.

Please cite this article as: S. Schütz and R. Sprangers, Methyl TROSY spectroscopy: A versatile NMR approach to study challenging biological systems, Progress in Nuclear Magnetic Resonance Spectroscopy, https://doi.org/10.1016/j.pnmrs.2019.09.004

[200] F.-A. Chao, J. Kim, Y. Xia, M. Milligan, N. Rowe, G. Veglia, FLAMEnGO 2.0: an enhanced fuzzy logic algorithm for structure-based assignment of methyl group resonances, J. Magn. Reson. San Diego Calif 1997 (245) (2014) 17–23, https://doi.org/10.1016/j.jmr.2014.04.012.

[201] I. Pritišanac, M.T. Degiacomi, T.R. Alderson, M.G. Carneiro, E. Ab, G. Siegal, A.J. Baldwin, Automatic assignment of methyl-NMR spectra of supramolecular machines using graph theory, J. Am. Chem. Soc. 139 (2017) 9523–9533, https://doi.org/10.1021/jacs.6b11358.

[202] Y.R. Monneau, P. Rossi, A. Bhaumik, C. Huang, Y. Jiang, T. Saleh, T. Xie, Q. Xing, C.G. Kalodimos, Automatic methyl assignment in large proteins by the MAGIC algorithm, J. Biomol. NMR 69 (2017) 215–227, https://doi.org/10.1007/s10858-017-0149-y.

[203] J. Janin, S. Miller, C. Chothia, Surface, subunit interfaces and interior of oligomeric proteins, J. Mol. Biol. 204 (1988) 155–164.

[204] M.C. Stoffregen, M.M. Schwer, F.A. Renschler, S. Wiesner, Methionine scanning as an NMR tool for detecting and analyzing biomolecular interaction surfaces, Struct. Lond. Engl. 1993 (20) (2012) 573–581, https://doi.org/10.1016/j.str.2012.02.012.

[205] S. Mari, N. Ruetalo, E. Maspero, M.C. Stoffregen, S. Pasqualato, S. Polo, S. Wiesner, Structural and functional framework for the autoinhibition of Nedd4-family ubiquitin ligases, Struct. Lond. Engl. 1993 (22) (2014) 1639–1649, https://doi.org/10.1016/j.str.2014.09.006.

[206] A.G. Palmer, H. Koss, Chemical exchange, Methods Enzymol. 615 (2019) 177–236, https://doi.org/10.1016/bs.mie.2018.09.028.

[207] D. Sheppard, R. Sprangers, V. Tugarinov, Experimental approaches for NMR studies of side-chain dynamics in high-molecular-weight proteins, Prog. Nucl. Magn. Reson. Spectrosc. 56 (2010) 1–45, https://doi.org/10.1016/j.pnmrs.2009.07.004.

[208] V. Tugarinov, L.E. Kay, Quantitative 13C and 2H NMR relaxation studies of the 723-residue enzyme malate synthase G reveal a dynamic binding interface, Biochemistry 44 (2005) 15970–15977, https://doi.org/10.1021/bi0519809.

[209] V. Tugarinov, J.E. Ollerenshaw, L.E. Kay, Probing side-chain dynamics in high molecular weight proteins by deuterium NMR spin relaxation: an application to an 82-kDa enzyme, J. Am. Chem. Soc. 127 (2005) 8214–8225, https://doi.org/10.1021/ja0508830.

[210] R. Ishima, A.P. Petkova, J.M. Louis, D.A. Torchia, Comparison of methyl rotation axis order parameters derived from model-free analyses of (2)H and (13)C longitudinal and transverse relaxation rates measured in the same protein sample, J. Am. Chem. Soc. 123 (2001) 6164–6171.

[211] D.R. Muhandiram, T. Yamazaki, B.D. Sykes, L.E. Kay, Measurement of 2H T1 and T1.rho. Relaxation times in uniformly 13C-labeled and fractionally 2H-labeled proteins in solution, J. Am. Chem. Soc. 117 (1995) 11536–11544, https://doi.org/10.1021/ja00151a018.

[212] O. Millet, D.R. Muhandiram, N.R. Skrynnikov, L.E. Kay, Deuterium spin probes of side-chain dynamics in proteins. 1. Measurement of five relaxation rates per deuteron in (13)C-labeled and fractionally (2)H-enriched proteins in solution, J. Am. Chem. Soc. 124 (2002) 6439–6448.

[213] V. Tugarinov, L.E. Kay, Relaxation rates of degenerate ^{1}H transitions in methyl groups of proteins as reporters of side-chain dynamics, J. Am. Chem. Soc. 128 (2006) 7299–7308, https://doi.org/10.1021/ja060817d.

[214] V. Tugarinov, R. Sprangers, L.E. Kay, Line narrowing in methyl-TROSY using zero-quantum 1H–13C NMR spectroscopy, J. Am. Chem. Soc. 126 (2004) 4921–4925, https://doi.org/10.1021/ja039732s.

[215] M.L. Gill, A.G. Palmer, Multiplet-filtered and gradient-selected zero-quantum TROSY experiments for 13C1H3 methyl groups in proteins, J. Biomol. NMR 51 (2011) 245–251, https://doi.org/10.1007/s10858-011-9533-1.

[216] V. Tugarinov, R. Sprangers, L.E. Kay, Probing side-chain dynamics in the proteasome by relaxation violated coherence transfer NMR spectroscopy, J. Am. Chem. Soc. 129 (2007) 1743–1750, https://doi.org/10.1021/ja067827z.

[217] H. Sun, R. Godoy-Ruiz, V. Tugarinov, Estimating side-chain order in methyl-protonated, perdeuterated proteins via multiple-quantum relaxation violated coherence transfer NMR spectroscopy, J. Biomol. NMR 52 (2012) 233–243, https://doi.org/10.1007/s10858-012-9604-y.

[218] H. Sun, L.E. Kay, V. Tugarinov, An optimized relaxation-based coherence transfer NMR experiment for the measurement of side-chain order in methyl-protonated, highly deuterated proteins, J. Phys. Chem. B. 115 (2011) 14878–14884, https://doi.org/10.1021/jp209049k.

[219] D.A. Capdevila, F. Huerta, K.A. Edmonds, M.T. Le, H. Wu, D.P. Giedroc, Tuning site-specific dynamics to drive allosteric activation in a pneumococcal zinc uptake regulator, ELife 7 (2018), https://doi.org/10.7554/eLife. 37268 e37268.

[220] Y. Wang, V.S. Manu, J. Kim, G. Li, L.G. Ahuja, P. Aoto, S.S. Taylor, G. Veglia, Globally correlated conformational entropy underlies positive and negative cooperativity in a kinase's enzymatic cycle, Nat. Commun. 10 (2019) 799, https://doi.org/10.1038/s41467-019-08655-7.

[221] V. Tugarinov, L.E. Kay, 1H,13C–1H,1H dipolar cross-correlated spin relaxation in methyl groups, J. Biomol. NMR 29 (2004) 369–376, https://doi.org/10.1023/B:JNMR.0000032562.07475.7f.

[222] B. Ergel, M.L. Gill, L. Brown, B. Yu, A.G. Palmer, J.F. Hunt, Protein dynamics control the progression and efficiency of the catalytic reaction cycle of the Escherichia coli DNA-repair enzyme AlkB, J. Biol. Chem. 289 (2014) 29584–29601, https://doi.org/10.1074/jbc.M114.575647.

[223] Y. Toyama, M. Osawa, M. Yokogawa, I. Shimada, NMR method for characterizing microsecond-to-millisecond chemical exchanges utilizing differential multiple-quantum relaxation in high molecular weight proteins, J. Am. Chem. Soc. 138 (2016) 2302–2311, https://doi.org/10.1021/jacs.5b12954.

[224] P. Lundström, M. Akke, Quantitative analysis of conformational exchange contributions to ^{1}H– ^{15}N multiple-quantum relaxation using field-dependent measurements. time scale and structural characterization of exchange in a calmodulin C-terminal domain mutant, J. Am. Chem. Soc. 126 (2004) 928–935, https://doi.org/10.1021/ja037529r.

[225] Y. Toyama, H. Kano, Y. Mase, M. Yokogawa, M. Osawa, I. Shimada, Dynamic regulation of GDP binding to G proteins revealed by magnetic field-dependent NMR relaxation analyses, Nat. Commun. 8 (2017) 14523, https://doi.org/10.1038/ncomms14523.

[226] V. Tugarinov, L.E. Kay, Estimating side-chain order in [U-^{2}H; ^{13}CH$_3$]-labeled high molecular weight proteins from analysis of HMQC/HSQC spectra, J. Phys. Chem. B. 117 (2013) 3571–3577, https://doi.org/10.1021/jp401088c.

[227] D.M. Korzhnev, P. Neudecker, A. Mittermaier, V.Yu. Orekhov, L.E. Kay, Multiple-site exchange in proteins studied with a suite of six NMR relaxation dispersion experiments: an application to the folding of a Fyn SH3 domain mutant, J. Am. Chem. Soc. 127 (2005) 15602–15611, https://doi.org/10.1021/ja054550e.

[228] H. Koss, M. Rance, A.G. Palmer, General expressions for carr-purcell-meiboom-gill relaxation dispersion for N-site chemical exchange, Biochemistry. 57 (2018) 4753–4763, https://doi.org/10.1021/acs.biochem.8b00370.

[229] A.J. Baldwin, An exact solution for R2, eff in CPMG experiments in the case of two site chemical exchange, J. Magn. Reson. San Diego Calif 1997 (244) (2014) 114–124, https://doi.org/10.1016/j.jmr.2014.02.023.

[230] J.G. Reddy, S. Pratihar, D. Ban, S. Frischkorn, S. Becker, C. Griesinger, D. Lee, Simultaneous determination of fast and slow dynamics in molecules using extreme CPMG relaxation dispersion experiments, J. Biomol. NMR 70 (2018) 1–9, https://doi.org/10.1007/s10858-017-0155-0.

[231] C.A. Smith, D. Ban, S. Pratihar, K. Giller, C. Schwiegk, B.L. de Groot, S. Becker, C. Griesinger, D. Lee, Population shuffling of protein conformations, Angew. Chem. Int. Ed. 54 (2015) 207–210, https://doi.org/10.1002/anie.201408890.

[232] N.R. Skrynnikov, F.A.A. Mulder, B. Hon, F.W. Dahlquist, L.E. Kay, Probing slow time scale dynamics at methyl-containing side chains in proteins by relaxation dispersion NMR measurements: application to methionine residues in a cavity mutant of T4 lysozyme, J. Am. Chem. Soc. 123 (2001) 4556–4566, https://doi.org/10.1021/ja004179p.

[233] P. Lundström, P. Vallurupalli, T.L. Religa, F.W. Dahlquist, L.E. Kay, A single-quantum methyl 13C-relaxation dispersion experiment with improved sensitivity, J. Biomol. NMR 38 (2007) 79–88, https://doi.org/10.1007/s10858-007-9149-7.

[234] T. Yuwen, R. Huang, P. Vallurupalli, L.E. Kay, A methyl-TROSY-based 1 H relaxation dispersion experiment for studies of conformational exchange in high molecular weight proteins, Angew. Chem. Int. Ed Engl. (2019), https://doi.org/10.1002/anie.201900241.

[235] V. Tugarinov, L.E. Kay, Separating degenerate (1)H transitions in methyl group probes for single-quantum (1)H-CPMG relaxation dispersion NMR spectroscopy, J. Am. Chem. Soc. 129 (2007) 9514–9521, https://doi.org/10.1021/ja0726456.

[236] M.J.C. Audin, J.P. Wurm, M.A. Cvetkovic, R. Sprangers, The oligomeric architecture of the archaeal exosome is important for processive and efficient RNA degradation, Nucleic Acids Res. 44 (2016) 2962–2973, https://doi.org/10.1093/nar/gkw062.

[237] U. Weininger, Z. Liu, D.D. McIntyre, H.J. Vogel, M. Akke, Specific 12 C β D 2 12 C γ D 2 S 13 C ε HD 2 isotopomer labeling of methionine to characterize protein dynamics by 1 H and 13 C NMR relaxation dispersion, J. Am. Chem. Soc. 134 (2012) 18562–18565, https://doi.org/10.1021/ja309294u.

[238] A.J. Baldwin, T.L. Religa, D.F. Hansen, G. Bouvignies, L.E. Kay, ^{13}CHD$_2$ methyl group probes of millisecond time scale exchange in proteins by ^{1}H relaxation dispersion: an application to proteasome gating residue dynamics, J. Am. Chem. Soc. 132 (2010) 10992–10995, https://doi.org/10.1021/ja104578n.

[239] R. Otten, J. Villali, D. Kern, F.A.A. Mulder, Probing microsecond time scale dynamics in proteins by methyl ^{1} H Carr–Purcell–Meiboom–Gill relaxation dispersion NMR measurements. Application to activation of the signaling protein NtrC^{r}, J. Am. Chem. Soc. 132 (2010) 17004–17014, https://doi.org/10.1021/ja107410x.

[240] E. Rennella, A.K. Schuetz, L.E. Kay, Quantitative measurement of exchange dynamics in proteins via (13)C relaxation dispersion of (13)CHD2-labeled samples, J. Biomol. NMR 65 (2016) 59–64, https://doi.org/10.1007/s10858-016-0038-9.

[241] D.M. Korzhnev, K. Kloiber, L.E. Kay, Multiple-quantum relaxation dispersion NMR spectroscopy probing millisecond time-scale dynamics in proteins: theory and application, J. Am. Chem. Soc. 126 (2004) 7320–7329, https://doi.org/10.1021/ja049968b.

[242] Y. Xiao, T. Lee, M.P. Latham, L.R. Warner, A. Tanimoto, A. Pardi, N.G. Ahn, Phosphorylation releases constraints to domain motion in ERK2, Proc. Natl. Acad. Sci. 111 (2014) 2506–2511, https://doi.org/10.1073/pnas.1318899111.

[243] G.P. Lisi, K.W. East, V.S. Batista, J.P. Loria, Altering the allosteric pathway in IGPS suppresses millisecond motions and catalytic activity, Proc. Natl. Acad. Sci. U. S. A. 114 (2017) E3414–E3423, https://doi.org/10.1073/pnas.1700448114.

[244] J.L. Kitevski-LeBlanc, T. Yuwen, P.N. Dyer, J. Rudolph, K. Luger, L.E. Kay, Investigating the dynamics of destabilized nucleosomes using methyl-TROSY NMR, J. Am. Chem. Soc. 140 (2018) 4774–4777, https://doi.org/10.1021/jacs.8b00931.

Please cite this article as: S. Schütz and R. Sprangers, Methyl TROSY spectroscopy: A versatile NMR approach to study challenging biological systems, Progress in Nuclear Magnetic Resonance Spectroscopy, https://doi.org/10.1016/j.pnmrs.2019.09.004

[245] T. Yuwen, P. Vallurupalli, L.E. Kay, Enhancing the sensitivity of CPMG relaxation dispersion to conformational exchange processes by multiple-quantum spectroscopy, Angew. Chem. Int. Ed Engl. 55 (2016) 11490–11494, https://doi.org/10.1002/anie.201605843.
[246] T. Yuwen, A. Sekhar, A.J. Baldwin, P. Vallurupalli, L.E. Kay, Measuring diffusion constants of invisible protein conformers by triple-quantum ^{1}H CPMG relaxation dispersion, Angew. Chem. Int. Ed. 57 (2018) 16777–16780, https://doi.org/10.1002/anie.201810868.
[247] A.B. Gopalan, T. Yuwen, L.E. Kay, P. Vallurupalli, A methyl 1H double quantum CPMG experiment to study protein conformational exchange, J. Biomol. NMR 72 (2018) 79–91, https://doi.org/10.1007/s10858-018-0208-z.
[248] A.B. Gopalan, P. Vallurupalli, Measuring the signs of the methyl 1H chemical shift differences between major and 'invisible' minor protein conformational states using methyl 1H multi-quantum spectroscopy, J. Biomol. NMR 70 (2018) 187–202, https://doi.org/10.1007/s10858-018-0171-8.
[249] A.J. Baldwin, L.E. Kay, Measurement of the signs of methyl 13C chemical shift differences between interconverting ground and excited protein states by R (1ρ): an application to αB-crystallin, J. Biomol. NMR 53 (2012) 1–12, https://doi.org/10.1007/s10858-012-9617-6.
[250] I.R. Kleckner, P. Gollnick, M.P. Foster, Mechanisms of allosteric gene regulation by NMR quantification of microsecond-millisecond protein dynamics, J. Mol. Biol. 415 (2012) 372–381, https://doi.org/10.1016/j.jmb.2011.11.019.
[251] D.F. Hansen, P. Vallurupalli, P. Lundström, P. Neudecker, L.E. Kay, Probing chemical shifts of invisible states of proteins with relaxation dispersion NMR spectroscopy: how well can we do?, J. Am. Chem. Soc. 130 (2008) 2667–2675, https://doi.org/10.1021/ja078337p.
[252] M. Bieri, P.R. Gooley, Automated NMR relaxation dispersion data analysis using NESSY, BMC Bioinformatics 12 (2011) 421, https://doi.org/10.1186/1471-2105-12-421.
[253] S. Morin, T.E. Linnet, M. Lescanne, P. Schanda, G.S. Thompson, M. Tollinger, K. Teilum, S. Gagné, D. Marion, C. Griesinger, M. Blackledge, E.J. d'Auvergne, relax: the analysis of biomolecular kinetics and thermodynamics using NMR relaxation dispersion data, Bioinforma. Oxf. Engl. 30 (2014) 2219–2220, https://doi.org/10.1093/bioinformatics/btu166.
[254] A. Mazur, B. Hammesfahr, C. Griesinger, D. Lee, M. Kollmar, ShereKhan–calculating exchange parameters in relaxation dispersion data from CPMG experiments, Bioinforma. Oxf. Engl. 29 (2013) 1819–1820, https://doi.org/10.1093/bioinformatics/btt286.
[255] K. Sugase, T. Konuma, J.C. Lansing, P.E. Wright, Fast and accurate fitting of relaxation dispersion data using the flexible software package GLOVE, J. Biomol. NMR 56 (2013) 275–283, https://doi.org/10.1007/s10858-013-9747-5.
[256] M. Niklasson, R. Otten, A. Ahlner, C. Andresen, J. Schlagnitweit, K. Petzold, P. Lundström, Comprehensive analysis of NMR data using advanced line shape fitting, J. Biomol. NMR 69 (2017) 93–99, https://doi.org/10.1007/s10858-017-0141-6.
[257] R. Ishima, J.M. Louis, D.A. Torchia, Transverse ^{13} C relaxation of CHD $_2$ methyl isotopmers to detect slow conformational changes of protein side chains, J. Am. Chem. Soc. 121 (1999) 11589–11590, https://doi.org/10.1021/ja992836b.
[258] U. Brath, M. Akke, D. Yang, L.E. Kay, F.A.A. Mulder, Functional dynamics of human FKBP12 revealed by methyl ^{13}C rotating frame relaxation dispersion NMR spectroscopy, J. Am. Chem. Soc. 128 (2006) 5718–5727, https://doi.org/10.1021/ja0570279.
[259] U. Weininger, A.T. Blissing, J. Hennig, A. Ahlner, Z. Liu, H.J. Vogel, M. Akke, P. Lundström, Protein conformational exchange measured by 1H R1ρ relaxation dispersion of methyl groups, J. Biomol. NMR 57 (2013) 47–55, https://doi.org/10.1007/s10858-013-9764-4.
[260] P. Vallurupalli, G. Bouvignies, L.E. Kay, Studying "Invisible" excited protein states in slow exchange with a major state conformation, J. Am. Chem. Soc. 134 (2012) 8148–8161, https://doi.org/10.1021/ja3001419.
[261] T. Yuwen, R. Huang, L.E. Kay, Probing slow timescale dynamics in proteins using methyl 1H CEST, J. Biomol. NMR 68 (2017) 215–224, https://doi.org/10.1007/s10858-017-0121-x.
[262] T. Yuwen, L.E. Kay, A new class of CEST experiment based on selecting different magnetization components at the start and end of the CEST relaxation element: an application to 1H CEST, J. Biomol. NMR 70 (2018) 93–102, https://doi.org/10.1007/s10858-017-0161-2.
[263] A. Sekhar, A. Velyvis, G. Zoltsman, R. Rosenzweig, G. Bouvignies, L.E. Kay, Conserved conformational selection mechanism of Hsp70 chaperone-substrate interactions, ELife 7 (2018), https://doi.org/10.7554/eLife. 32764 e32764.
[264] G. Bouvignies, L.E. Kay, A 2D ^{13}C-CEST experiment for studying slowly exchanging protein systems using methyl probes: an application to protein folding, J. Biomol. NMR 53 (2012) 303–310, https://doi.org/10.1007/s10858-012-9640-7.
[265] E. Rennella, R. Huang, A. Velyvis, L.E. Kay, 13CHD2–CEST NMR spectroscopy provides an avenue for studies of conformational exchange in high molecular weight proteins, J. Biomol. NMR 63 (2015) 187–199, https://doi.org/10.1007/s10858-015-9974-z.
[266] M. Leninger, W.M. Marsiglia, A. Jerschow, N.J. Traaseth, Multiple frequency saturation pulses reduce CEST acquisition time for quantifying conformational exchange in biomolecules, J. Biomol. NMR 71 (2018) 19–30, https://doi.org/10.1007/s10858-018-0186-1.
[267] T. Yuwen, G. Bouvignies, L.E. Kay, Exploring methods to expedite the recording of CEST datasets using selective pulse excitation, J. Magn. Reson. 292 (2018) 1–7, https://doi.org/10.1016/j.jmr.2018.04.013.
[268] T. Yuwen, L.E. Kay, G. Bouvignies, Dramatic decrease in CEST measurement times using multi-site excitation, ChemPhysChem 19 (2018) 1707–1710, https://doi.org/10.1002/cphc.201800249.
[269] N.L. Fawzi, J. Ying, R. Ghirlando, D.A. Torchia, G.M. Clore, Atomic-resolution dynamics on the surface of amyloid-β protofibrils probed by solution NMR, Nature 480 (2011) 268–272, https://doi.org/10.1038/nature10577.
[270] N.L. Fawzi, D.S. Libich, J. Ying, V. Tugarinov, G.M. Clore, Characterizing methyl-bearing side chain contacts and dynamics mediating amyloid β protofibril interactions using $^{13}\zeta_{\text{meth}}$yl -DEST and lifetime line broadening, Angew. Chem. Int. Ed. 53 (2014) 10345–10349, https://doi.org/10.1002/anie.201405180.
[271] D.S. Libich, V. Tugarinov, G.M. Clore, Intrinsic unfoldase/foldase activity of the chaperonin GroEL directly demonstrated using multinuclear relaxation-based NMR, Proc. Natl. Acad. Sci. 112 (2015) 8817–8823, https://doi.org/10.1073/pnas.1510083112.
[272] N.A. Farrow, O. Zhang, J.D. Forman-Kay, L.E. Kay, Characterization of the backbone dynamics of folded and denatured states of an SH3 domain, Biochemistry 36 (1997) 2390–2402, https://doi.org/10.1021/bi962548h.
[273] M.P. Latham, A. Sekhar, L.E. Kay, Understanding the mechanism of proteasome 20S core particle gating, Proc. Natl. Acad. Sci. 111 (2014) 5532–5537, https://doi.org/10.1073/pnas.1322079111.
[274] K. Kloiber, R. Spitzer, S. Grutsch, C. Kreutz, M. Tollinger, Longitudinal exchange: an alternative strategy towards quantification of dynamics parameters in ZZ exchange spectroscopy, J. Biomol. NMR 51 (2011) 123–129, https://doi.org/10.1007/s10858-011-9547-8.
[275] K.H. Mok, T. Nagashima, I.J. Day, J.A. Jones, C.J.V. Jones, C.M. Dobson, P.J. Hore, Rapid sample-mixing technique for transient NMR and photo-CIDNP spectroscopy: applications to real-time protein folding, J. Am. Chem. Soc. 125 (2003) 12484–12492, https://doi.org/10.1021/ja036357v.
[276] R. Franco, A. Favier, P. Schanda, B. Brutscher, Optimized fast mixing device for real-time NMR applications, J. Magn. Reson. San Diego Calif 1997 (281) (2017) 125–129, https://doi.org/10.1016/j.jmr.2017.05.016.
[277] C. Charlier, J.M. Courtney, T.R. Alderson, P. Anfinrud, A. Bax, Monitoring 15N chemical shifts during protein folding by pressure-jump NMR, J. Am. Chem. Soc. 140 (2018) 8096–8099, https://doi.org/10.1021/jacs.8b04833.
[278] G. Mas, J.-Y. Guan, E. Crublet, E.C. Debled, C. Moriscot, P. Gans, G. Schoehn, P. Macek, P. Schanda, J. Boisbouvier, Structural investigation of a chaperonin in action reveals how nucleotide binding regulates the functional cycle, Sci. Adv. 4 (2018), https://doi.org/10.1126/sciadv.aau4196, eaau4196.
[279] P. Macek, R. Kerfah, E. Boeri Erba, E. Crublet, C. Moriscot, G. Schoehn, C. Amero, J. Boisbouvier, Unraveling self-assembly pathways of the 468-kDa proteolytic machine TET2, Sci. Adv. 3 (2017), https://doi.org/10.1126/sciadv.1601601, e1601601.
[280] E.F. DeRose, T.W. Kirby, G.A. Mueller, W.A. Beard, S.H. Wilson, R.E. London, Transitions in DNA polymerase β μs-ms dynamics related to substrate binding and catalysis, Nucleic Acids Res. 46 (2018) 7309–7322, https://doi.org/10.1093/nar/gky503.
[281] K. Weinhäupl, C. Lindau, A. Hessel, Y. Wang, C. Schütze, T. Jores, L. Melchionda, B. Schönfisch, H. Kalbacher, B. Bersch, D. Rapaport, M. Brennich, K. Lindorff-Larsen, N. Wiedemann, P. Schanda, Structural basis of membrane protein chaperoning through the mitochondrial intermembrane space, Cell 175 (2018) 1365–1379.e25, https://doi.org/10.1016/j.cell.2018.10.039.
[282] Y. Toyama, H. Kano, Y. Mase, M. Yokogawa, M. Osawa, I. Shimada, Structural basis for the ethanol action on G-protein–activated inwardly rectifying potassium channel 1 revealed by NMR spectroscopy, Proc. Natl. Acad. Sci. 115 (2018) 3858–3863, https://doi.org/10.1073/pnas.1722257115.
[283] A.K. Schuetz, L.E. Kay, A Dynamic molecular basis for malfunction in disease mutants of p97/VCP, ELife 5 (2016), https://doi.org/10.7554/eLife. 20143.
[284] A.K. Schütz, E. Rennella, L.E. Kay, Exploiting conformational plasticity in the AAA+ protein VCP/p97 to modify function, Proc. Natl. Acad. Sci. 114 (2017) E6822–E6829, https://doi.org/10.1073/pnas.1707974114.
[285] M. Larion, A.L. Hansen, F. Zhang, L. Bruschweiler-Li, V. Tugarinov, B.G. Miller, R. Brüschweiler, Kinetic cooperativity in human pancreatic glucokinase originates from millisecond dynamics of the small domain, Angew. Chem. Int. Ed. 54 (2015) 8129–8132, https://doi.org/10.1002/anie.201501204.
[286] K.H. Gardner, M.K. Rosen, L.E. Kay, Global folds of highly deuterated, methyl-protonated proteins by multidimensional NMR, Biochemistry 36 (1997) 1389–1401, https://doi.org/10.1021/bi9624806.
[287] C.N. Chi, D. Strotz, R. Riek, B. Vögeli, NOE-derived methyl distances from a 360 kDa proteasome complex, Chem. Weinh. Bergstr. Ger. 24 (2018) 2270–2276, https://doi.org/10.1002/chem.201705551.
[288] A. Lapinaite, B. Simon, L. Skjaerven, M. Rakwalska-Bange, F. Gabel, T. Carlomagno, The structure of the box C/D enzyme reveals regulation of RNA methylation, Nature 502 (2013) 519–523, https://doi.org/10.1038/nature12581.
[289] R. Sprangers, L.E. Kay, Probing supramolecular structure from measurement of methyl (1)H-(13)C residual dipolar couplings, J. Am. Chem. Soc. 129 (2007) 12668–12669, https://doi.org/10.1021/ja075846i.
[290] C. Guo, R. Godoy-Ruiz, V. Tugarinov, High resolution measurement of methyl 13C(m)-13C and 1H(m)-13C(m) residual dipolar couplings in large proteins, J. Am. Chem. Soc. 132 (2010) 13984–13987, https://doi.org/10.1021/ja1041435.

Please cite this article as: S. Schütz and R. Sprangers, Methyl TROSY spectroscopy: A versatile NMR approach to study challenging biological systems, Progress in Nuclear Magnetic Resonance Spectroscopy, https://doi.org/10.1016/j.pnmrs.2019.09.004

[291] X. Liao, R. Godoy-Ruiz, C. Guo, V. Tugarinov, Simultaneous measurement of $^{1}H–^{15}N$ and methyl $^{1}Hm–^{13}Cm$ residual dipolar couplings in large proteins, J. Biomol. NMR 51 (2011) 191–198, https://doi.org/10.1007/s10858-011-9553-x.

[292] A.M. Ruschak, L.E. Kay, Proteasome allostery as a population shift between interchanging conformers, Proc. Natl. Acad. Sci. 109 (2012) E3454–E3462, https://doi.org/10.1073/pnas.1213640109.

[293] A. Velyvis, H.K. Schachman, L.E. Kay, Application of methyl-TROSY NMR to test allosteric models describing effects of nucleotide binding to aspartate transcarbamoylase, J. Mol. Biol. 387 (2009) 540–547, https://doi.org/10.1016/j.jmb.2009.01.066.

[294] K. Pederson, G.R. Chalmers, Q. Gao, D. Elnatan, T.A. Ramelot, L.-C. Ma, G.T. Montelione, M.A. Kennedy, D.A. Agard, J.H. Prestegard, NMR characterization of HtpG, the E. coli Hsp90, using sparse labeling with 13C-methyl alanine, J. Biomol. NMR 68 (2017) 225–236, https://doi.org/10.1007/s10858-017-0123-8.

[295] A.J. Baldwin, D.F. Hansen, P. Vallurupalli, L.E. Kay, Measurement of methyl axis orientations in invisible, excited states of proteins by relaxation dispersion NMR spectroscopy, J. Am. Chem. Soc. 131 (2009) 11939–11948, https://doi.org/10.1021/ja903896p.

[296] D.F. Hansen, L.E. Kay, Determining valine side-chain rotamer conformations in proteins from methyl 13C chemical shifts: application to the 360 kDa half-proteasome, J. Am. Chem. Soc. 133 (2011) 8272–8281, https://doi.org/10.1021/ja2014532.

[297] A. Grishaev, V. Tugarinov, L.E. Kay, J. Trewhella, A. Bax, Refined solution structure of the 82-kDa enzyme malate synthase G from joint NMR and synchrotron SAXS restraints, J. Biomol. NMR 40 (2008) 95–106, https://doi.org/10.1007/s10858-007-9211-5.

[298] M. Groll, T. Clausen, Molecular shredders: how proteasomes fulfill their role, Curr. Opin. Struct. Biol. 13 (2003) 665–673.

[299] A.M. Ruschak, T.L. Religa, S. Breuer, S. Witt, L.E. Kay, The proteasome antechamber maintains substrates in an unfolded state, Nature 467 (2010) 868–871, https://doi.org/10.1038/nature09444.

[300] A. Velyvis, L.E. Kay, Measurement of active site ionization equilibria in the 670 kDa proteasome core particle using methyl-TROSY NMR, J. Am. Chem. Soc. 135 (2013) 9259–9262, https://doi.org/10.1021/ja403091c.

[301] R. Sprangers, X. Li, X. Mao, J.L. Rubinstein, A.D. Schimmer, L.E. Kay, TROSY-based NMR evidence for a novel class of 20S proteasome inhibitors, Biochemistry 47 (2008) 6727–6734, https://doi.org/10.1021/bi8005913.

[302] X. Mao, X. Li, R. Sprangers, X. Wang, A. Venugopal, T. Wood, Y. Zhang, D.A. Kuntz, E. Coe, S. Trudel, D. Rose, R.A. Batey, L.E. Kay, A.D. Schimmer, Clioquinol inhibits the proteasome and displays preclinical activity in leukemia and myeloma, Leukemia 23 (2009) 585–590, https://doi.org/10.1038/leu.2008.232.

[303] X. Li, T.E. Wood, R. Sprangers, G. Jansen, N.E. Franke, X. Mao, X. Wang, Y. Zhang, S.E. Verbrugge, H. Adomat, Z.H. Li, S. Trudel, C. Chen, T.L. Religa, N. Jamal, H. Messner, J. Cloos, D.R. Rose, A. Navon, E. Guns, R.A. Batey, L.E. Kay, A. D. Schimmer, Effect of noncompetitive proteasome inhibition on bortezomib resistance, J. Natl. Cancer Inst. 102 (2010) 1069–1082, https://doi.org/10.1093/jnci/djq198.

[304] E. Lorentzen, J. Basquin, E. Conti, Structural organization of the RNA-degrading exosome, Curr. Opin. Struct. Biol. 18 (2008) 709–713, https://doi.org/10.1016/j.sbi.2008.10.004.

[305] R. Rosenzweig, S. Moradi, A. Zarrine-Afsar, J.R. Glover, L.E. Kay, Unraveling the mechanism of protein disaggregation through a ClpB-DnaK interaction, Science 339 (2013) 1080–1083, https://doi.org/10.1126/science.1233066.

[306] R. Rosenzweig, P. Farber, A. Velyvis, E. Rennella, M.P. Latham, L.E. Kay, ClpB N-terminal domain plays a regulatory role in protein disaggregation, Proc. Natl. Acad. Sci. 112 (2015) E6872–E6881, https://doi.org/10.1073/pnas.1512783112.

[307] A. Sekhar, R. Rosenzweig, G. Bouvignies, L.E. Kay, Mapping the conformation of a client protein through the Hsp70 functional cycle, Proc. Natl. Acad. Sci. U. S. A. 112 (2015) 10395–10400, https://doi.org/10.1073/pnas.1508504112.

[308] A. Sekhar, J. Nagesh, R. Rosenzweig, L.E. Kay, Conformational heterogeneity in the Hsp70 chaperone-substrate ensemble identified from analysis of NMR-detected titration data, Protein Sci. Publ. Protein Soc. 26 (2017) 2207–2220, https://doi.org/10.1002/pro.3276.

[309] R. Rosenzweig, A. Sekhar, J. Nagesh, L.E. Kay, Promiscuous binding by Hsp70 results in conformational heterogeneity and fuzzy chaperone-substrate ensembles, ELife 6 (2017), https://doi.org/10.7554/eLife. 28030.

[310] A. Zhuravleva, E.M. Clerico, L.M. Gierasch, An interdomain energetic tug-of-war creates the allosterically active state in Hsp70 molecular chaperones, Cell 151 (2012) 1296–1307, https://doi.org/10.1016/j.cell.2012.11.002.

[311] W. Meng, E.M. Clerico, N. McArthur, L.M. Gierasch, Allosteric landscapes of eukaryotic cytoplasmic Hsp70s are shaped by evolutionary tuning of key interfaces, Proc. Natl. Acad. Sci. 115 (2018) 11970–11975, https://doi.org/10.1073/pnas.1811105115.

[312] G.E. Karagöz, A.M.S. Duarte, E. Akoury, H. Ippel, J. Biernat, T. Morán Luengo, M. Radli, T. Didenko, B.A. Nordhues, D.B. Veprintsev, C.A. Dickey, E. Mandelkow, M. Zweckstetter, R. Boelens, T. Madl, S.G.D. Rüdiger, Hsp90-Tau complex reveals molecular basis for specificity in chaperone action, Cell. 156 (2014) 963–974, https://doi.org/10.1016/j.cell.2014.01.037.

[313] T. Saio, S. Kawagoe, K. Ishimori, C.G. Kalodimos, Oligomerization of a molecular chaperone modulates its activity, ELife 7 (2018), https://doi.org/10.7554/eLife. 35731.

[314] A.S. Solt, M.J. Bostock, B. Shrestha, P. Kumar, T. Warne, C.G. Tate, D. Nietlispach, Insight into partial agonism by observing multiple equilibria for ligand-bound and Gs-mimetic nanobody-bound β1-adrenergic receptor, Nat. Commun. 8 (2017) 1795, https://doi.org/10.1038/s41467-017-02008-y.

[315] M. Casiraghi, M. Damian, E. Lescop, E. Point, K. Moncoq, N. Morellet, D. Levy, J. Marie, E. Guittet, J.-L. Banères, L.J. Catoire, Functional modulation of a G protein-coupled receptor conformational landscape in a lipid bilayer, J. Am. Chem. Soc. 138 (2016) 11170–11175, https://doi.org/10.1021/jacs.6b04432.

[316] F. Bumbak, A.C. Keen, N.J. Gunn, P.R. Gooley, R.A.D. Bathgate, D.J. Scott, Optimization and 13CH3 methionine labeling of a signaling competent neurotensin receptor 1 variant for NMR studies, Biochim. Biophys. Acta BBA - Biomembr. 2018 (1860) 1372–1383, https://doi.org/10.1016/j.bbamem.2018.03.020.

[317] J. Okude, T. Ueda, Y. Kofuku, M. Sato, N. Nobuyama, K. Kondo, Y. Shiraishi, T. Mizumura, K. Onishi, M. Natsume, M. Maeda, H. Tsujishita, T. Kuranaga, M. Inoue, I. Shimada, Identification of a conformational equilibrium that determines the efficacy and functional selectivity of the μ-opioid receptor, Angew. Chem. Int. Ed. 54 (2015) 15771–15776, https://doi.org/10.1002/anie.201508794.

[318] J. Xu, Y. Hu, J. Kaindl, P. Risel, H. Hübner, S. Maeda, X. Niu, H. Li, P. Gmeiner, C. Jin, B.K. Kobilka, Conformational complexity and dynamics in a muscarinic receptor revealed by NMR spectroscopy, Mol. Cell. S109727651930320X (2019), https://doi.org/10.1016/j.molcel.2019.04.028.

[319] Y. Shiraishi, M. Natsume, Y. Kofuku, S. Imai, K. Nakata, T. Mizukoshi, T. Ueda, H. Iwaï, I. Shimada, Phosphorylation-induced conformation of β2-adrenoceptor related to arrestin recruitment revealed by NMR, Nat. Commun. 9 (2018) 194, https://doi.org/10.1038/s41467-017-02632-8.

[320] J.J. Liu, R. Horst, V. Katritch, R.C. Stevens, K. Wüthrich, Biased signaling pathways in β2-adrenergic receptor characterized by 19F-NMR, Science 335 (2012) 1106–1110, https://doi.org/10.1126/science.1215802.

[321] A. Manglik, T.H. Kim, M. Masureel, C. Altenbach, Z. Yang, D. Hilger, M.T. Lerch, T.S. Kobilka, F.S. Thian, W.L. Hubbell, R.S. Prosser, B.K. Kobilka, Structural insights into the dynamic process of β2-adrenergic receptor signaling, Cell 161 (2015) 1101–1111, https://doi.org/10.1016/j.cell.2015.04.043.

[322] D. Goricanec, R. Stehle, P. Egloff, S. Grigoriu, A. Plückthun, G. Wagner, F. Hagn, Conformational dynamics of a G-protein α subunit is tightly regulated by nucleotide binding, Proc. Natl. Acad. Sci. 113 (2016) E3629–E3638, https://doi.org/10.1073/pnas.1604125113.

[323] D. Goricanec, F. Hagn, NMR backbone and methyl resonance assignments of an inhibitory G-alpha subunit in complex with GDP, Biomol. NMR Assign. 13 (2019) 131–137, https://doi.org/10.1007/s12104-018-9865-9.

[324] H. van Ingen, A.M.J.J. Bonvin, Information-driven modeling of large macromolecular assemblies using NMR data, J. Magn. Reson. San Diego Calif 1997 (241) (2014) 103–114, https://doi.org/10.1016/j.jmr.2013.10.021.

[325] X. Bai, G. McMullan, S.H.W. Scheres, How cryo-EM is revolutionizing structural biology, Trends Biochem. Sci. 40 (2015) 49–57, https://doi.org/10.1016/j.tibs.2014.10.005.

[326] E. Nogales, The development of cryo-EM into a mainstream structural biology technique, Nat. Methods 13 (2016) 24–27.

[327] S. Kaledhonkar, Z. Fu, K. Caban, W. Li, B. Chen, M. Sun, R.L. Gonzalez, J. Frank, Late steps in bacterial translation initiation visualized using time-resolved cryo-EM, Nature (2019), https://doi.org/10.1038/s41586-019-1249-5.

[328] R. Huang, Z.A. Ripstein, R. Augustyniak, M. Lazniewski, K. Ginalski, L.E. Kay, J. L. Rubinstein, Unfolding the mechanism of the AAA+ unfoldase VAT by a combined cryo-EM, solution NMR study, Proc. Natl. Acad. Sci. U. S. A. 113 (2016) E4190–E4199, https://doi.org/10.1073/pnas.1603980113.

[329] S. Vahidi, Z.A. Ripstein, M. Bonomi, T. Yuwen, M.F. Mabanglo, J.B. Juravsky, K. Rizzolo, A. Velyvis, W.A. Houry, M. Vendruscolo, J.L. Rubinstein, L.E. Kay, Reversible inhibition of the ClpP protease via an N-terminal conformational switch, Proc. Natl. Acad. Sci. 115 (2018) E6447–E6456, https://doi.org/10.1073/pnas.1805125115.

[330] F. Delaglio, S. Grzesiek, G.W. Vuister, G. Zhu, J. Pfeifer, A. Bax, NMRPipe: a multidimensional spectral processing system based on UNIX pipes, J. Biomol. NMR 6 (1995) 277–293.

[331] P. Li, I.R.S. Martins, M.K. Rosen, The feasibility of parameterizing four-state equilibria using relaxation dispersion measurements, J. Biomol. NMR 51 (2011) 57–70, https://doi.org/10.1007/s10858-011-9541-1.

[332] A. Förster, E.I. Masters, F.G. Whitby, H. Robinson, C.P. Hill, The 1.9 A structure of a proteasome-11S activator complex and implications for proteasome-PAN/PA700 interactions, Mol. Cell. 18 (2005) 589–599, https://doi.org/10.1016/j.molcel.2005.04.016.

[333] E. Lorentzen, A. Dziembowski, D. Lindner, B. Seraphin, E. Conti, RNA channelling by the archaeal exosome, EMBO Rep. 8 (2007) 470–476, https://doi.org/10.1038/sj.embor.7400945.

[334] C. Deville, M. Carroni, K.B. Franke, M. Topf, B. Bukau, A. Mogk, H.R. Saibil, Structural pathway of regulated substrate transfer and threading through an Hsp100 disaggregase, Sci. Adv. 3 (2017), https://doi.org/10.1126/sciadv.1701726 e1701726.

[335] R. Qi, E.B. Sarbeng, Q. Liu, K.Q. Le, X. Xu, H. Xu, J. Yang, J.L. Wong, C. Vorvis, W. A. Hendrickson, L. Zhou, Q. Liu, Allosteric opening of the polypeptide-binding site when an Hsp70 binds ATP, Nat. Struct. Mol. Biol. 20 (2013) 900–907, https://doi.org/10.1038/nsmb.2583.

[336] K. Krishna Kumar, M. Shalev-Benami, M.J. Robertson, H. Hu, S.D. Banister, S.A. Hollingsworth, N.R. Latorraca, H.E. Kato, D. Hilger, S. Maeda, W.I. Weis, D.L. Farrens, R.O. Dror, S.V. Malhotra, B.K. Kobilka, G. Skiniotis, Structure of a

Please cite this article as: S. Schütz and R. Sprangers, Methyl TROSY spectroscopy: A versatile NMR approach to study challenging biological systems, Progress in Nuclear Magnetic Resonance Spectroscopy, https://doi.org/10.1016/j.pnmrs.2019.09.004

signaling cannabinoid receptor 1-G protein complex, Cell 176 (2019) 448–458.e12, https://doi.org/10.1016/j.cell.2018.11.040.

[337] G. Mas, E. Crublet, O. Hamelin, P. Gans, J. Boisbouvier, Specific labeling and assignment strategies of valine methyl groups for NMR studies of high molecular weight proteins, J. Biomol. NMR 57 (2013) 251–262, https://doi.org/10.1007/s10858-013-9785-z.

Glossary

γ_C: Gyromagnetic ratio of carbon ($67.28 \cdot 10^6$ rad·s^{-1}·T^{-1})
γ_D: Gyromagnetic ratio of deuterium ($41.07 \cdot 10^6$ rad·s^{-1}·T^{-1})
γ_H: Gyromagnetic ratio of proton ($267.52 \cdot 10^6$ rad·s^{-1}·T^{-1})
ω_A: Frequency of spin A
ω_B: Frequency of spin B
$\Delta\omega$: Frequency difference
ħ: Reduced Planck's constant ($1.05 \cdot 10^{-34}$ J·s)
μ_0: Vacuum permeability ($1.26 \cdot 10^{-6}$N·A^{-2})
μs: microsecond
τ_C: Correlation time for overall (isotropic) tumbling of the protein
$|1\rangle$ - $|8\rangle$: Proton spin states
$|\alpha\rangle$, $|\beta\rangle$: Carbon spin states
A: Alanine
A: State A
Ala: Alanine
B: State B
B_0: External magnetic field strength
CEST: Chemical Exchange Saturation Transfer
CHO: Chinese hamster ovary
COSY: Correlated Spectroscopy
CPMG: Carr-Purcell-Meiboom-Gill
Cryo-EM: Cryogenic electron microscopy
CSA: Chemical shift anisotropy
CSP: Chemical shift perturbation
DD: Dipole-dipole
DEST: Dark-state Exchange Saturation Transfer
DQ: Double quantum
E. coli: Escherichia coli
GHz: Gigaherz
Gly: Glycine
GPCR: G-protein-coupled receptor
HSQC: Heteronuclear single quantum coherence
I: Isoleucine
Ile: Isoleucine
INEPT: Insensitive nuclei enhanced by polarization transfer
J_{HC}: One bond scalar coupling constant between ^{1}H and ^{13}C (approx. 125 Hz within a methyl group)
kDa: Kilodalton
k_{AB}: Forward rate
k_{BA}: Reverse rate
k_{ex}: Exchange rate ($k_{ex} = k_{AB} + k_{BA}$)
L: Leucine
L: Liter
LEGO NMR: A method to "label, express, and generate oligomers" for NMR
Leu: Leucine
M: Methionine
MBP: Maltose binding protein
MDa: Megadalton
Met: Methionine
MHz: Megahertz
MMTS: Methyl-methanethiosulfonate
MQ: Multiple quantum
ms: millisecond
MSG: Malate synthase G
MTC: S-methylthiocysteine
NMR: Nuclear magnetic resonance
NOESY: Nuclear Overhauser effect spectroscopy
ns: nanosecond
NUS: Non-uniform sampling
p_A: Fractional population of state A
p_B: Fractional population of state B
PDBID: Protein databank identification code
PCS: Pseudo-contact shift
RDC: Residual dipolar coupling
PRE: Paramagnetic relaxation enhancement
r_{HC}: Proton-carbon distance ($1.135 \cdot 10^{-10}$ m within a methyl group)
r_{HH}: Proton-proton distance ($1.763 \cdot 10^{-10}$ m within a methyl group)
r_{HD}: Proton-deuterium distance
RecA-like: RecA-like domain 1 of the RNA helicase Dhh1
RNA: Ribonucleic acid
$R_{1\rho}$: Rotating-frame relaxation rate
$R_{1,EXT}$: ^{1}H spin flip rate that is due to external protons
$R_{2,EXT}$: Dephasing rate of ^{1}H coherences that is due to dipolar interactions with external proton and deuterium spins.
R_2: Transverse relaxation rate
$R_{2,C}^{SLOW}$: Slowly relaxing single quantum carbon transition
$R_{2,CH}^{SLOW}$: Slowly relaxing multiple quantum carbon transition
$R_{2,C/CH}^{SLOW}$: Slowly relaxing single or multiple quantum carbon transition
$R_{2,H}^{SLOW}$: Slowly relaxing proton transition
$R_{2,C}^{FAST}$: Fast relaxing single quantum carbon transition
$R_{2,CH}^{FAST}$: Fast relaxing multiple quantum carbon transition
$R_{2,C/CH}^{FAST}$: Fast relaxing single or multiple quantum carbon transition
$R_{2,H}^{FAST}$: Fast relaxing proton transition
RF: Radio frequency
S^2_{Axis}: Order parameter that describes the amplitude of the motion of a bond connecting a methyl group to its directly attached carbon
SAM: S-adenosyl-methionine
SANS: Small-angle neutron scattering
SAXS: Small-angle X-ray scattering
SOFAST: Band-Selective Optimized Flip-Angle Short-Transient
t_1: Carbon chemical shift evolution time (indirect dimension)
t_2: Proton chemical shift evolution time (direct dimension)
T_2: Transverse relaxation time
Thr: Threonine
TOCSY: Total Correlation Spectroscopy
TQ: Triple quantum
TROSY: Transverse relaxation optimized spectroscopy
V: Valine
Val: Valine
WT: Wild-type
ZQ: Zero quantum

Please cite this article as: S. Schütz and R. Sprangers, Methyl TROSY spectroscopy: A versatile NMR approach to study challenging biological systems, Progress in Nuclear Magnetic Resonance Spectroscopy, https://doi.org/10.1016/j.pnmrs.2019.09.004